To the Graduate Council:

I am submitting herewith a dissertation written by Yoshiaki Ide, entitled "The Rheology of Fiber Formation." I recommend that it be accepted in partial fulfillment of the requirements for the degree of Doctor of Philosophy, with a major in Chemical Engineering.

James L. White, Major Professor

We have read this dissertation
and recommend its acceptance:

Accepted for the Council:

Vice Chancellor
Graduate Studies and Research

Thesis
Ph.
.I332
1976

THE RHEOLOGY OF FIBER FORMATION

A Dissertation

Presented for the

Doctor of Philosophy

Degree

The University of Tennessee

Yoshiaki Ide

June 1976

128705

ACKNOWLEDGEMENTS

The author is indebted to the many persons who have been of assistance in various ways to make this investigation possible.

First of all, sincere appreciation goes to Professor James L. White, the author's advisor throughout his graduate study at the University of Tennessee. Prof. White has always provided guidance and patient encouragement in all aspects of the author's graduate work.

The author is very grateful to Prof. Donald C. Bogue and Prof. Nobuo Mitsuishi for providing the opportunity to study at this university. And financial support by Prof. H.F. Johnson, head of the department, and the "Polymer Consortium" is gratefully acknowledged.

Thanks are extended to all of the faculty members and student colleagues who have given useful suggestions and stimulating discussions during the study. Members of the Laboratory Service Shops have been very helpful in the experimental study.

Finally, the author is extremely grateful to his wife Mary for her love and continuous encouragement. Her efforts in helping with experiments, typing, and drawing figures were essential to the preparation of this dissertation.

ABSTRACT

Elongational flow behaviors of polymer melts were investigated for various kinds of polymers including low and high density polyethylenes (LDPE and HDPE), polystyrenes (PS), polypropylenes (PP), and polymethyl methacrylate (PMMA). Simple equipment to provide a constant stretch rate condition was developed and used for the study. The elongational viscosity functions for the various polymer melts were obtained. The stress responses were described reasonably well by the Bogue and White model or a generalized convected Maxwell model.

A mathematical theory integrating all instability mechanisms: capillarity, ductility, and fracture has been developed and sucessfully applied to the filament spinnability problem. The extensibility is predicted to show a maximum due to the three competing mechanisms. Different failure characterisitcs observed for LDPE and PS versus HDPE and PP were interpreted as due to different dependences of relaxation time upon deformation rate.

The instability concepts developed for tensile tests were applied to the continuous melt spinning process. It is suggested that draw resonance is an analogue of ductile instability and accumulation of material in the spinpath is responsible for such severe fluctuations. The threadline instabilities were discussed for isothermal and non-isothermal conditions.

TABLE OF CONTENTS

CHAPTER		PAGE
I.	INTRODUCTION	1
II.	BACKGROUND	4
	A. Mathematical Statements of the Principles of Conservation	4
	B. Constitutive Equations	5
	Differential Type Constitutive Equations	7
	Integral Type Constitutive Equations .	9
	Linear Theory	9
	Nonlinear Theory	11
	C. Rheological Response to Imposed Kinematics	16
	Simple Shear Flow	16
	Simple Uniaxial Elongation	18
	Theoretical Study	18
	Experimental Study	25
	D. Filament Stability	28
	General	28
	Capillary Instability	30
	Surface Tension	30
	Break Up of a Capillary Column . .	32
	Tensile Failure of Materials	37

CHAPTER PAGE

III. UNIAXIAL STRETCHING OF POLYMER MELTS 41

A. Experimental 41

Materials 41

Apparatus 41

Uniaxial Stretching 47

Procedure 47

Data Processing 49

Stress Relaxation 52

Procedure 52

Data Processing 52

B. Stress Development in Elongational Flow 57

Results 57

Low Density Polyethylene (LDPE) . 57

High Density Polyethylene (HDPE) . 61

Polystyrene (PS) 64

Polypropylene (PP) 64

Polymethyl Methacrylate (PMMA) . . 68

Discussion of Elongational Viscosity . 71

C. Comparison of Elongational Flow Behavior With Viscoelastic Fluid Theories 74

Bogue and White Model 74

Formulation of Transient Stress for Constant Rate Stretching . . 74

CHAPTER PAGE

Stress Growth Data and Comparisons with the Model 80
Generalized Maxwell Model 90
Formulation of the Transient Stress for Constant Rate Stretching 90
Comparison 95
D. Mechanisms and Elongation to Failure . . 102
Qualitative Observations 102
Total Elongation before Failure . . . 105
Interpretation of Failure 112
IV. THEORETCIAL INVESTIGATION OF THE SPINNABILITY. 115
A. Fundamental Equations for a Cylindrical Filament 115
B. Stability Analysis of Liquid Filaments . 118
Disturbances and Linearized Disturbance Equations 118
Newtonian Fluid Filaments 122
Capillary Instability 123
Interaction of Capillary and Ductile Instability 124
Viscoelastic Fluid Filaments 128
Perturbed Equation of State . . . 128
Capillary Instability 132

CHAPTER PAGE

Interaction of Capillarity and Ductility 133
Ductile Instability of Constant Relaxation Time Viscoelastic Fluids 135
Ductile Instability of Nonlinear Relaxation Time Viscoelastic Fluids 142
C. Prediction of Elongation to Break . . . 147
Interpretation from Stability Theory . 147
Extensibility as a Function of Weissenberg Number 153
Extensibility as a Function of Molecular Weight 158
V. CONSIDERATIONS OF MELT SPINNING PROCESS . . . 163
A. Background Literature 163
Stable Melt Spinning Process 163
Isothermal Melt Spinning 163
Non-isothermal Melt Spinning . . . 169
Unstable Melt Spinning Process 171
Spinnability in the Continuous Process 171
Draw Resonance Phenomena 172
B. Theoretical Investigation 175

CHAPTER PAGE

Stable Spinning of a Viscoelastic Fluid 175
Analogy between Ductile Instability and Draw Resonance Analyses 180
C. Experimental Study on Limitations of Melt Spinning 185
Materials 185
Melt Spinning Apparatus 186
Melt Spinning into Quiescent Air . . . 189
Qualitative Observations 189
Quantitative Data 190
Draw Resonance Experiments 191
Qualitative Observations 191
Quantitative Data 195
Interpretations of the Failures of Stable Melt Spinning Process 198
VI. CONCLUSIONS AND RECOMMENDATIONS 202
LIST OF REFERENCES 206
APPENDIX 216
VITA 218

LIST OF TABLES

TABLE PAGE

I. Predictions of Constitutive Equations at Steady State 19

II. Materials Used in the Experiments 42

III. Material Parameters Determined by Relaxation Experiment 56

IV. Material Constants (Data of Chen [23]) 82

LIST OF FIGURES

FIGURE		PAGE
2.1	Mechanisms of Filament Instability	29
3.1	Experimental Set Up for Constant Rate Stretching	45
3.2	Schematic Diagram of the Experimental Apparatus	46
3.3	Load-time Curve for a Low Density Polyethylene	51
3.4	An Illustration of Procedure X	54
3.5	Stress Developments at Various Stretch Rates for LDPE (MI = 1.7)	59
3.6	Stress Development at Various Stretch Rates for LDPE (MI = 5.0)	60
3.7	Stress Developments at Various Stretch Rates for HDPE (MI = 0.1)	62
3.8	Stress Developments at Various Stretch Rates for HDPE (MI = 2.6)	63
3.9	Stress Developments at Various Stretch Rates for PS (Shell TC3-30)	65
3.10	Stress Developments at Various Stretch Rates for PS (Dow Styron 678 U)	66
3.11	Stress Developments at Various Stretch Rates for PP (MI = 0.42)	67

FIGURE PAGE

3.12 Stress Development at Various Stretch Rates for PP (MI = 6.6) 69

3.13 Stress Development at Various Stretch Rates for PMMA 70

3.14 Maximum Attained Elongational Viscosities for Various Polymers as a Function of Elongation Rate 72

3.15 Stress Development Data of LDPE (MI = 1.7) and the Bogue and White Model Prediction Based upon Chen Oscillation Data 83

3.16 Stress Development Data of HDPE (MI = 2.6) and the Bogue and White Model Prediction Based upon Chen Oscillation Data 85

3.17 Predicted Tensile Stress by Takaki and Bogue and Stress Development Data of Shell TC3-30 at 160 °C 87

3.18 Stress Development Data of LDPE (MI = 1.7) and the Bogue and White Model Based upon Stress Relaxation Data 88

3.19 Stress Development Data of HDPE (MI = 0.1) and the Bogue and White Model Based upon Stress Relaxation Data 89

3.20 Stress Development Data of PS (Dow Styron 678 U) and the Bogue and White Model Based upon Stress Relaxation Data 91

FIGURE PAGE

3.21 Stress Development Data of PP (MI = 0.42) and the Bogue and White Model Based upon Stress Relaxation Data 92

3.22 Deformation Rate Dependence of the Characteristic Relaxation Time (Calculated by Steady Shear Data of Chen) 96

3.23 Comparison of White and Metzner Model and Generalized Maxwell Model with Experimental Data 99

3.24 Stress Development Data of PS (Shell TC3-30) and the Generalized Maxwell Model (Material Parameters Were Determined by Takaki and Bogue) 101

3.25 Experimental Apparatus for Study of Tensile Failure of Molten Polymer Filaments 103

3.26 Time to Break as a Function of Stretch Rate at 160°C 106

3.27 Total Elongation as a Function of Stretch Rate at 160°C 107

3.28 Total Elongation of LDPE as a Function of Stretch Rate at 130°C 108

3.29 Total Elongation of HDPE at 160°C 110

3.30 Total Elongation for Various Polymers Plotted Against Stretch Rate 111

FIGURE PAGE

4.1 Filament Containing a Periodic Disturbance in Its Diameter 119

4.2 Orowan-Chang-Lodge Model of Disturbance in a Filament Being Stretched 127

4.3 Disturbance Growth Plotted Against Strain Et for Varying Viscoelasticity Levels λE for a=0 137

4.4 Comparison of Disturbance Growth Analyses for Neglected τ_{22} (Eq. (4.69)) and Included τ_{22} (Eq. (4.78)) 143

4.5 Disturbance Growth of Viscoelastic Fluids at Various Values of a and λE 146

4.6 Elongation to Break as a Function of Inverse of Capillarity Number for Varying Defect Sizes 149

4.7 Viscoelastic Ductile Failure at Various Levels of Relaxation Time Dependence upon Stretch Rate 151

4.8 Cohesive Fracture of Visocelastic Fluids for Various Values of a 154

4.9 Predicted Viscoelastic Filament Failure: Elongation to Break and Failure Mechanisms . 155

4.10 Comparison of Elongation to Break Data with Theoretical Predictions 159

FIGURE PAGE

4.11 Predicted Spinnability as a Function of Molecular Weight 160

5.1 Continuous Melt Spinning Process 164

5.2 Velocity Distribution Along the Threadline for Various Values of an Effective Deborah Number 178

5.3 Schematic Diagram of the Melt Spinning Apparatus 187

5.4 Experimental Set Up for the Draw Resonance Experiments 188

5.5 Maximum Draw Ratio Attained Plotted Against Deborah Number 192

5.6 Force and Diameter Fluctuations During Draw Resonance 194

5.7 Transient States of the Draw Resonance Phenomena 196

5.8 Spinline Tension as a Function of Draw Ratio 197

5.9 Resonance Periods for Various Process Variables 199

CHAPTER I

INTRODUCTION

Elongation is one of the most basic deformations that a material experiences. Elongational flow occurs in many polymer processing operations. In fiber spinning and sheet forming, which are two major polymer processing operations, elongational flow is an indispensible part of the forming process. However, it is only very recently that elongational flow received particular scientific attention. In fact, most of the earlier rheological studies were devoted to shearing flows, and the viscoelastic fluid theories developed were all tested in a shear flow. Thus the study of elongational flow is not only significant to major polymer processing industries but also of academic interest to the field of rheology.

In this dissertation, uniaxial elongation is studied with particular attention to fiber formation. Fibers are manufactured by stretching polymeric materials into thin filaments. There are some fundamental problems associated with it, since one cannot easily form fibers from all polymer melts nor from all polymer solutions. A fluid must have necessary characteristics if it is to be stretched out into continuous filaments of small diameter. We shall refer to this ability as the spinnability of the fluid.

The problem of spinnability is one of the most important

aspects of fiber formation. It is known that the spinnability depends not only on the physical properties of the liquid but also on the conditions of the experiment.

In the production of commercial fibers, polymer fluids are continuously extruded through a set of small circular holes called a spinneret and drawn down by a take up device. In this continuous process, various kinds of instabilities can occur and always limit the production rate. In the early 1930's, when Du Pont's melt spinning method was developed [12,17], Carothers and Van Natta [18] were concerned with the spinnability of aliphatic polyesters with different molecular weights. They reported that the melts were spinnable only in the moderately high molecular weight range. If a material is spinnable, the rheological problem of the process is the dependence of the spinline stress and fiber diameter upon the take up velocities. One must also be concerned with the stability of the process because under certain conditions it is found that the fiber taken up contains non-uniform diameter. This may be caused by temperature fluctuations, forced oscillations, or inherent instability in the system called "draw resonance." The draw resonance gives most severe diameter variation and has received particular attention.

In the investigation of elongational flow, many people turned their attention directly toward melt spinning (isothermal). In this process the kinematics cannot be controlled. For the study of viscoelastic fluids, however,

the control of the kinematics is essential. Thus study of the uniaxial elongation under controlled kinematics (preferably constant stretch rate) must be pursued first.

In this light, two types of problems are considered sequentially in this dissertation. The first is the fundamental problem of uniaxial deformation of a fluid filament at constant rate. Both homogeneous and nonhomogeneous deformations are analyzed. This provides basic understandings on an elongational flow and the criteria of spinnability. The other is the more practical problem of the spinline rheology in a continuous melt spinning process. This problem can be thought of as a direct application of the elongational rheology considered earlier. Discussion of both stable and unstable spinline dynamics is presented.

CHAPTER II

BACKGROUND

A. Mathematical Statements of the Principles of Conservation

When forces act upon a material the responses of the body have to satisfy the principle of momentum conservation. In a continuum this principle can be expressed as a force balance at a point in the body as follows.

$$\rho \frac{D\underline{v}}{Dt} = \nabla \cdot \underline{\sigma} + \rho \underline{f} \tag{2.1}$$

This is a continuum statement of Newtonian mechanics known as Cauchy's law of motion. The first term represents acceleration or inertia, the second term is stress divergence, and the third represents the external body force. The total stress tensor $\underline{\sigma}$ is usually divided into two parts for convenience:

$$\underline{\sigma} = - p\underline{I} + \underline{\tau} \tag{2.2}$$

where p is an isotropic pressure and $\underline{\tau}$ is the extra stress tensor associated with deformation. When a fluid is at static condition ($\underline{\tau} = \underline{0}$) p is identified as the hydrodynamic pressure. In a dynamic situation p should be considered as a scalar value to be determined by boundary conditions. In addition to the linear momentum equation (Eq. (2.1)), the body is subjected to the angular momentum balance. This causes the stress tensor to be symmetric:

$$\sigma_{ij} = \sigma_{ji} \tag{2.3}$$

The body must also satisfy the principle of mass conservation to be a continuous body. For an incompressible material this principle known as "continuity equation" takes the following form:

$$\nabla \cdot \underset{\sim}{v} = 0 \tag{2.4}$$

This states that the net flux of mass at a point in a continuum has to be zero to be continuous.

The system is also subjected to the additional requirement of the principle of energy conservation:

$$\rho C_p \frac{DT}{Dt} = -\nabla \cdot \underset{\sim}{q} + (\underset{\sim}{\tau} \cdot \nabla \underset{\sim}{v}) \tag{2.5}$$

Where ρ is the fluid density, C_p is the heat capacity per unit mass. This is a scalar equation of energy balance stating that the internal energy increase is balanced by negative divergence of heat flux $\underset{\sim}{q}$ and the frictional dissipation term.

B. Constitutive Equations

When a material is exposed to external forces, the stresses of the material respond to it according to the force balance equation (Eq. (2.1)). However the internal response of a material to the stresses differs from material to material. The constitutive equation describes the material's responses to the imposed stresses.

Low molecular weight organic compounds generally respond to stresses by flowing. And the stress is proportional to instantaneous deformation rate. This is the Newtonian fluid described by

$$\underline{\tau} = 2\eta\,\underline{d} \tag{2.6a}$$

where

$$\underline{d} = \frac{1}{2}\left[(\nabla\underline{v}) + (\nabla\underline{v})^{T}\right] \tag{2.6b}$$

is the deformation rate tensor and η is the shear viscosity. The well known Navier-Stokes equation can be obtained by substituting Eq. (2.6) with Eq. (2.2) into Eq. (2.1).

It is well known that polymeric materials show a wide variety of responses; notably stress relaxation, recoil, die swell, non-Newtonian viscosity, and normal stresses in simple shear flow. They exhibit a combined behavior of the properties of elastic solids and of Newtonian fluids and show not only viscous but also elastic responses to applied stresses. They are thus called viscoelastic fluids. Whether a viscoelastic material behaves as a viscous liquid or an elastic solid depends upon the time scale of the experiment. If the deformation is greater than the relaxation rate of the material, the material would behave more like an elastic solid and if the deformation rate is slower than relaxation rate it would behave more as a viscous liquid. This rate dependent response is the most important feature of the viscoelastic fluid.

Before attempting any theoretical study of viscoelastic fluids, it is necessary to choose a rheological constitutive equation which will properly express the stress-deformation relationship within the fluid. Many rheological equations of state or constitutive equations for viscoelastic fluids have been developed. These have all been classified as either differential or integral types.

Differential Type Constitutive Equations

The historical development of the differential type constitutive equations is based upon Maxwell's equation [79,115]

$$\tau + \lambda \frac{d\tau}{dt} = G\lambda \frac{d\varepsilon}{dt} , \quad G\lambda = \eta \tag{2.7}$$

where τ is the stress, ε is the strain, G is the elastic modulus and λ denotes the relaxation time. This is the simplest viscoelastic fluid model in one dimensional linear form and is often represented by the mechanical analog of a spring and dashpot in series. We note that as deformation is ceased ($d\varepsilon/dt = 0$), the stress relaxes exponentially.

$$\tau(t) = \tau(0)e^{-t/\lambda} \tag{2.8}$$

Note that the above form gives a definition of relaxation time λ.

The first generalization of Eq. (2.7) independent of coordinate system (the principle of invariance) and also

valid for large deformation was given by Zaremba [159]. Zaremba argued that the constitutive equation of a material should be framed in a coordinate system embedded in the material; that is, from the point of view of an observer attached to material points. However, human observers are usually in a stationary coordinate system fixed in a space, and so it is necessary to transform tensors from a convected to a stationary coordinate system. Tensor transformations into another coordinate system are not unique. There exist different ways to transform which include covariant and contravariant transformations.

As the constitutive equation relates stresses to deformation, it should be independent of translation or rigid rotation of a material. Thus Zaremba [159] considers a convected coordinate system which translates and rotates with a material point. This analysis was later repeated by Hencky [59] and De Witt [31]. Zaremba's theory predicts both non-Newtonian viscosity and normal stresses in simple shear but the predictions are only qualitative. Oldroyd [103,104] considered a coordinate system which translates, rotates, and deforms with the fluid as the convective coordinate system. In succeeding years, other generalizations were developed by Noll [100], White and Metzner [150], Williams and Bird [153], and Spriggs and Bird [126,127].

When one tries to apply these constitutive equations for various flow problems, one encounters a number of difficulties. First, the stress can not be expressed

explicitly except for simplest flows. Secondly, they contain too many material constants to be used in practical problems. The expression developed by White and Metzner [150] is the simplest but still describes many important features of the non-linear viscoelasticity (behavior at large deformations). This is written as

$$\underset{\sim}{\tau} + \lambda \frac{\delta \underset{\sim}{\tau}}{\delta t} = 2\eta \underset{\sim}{d} \quad , \quad \eta = G\lambda \tag{2.9a}$$

where

$$\frac{\delta \underset{\sim}{\tau}}{\delta t} = \frac{\partial \underset{\sim}{\tau}}{\partial t} + \underset{\sim}{v} \cdot \nabla \underset{\sim}{\tau} - \nabla \underset{\sim}{v} \cdot \underset{\sim}{\tau} - \underset{\sim}{\tau} \cdot (\nabla \underset{\sim}{v})^T \tag{2.9b}$$

is the Oldroyd contravariant convective derivative. The last two terms arise from the differentiation of a metric tensor relating a convected coordinate (which undergoes translation, rotation, and deformation with the material) and stationary coordinate. White and Metzner [150] proposed this form with the relaxation time λ a function of second invariant of $\underset{\sim}{d}$ ($\mathrm{II}_d = \mathrm{tr}\ \underset{\sim}{d}^2$). We note that when λ goes to zero, we obtain the Newtonian fluid model (Eq. (2.6)).

Integral Type Constitutive Equations

Linear theory. Integral theories are based upon Boltzmann's [13] superposition principle of responses to a series of infinitesimal strains. Boltzmann first developed a constitutive equation which has "fading memory" function. This may be written in one dimensional form:

$$\tau(t) = \sum_j G(t - t_j)\Delta\epsilon_j = \int_{-\infty}^{t} G(t - s)\frac{d\epsilon}{dt}ds \qquad (2.10)$$

Here, $G(t)$ is a fading memory function of time, ϵ is a strain and s is time. The stress is supposed to depend not only on the instantaneous deformation rate but also on previous deformation weighted by a fading memory function $G(t - s)$. The above relation can be written as

$$\tau(t) = \int_{-\infty}^{t} \phi(t - s)\epsilon(s)ds \qquad (2.11a)$$

where

$$\phi(t) = -\frac{dG(t)}{dt} \qquad (2.11b)$$

The Maxwell equation (Eq. (2.7)) is a special case of the Boltzmann equation for which

$$G(t) = G_0 e^{-t/\lambda} \quad , \quad \phi(t) = \frac{G_0}{\lambda} e^{-t/\lambda} \qquad (2.12a,b)$$

One generalization of the Maxwell model is the summation of various relaxation modes.

$$G(t) = \sum_i G_i e^{-t/\lambda_i} \quad , \quad \phi(t) = \sum_i \frac{G_i}{\lambda_i} e^{-t/\lambda_i} \qquad (2.13a,b)$$

The relaxation spectrum $H(\lambda)$ is introduced to represent relaxation functions of a generalized Maxwell model in a continuous spectrum.

$$G(t) = \int_0^\infty \frac{H(\lambda)}{\lambda} e^{-t/\lambda} \, d\lambda = \int_{-\infty}^{\infty} H(\lambda) e^{-t/\lambda} \, d(\ln\lambda) \qquad (2.14a)$$

$$\phi(t) = \int_0^\infty \frac{H(\lambda)}{\lambda^2} e^{-t/\lambda} \, d\lambda = \int_{-\infty}^{\infty} \frac{H(\lambda)}{\lambda} e^{-t/\lambda} d(\ln\lambda) \qquad (2.14b)$$

Nonlinear theory. The one dimensional Boltzmann constitutive equation is limited to infinitesimal deformations. Besides, it does not satisfy the principle of material invariance (objectivity) because it is not a tensor form. It was necessary to extend the Boltzmann theory to be valid at large deformations and to describe many nonlinear viscoelastic behaviors. The first generalization to finite strains was considered by Oldroyd [103] and more specifically by Lodge [71]. On the basis of the statistical mechanical theory of rubber elasticity [139] and arguments by Green and Tobolsky [52] concerning the replacement of the permanent crosslinks with temporary junctions between entangling chains, Yamamoto [155,156] and Lodge [72] developed a nonlinear generalization of Boltzmann's theory. Lodge's theory is the simplest and was applied to many flow problems in his monograph [74] and succeeding papers [21,22,73].

Lodge's constitutive equation known as the "Lodge fluid" is a tensor generalization of Boltzmann's equation employing an embedded coordinate system. Consider the embedded coordinate system X^α and its metric tensor $G^{\alpha\beta}(X,s)$ which measures the distance in any curvilinear coordinate system. As deformation proceeds, the distance

between two points changes with time but not the coordinate system X^{α} because it is embedded in the material. Thus the metric tensor $G^{\alpha\beta}(X,s)$ becomes function of time and measures the strain. In a convected coordinate system the Boltzmann theory (Eq. (2.11)) may be written in tensor form as [136]

$$\pi^{\alpha\beta}(X,t) = \int_{-\infty}^{t} \phi\,(t - s)\; G^{\alpha\beta}(X,s)ds \qquad (2.15)$$

We now transform the above constitutive equation into stationary coordinate system using the contravariant transformation law:

$$\pi^{\alpha\beta} = \frac{\partial x^{\alpha}}{\partial x^{i}} \cdot \frac{\partial x^{\beta}}{\partial x^{j}}\, \tau^{ij} \qquad (2.16)$$

Then it is found that Eq. (2.15) takes the following form in a stationary coordinate system:

$$\tau^{ij}(x,t) = \int_{-\infty}^{t} \phi\,(t - s) \frac{\partial x^{i}}{\partial X^{k}} \cdot \frac{\partial x^{j}}{\partial X^{\ell}} G^{k\ell}(X)ds$$

$$= \int_{-\infty}^{t} \phi\,(t - s) C^{-1ij}(x,t,s)ds \qquad (2.17)$$

where C^{-1ij} is the Finger deformation tensor [141]. In the Cartesian coordinate system ($G^{k\ell} = \delta^{k\ell}$) the Finger strain tensor is written as

$$C^{-1ij} = \sum_{m} \frac{\partial x^i(t)}{\partial X^m(s)} \frac{\partial x^j(t)}{\partial X^m(s)} \qquad (2.18)$$

where $x^i(t)$ is the coordinate position at present time t and $X^m(s)$ is the position at past time s.

In succeeding years, there were numerous efforts to modify Eq. (2.17) to improve its agreement with experiments. A general constitutive theory accounting for nonlinear effects was developed by Green and Rivlin [51] presuming that the stress is an hereditary function of the deformation history. An equivalent but more elegant formulation of the Green and Rivlin concepts has been given by Coleman and Noll [30,101]. This is expressed as a functional of strain history

$$\underset{\sim}{\tau} = F\left[\underset{s=-\infty}{\overset{s=t}{\underset{\sim}{e}(t-s)}}\right] . \qquad (2.19)$$

Here $\underset{\sim}{e}(s)$ is a Finger type strain tensor which measures deformation from the present state to some past time. This is known as Coleman and Noll's "simple fluid" [30,101]. The Green-Rivlin-Coleman-Noll theory may be expressed by a Frechet expansion of the functional yielding a multi-integral form (which is not practically useful except in certain asymptotic cases). If the kernel functions of the multiple integrals are products of a single relaxation function and Dirac delta functions, the multi-integral theory may be simplified to a single integral theory using the Cayley-Hamilton theorem as follows:

$$\underset{\sim}{\tau}(t) = 2\int_{-\infty}^{t}[a_1(t-s,I_e,\ II_e)\underset{\sim}{e}(s)+a_2(t-s,I_e,II_e)\underset{\sim}{e}^2(s)]ds \quad (2.20)$$

Here relaxation moduli $a_1(t-s,I_e,II_e)$ and $a_2(t-s,I_e.II_e)$ are dependent not only on time but also deformation invariants $I_e = tr\ \underset{\sim}{e}$ and $II_e = tr\ \underset{\sim}{e}^2$. Justification for such a procedure is found in the experiments of Zapas and Craft [158].

The constitutive equations of Bernstein, Kearsley, and Zapas [8], Bogue [9], Spriggs, Huppler and Bird [128], Bogue and White [11], Chen and Bogue [24], and Carreau [19] are generally equivalent to Eq. (2.20) and are expressed in the equivalent form:

$$\underset{\sim}{\tau}(t) = \int_{-\infty}^{t}[m_1(t-s)\ \underset{\sim}{C}^{-1}(t-s) - m_2(t-s)\ \underset{\sim}{C}(t-s)]ds \quad (2.21)$$

where $\underset{\sim}{C}$ is the Cauchy deformation tensor which is the transpose of the Finger deformation tensor $\underset{\sim}{C}^{-1}$. The memory functions $m_1(t-s)$, $m_2(t-s)$ are dependent on the invariants of $\underset{\sim}{C}^{-1}$, $\underset{\sim}{C}$, or $\underset{\sim}{d}$. The forms of $m_1(t-s)$ and $m_2(t-s)$ suggested by Bogue [9] and Bogue and White [11] are simple and have been found successful by Chen and Bogue[24], Chen et al. [25], and Takaki and Bogue [132] in a wide range of experiments on polyethylene and polystyrene melts. Middleman [88] has also succeeded in representing deformation behaviors of polyisobutylene. These forms are:

$$m_1(t) = (1+\frac{\epsilon}{2}) \sum_i \frac{G_i}{\lambda_{ieff}} e^{-t/\lambda_{ieff}} \qquad (2.22a)$$

$$m_2(t) = -\frac{\epsilon}{2} \sum_i \frac{G_i}{\lambda_{ieff}} e^{-t/\lambda_{ieff}} \qquad (2.22b)$$

Here ϵ is a constant representing a deviation from Weissenberg's hypothesis ($\epsilon = 0$) and specifically expresses the ratio of second normal stress difference to principal normal stress difference in a simple shear flow. G_i are the relaxation moduli and λ_{ieff} are effective relaxation times dependent upon invariants. For small strain rates the λ_{ieff} become λ_i and the relaxation functions are those of a generalized Maxwell model (Eq. (2.13)). Time averaged invariants of the rate of deformation suggested by Bogue [24] fit the overshoot phenomena in transient shear flow reasonably well [24,44,88].

$$\lambda_{ieff} = \frac{\lambda_i}{1+a\lambda_i \langle II_d^{\frac{1}{2}} \rangle} \qquad (2.23a)$$

$$\langle II_d^{\frac{1}{2}} \rangle = \frac{1}{z} \int_0^z [2 \text{ tr } \underset{\sim}{d}^2]^{\frac{1}{2}} dz \qquad (2.23b)$$

where $z = t-s$ is the back running time from the present. Similar forms of $m_1(z)$ and $m_1(z)$ are suggested by Bernstein, Kearsley, and Zapas [8] and Carreau [19] who takes different forms for the λ_{ieff} in the denominator and exponential. This introduces additional parameters and

greater flexibility in fitting data but makes the constitutive equation more complicated and thus has limited utility for various flow problems.

C. Rheological Response to Imposed Kinematics

Simple Shear Flow

The most widely studied class of deformations is shearing flow. This type of flow includes simple shear flow between a cone and a plate or parallel plates, Poisuille flow in tubes, Couette flow between coaxial cylinders. The cone-plate geometry which provides a uniform shear rate in the entire sample is utilized in the Weissenberg rheogoniometer. This instrument can provide various kinds of experiments which include not only steady flow measurements but also oscillatory measurements. For this reason this instrument has been used not only to measure material parameters but also to test proposed constitutive equations.

For shear flow, the imposed kinematics can be written as

$$\underset{\sim}{v} = (v_1(x_2),0,0) \tag{2.24}$$

The rheological response of the Newtonian fluid (Eq. (2.6)) to this type of deformation is rather simple. In terms of stress field, only the shear stress arises:

$$\sigma_{12} = \sigma_{21} = \eta\dot{\gamma} \tag{2.25}$$

where $\dot{\gamma} = dv_1/dx_2$ is the shear rate and η is the shear viscosity. For a viscoelastic fluid, one obtains not only shearing stresses but also normal stresses:

$$\underset{\sim}{\sigma} = -p\underset{\sim}{I} + \begin{vmatrix} \beta_1\dot{\gamma}^2 & \eta\dot{\gamma} & 0 \\ \eta\dot{\gamma} & \beta_2\dot{\gamma}^2 & 0 \\ 0 & 0 & 0 \end{vmatrix} \tag{2.26}$$

Here, unequal normal stresses arise in the direction and perpendicular to the direction of flow. One usually defines two normal stress differences, the principal and second normal stress differences, as net stresses to avoid unknown isotropic pressure.

$$\sigma_{11}-\sigma_{22} - \Psi_1\dot{\gamma}^2 = (\beta_1-\beta_2)\dot{\gamma}^2 \tag{2.27a}$$

$$\sigma_{22}-\sigma_{33} = \Psi_2\dot{\gamma}^2 = \beta_2\dot{\gamma}^2 \tag{2.27b}$$

where Ψ_1 and Ψ_2 are principal and second normal stress difference coefficients respectively.

We may define a characteristic relaxation time $\bar{\lambda}$ by the ratio of the second to the first moment of the kernel of relaxation functions. For low deformation rates we generally have

$$\bar{\lambda}_0 = \frac{\int_0^\infty s\, G(s)ds}{\int_0^\infty G(s)ds} = \frac{\sum_i \lambda_i^2 G_i}{\sum_i \lambda_i G_i}$$

$$= \left|\frac{\Psi_1}{2\eta}\right|_{\dot{\gamma}\to 0} = \left|\frac{\sigma_{11}-\sigma_{22}}{2\sigma_{12}\dot{\gamma}}\right|_{\dot{\gamma}\to 0} \tag{2.28}$$

At higher deformation rate the characteristic relaxation time seems to have a similar significance, but we must have a specific constitutive equation. For example using Eqs. (2.21) and (2.22), we obtain:

$$\bar{\lambda}_{eff} = \frac{\sum_i \lambda_{ieff}^2 G_i}{\sum_i \lambda_{ieff} G_i} = \frac{\sigma_{11}-\sigma_{22}}{2\sigma_{12}\dot{\gamma}} \qquad (2.29)$$

Values of material parameters η, Ψ_1, and Ψ_2 for some of the constitutive equations discussed earlier are summarized in Table I together with elongational viscosities which will be discussed later (page 22). Generally, the three material parameters η, Ψ_1, and Ψ_2 are decreasing functions of shear rate which have limiting values at very low shear rates. The character of the $\eta(\dot{\gamma})$ function for polymer solutions and melts is well known and have been reviewed by several authors [11, 115, 128]. Less rheological data is available for Ψ_1 and Ψ_2 but it is now known that Ψ_1 is positive and Ψ_2 is negative and the numerical value of Ψ_2 is about 10 to 30% of Ψ_1 [16,69,90,102, 133].

Simple Uniaxial Elongation

Theoretical study. As early as 1906, Trouton [140] showed that the elongational viscosity of Newtonian fluids is three times the shear viscostiy, both theoretically and experimentally. This fact is equivalent to Young's modulus for an incompressible solid being three times shear

TABLE I

PREDICTIONS OF CONSTITUTIVE EQUATIONS AT STEADY STATE

CONSTITITIVE EQUATIONS	SIMPLE SHEAR η(1)	Ψ_1(2)	Ψ_2(3)	SIMPLE ELONGATION χ(4)
Newtonian Fluid Eq. (2.6)	η	0	0	3η
Convected Maxwell (White-Metzner) Model, Eq. (2.9)	$\eta(\dot{\gamma})$	$2\eta\lambda(\dot{\gamma})$	0	$\frac{3\eta}{(1-2\lambda E)(1+\lambda E)}$, $\lambda E<\frac{1}{2}$
Single Integral Lodge Model Eq. (2.17)	$\sum_i G_i\lambda_i$	$2\sum_i G_i\lambda_i^2$	0	$\sum_i \frac{3G_i\lambda_i}{(1-2\lambda_i E)(1+\lambda_i E)}$, $\lambda_{max}E<\frac{1}{2}$
Bogue White Model, Eqs. (2.21)-(2.23)	$\sum_i G_i\lambda_{ieff}$	$2\sum_i G_i\lambda_{ieff}^2$	$\frac{\varepsilon}{2}\Psi_1$	$(1+\frac{\varepsilon}{2})\sum_i \frac{3G_i\lambda_{ieff}}{(1-2\lambda_{ieff}E)(1+\lambda_{ieff}E)} - \frac{\varepsilon}{2}\sum_i \frac{3G_i\lambda_{ieff}}{(1+2\lambda_{ieff}E)(1-\lambda_{ieff}E)}$,
	$\lambda_{ieff} = (\lambda_i)/(1+a\lambda_i\dot{\gamma})$			$\lambda_{ieff} = (\lambda_i)/(1+\sqrt{3}a\lambda_i E)$, $(\lambda_{eff})_{max}E<\frac{1}{2}$ $\lambda_{max}E<1/(2(1-\sqrt{3}a))$

(1) η : shear viscosity

(2) Ψ_1: principal normal stress difference coefficient

(3) Ψ_2: second normal stress difference coefficient

(4) χ : elongational viscosity

modulus. The first discussions of elongational viscosity of polymer fluids were those of Nitschmann and Schrade [99] who suggested that elongational viscosity increases with elongation rate. In 1957, Yamamoto [156] first derived the elongational viscosity for nonlinear viscoelastic fluids. He showed that, depending on the constitutive equation, the elongational viscosity first increases with elongation rate and then either goes to infinity at finite elongation rate or decreases after exhibiting a maximum. The infinite resistance to elongation at finite elongation rate was also shown by Lodge [74] and others in the mid 1960's. However, it was pointed out by Denn and Marrucci [34] that the infinite stress represents a never achievable steady state and one should rather study the stress buildup in an elongation experiment.

For a fluid filament in uniaxial elongation, the imposed kinematics can be given by

$$\underset{\sim}{v} = (v_1(x_1),\ v_2(x_2),\ v_3(x_3)) \tag{2.30}$$

with $v_2(x_2) = v_3(x_3)$. One notes that the individual velocities vary only with their own directions. The rate of deformation tensor takes the following form after applying continuity equation:

$$\underset{\sim}{d} = \tfrac{1}{2}\left|\frac{\partial v_j}{\partial x_j} + \frac{\partial v_1}{\partial x_1}\right| = \begin{vmatrix} E & 0 & 0 \\ 0 & -E/2 & 0 \\ 0 & 0 & -E/2 \end{vmatrix} \tag{2.31}$$

where $E = \partial v_1 / \partial x_1$ is the elongation rate. If elongation rate is constant with time, the cylinder deforms according to

$$L(t) = L(0)e^{Et} \quad , \quad R(t) = R(0)e^{-\frac{E}{2}t} \qquad (2.32a,b)$$

where L is the filament length and R is its radius.

We note that the stress field in a stretching filament may be expressed as

$$\underset{\sim}{\sigma} = -p\underset{\sim}{I} + \begin{vmatrix} \tau_{11} & 0 & 0 \\ 0 & \tau_{22} & 0 \\ 0 & 0 & \tau_{33} \end{vmatrix} \qquad (2.33)$$

The boundary conditions to be satisfied are

$$\sigma_{11} = F/(\pi R^2) \quad , \sigma_{22} = \sigma_{33} = -\gamma/R \qquad (2.34a,b)$$

where γ is the surface tension and F is the applied force. If we eliminate the pressure term this leads to

$$\underset{\sim}{\sigma} = -\frac{\gamma}{R} + \begin{vmatrix} \tau_{11}-\tau_{22} & 0 & 0 \\ 0 & 0 & 0 \\ 0 & 0 & 0 \end{vmatrix} \qquad (2.35)$$

We note that the stress field subjected to this type of deformation is very simple, having dynamic stress (which is associated with deformation) only in the axial direction. Therefore, when considering the force balance, we only need to consider the axial component which makes the problem one dimensional.

For a Newtonian fluid (Eq. (2.6)), the total stress responding to this deformation becomes

$$\sigma_{11} = -\frac{\gamma}{R} + \tau_{11} - \tau_{22} = -\frac{\gamma}{R} + 3\eta E \qquad (2.36)$$

The elongational viscosity χ becomes

$$\chi = \sigma_{11}/E = 3\eta \qquad (2.37)$$

if we neglect surface tension. This is due to Trouton [140] and the elongational viscosity of 3η is often referred to as Trouton viscosity.

The rheological response of the convected Maxwell fluid (White-Metzner form with constant λ, Eq. (2.9)) has been treated by Denn and Marrucci [34]. The transient stress when stretched at constant rate E is given by

$$\sigma_{11}(t) = -\frac{\gamma}{R} + \tau_{11} - \tau_{22} = -\frac{\gamma}{R} + \frac{2\eta E}{1-2\lambda E}\left[1-e^{-(1-2\lambda E)t/\lambda}\right]$$

$$+ \frac{\eta E}{1+\lambda E}\left[1-e^{-(1+\lambda E)t/\lambda}\right] \qquad (2.38)$$

The first term (after γ/R) arises from τ_{11} and the second from τ_{22}. At the very least, τ_{11} is two times τ_{22} (Newtonian fluids) and when λE is more than $\frac{1}{2}$, τ_{22} becomes negligible compared to τ_{11} as time proceeds. For small E the response of Eq. (2.38) is the same as that of a linear Maxwell model yielding

$$\sigma_{11}(t) = -\frac{\gamma}{R} + 3\eta E[1-e^{-t/\lambda}] \quad (\lambda E \ll 1) \tag{2.39}$$

When λE becomes equal to $\frac{1}{2}$, it becomes

$$\lim_{\lambda E \to \frac{1}{2}} \sigma_{11}(t) = -\frac{\gamma}{R} + 2\eta E \frac{t}{\lambda} + \frac{2}{3}\eta E(1-e^{-3t/2\lambda}) \tag{2.40}$$

where in essence $\sigma_{11}(t)$ increases linearly with time. When λE is greater than $\frac{1}{2}$, $\sigma_{11}(t)$ increases rapidly in an unbounded manner at finite time. And when $\lambda E \gg 1$ we have the asymptote of rubber elasticity [139].

$$\sigma_{11}(t) = -\frac{\gamma}{R} + G(e^{2Et} - e^{-Et}) \quad (\lambda E \gg 1) \tag{2.41}$$

We note that for increasing E and time, the τ_{22} term becomes negligible compared to τ_{11}. When stretch rate is slower than $1/2\lambda$, we obtain steady state stress and the elongational viscosity becomes

$$\chi = \frac{3\eta}{(1-2\lambda E)(1+\lambda E)} \quad (\lambda E < \tfrac{1}{2}) \tag{2.42}$$

One notices that while the model predicts a constant shear viscosity $\eta = G\lambda$, χ is a function of E. It may be seen that at small λE, χ is approximately 3η (Trouton viscosity) but as λE increases, χ also increases and goes to infinity at λE equal to $\frac{1}{2}$.

For the Lodge fluid, Chang and Lodge [21] obtained the transient stress response when constant stretch rate is imposed.

$$\sigma_{11}(t) = -\frac{\gamma}{R} + \sum_i \frac{G_i}{1-2\lambda_i E}\left[1-2\lambda_i E e^{-(1-2\lambda_i E)t/\lambda_i}\right]$$

$$-\sum_i \frac{G_i}{1+\lambda_i E}\left[1+\lambda_i E e^{-(1+\lambda_i E)t/\lambda_i}\right] \qquad (2.43)$$

This is the generalized form of Eq. (2.38) using the relaxation function in series. The result for a single relaxation time (i=1) of the the above expression should be the same as Eq. (2.38). Their different appearances are due to

$$\tau_{11}^{(L)} = \tau_{11}^{(M)} + G\,, \quad \tau_{22}^{(L)} = \tau_{22}^{(M)} + G \qquad (2.44a,b)$$

where superscript L and M denote Lodge and Maxwell fluids, respectively. But both become the same when we take $\tau_{11} - \tau_{22} = \sigma_{11}$ as a total stress. General features of the response are very similar. For small E linear viscoelastic response is predicted and only when E is slower than $\frac{1}{2}\lambda_m^{-1}$, where λ_m is the maximum relaxation time, does stress reach the steady state. The elongational viscosity at this condition is obtained as

$$\chi = \sum_i \frac{3G_i\lambda_i}{(1-2\lambda_i E)(1+\lambda_i E)} \qquad (\lambda_m E < \tfrac{1}{2}) \qquad (2.45)$$

The elongational viscosity and the transient stress have been worked out for several different constitutive equations with a variety of results. Many constitutive equations predict that χ goes to infinity at finite E,

while others show χ exhibiting maxima and some yield almost constant χ. This elongational function has been reviewed, for example, by Dealy [32]. White [49] derived this χ function for the Bogue-White model as

$$\chi = (1+\frac{\xi}{2})\sum_i \frac{3G_i\lambda_{ieff}}{(1-2\lambda_{ieff}\dot{E})(1+\lambda_{ieff}\dot{E})}$$

$$-\frac{\xi}{2}\sum_i \frac{3G_i\lambda_{ieff}}{(1+2\lambda_{ieff}\dot{E})(1-\lambda_{ieff}\dot{E})} \quad (\lambda_{meff}\dot{E} < \tfrac{1}{2}) \quad (2.46)$$

The elongational viscosities for the various constitutive equations were summarized in Table I (page 19).

Experimental study. The earliest scientific experiments on elongational flow are due to Trouton [140] who studied tensile stretching of Newtonian filiments as well as continuous gravity spinning. Trouton showed for pitch, tar, and wax that the elongational viscosity is three times the shear viscosity as discussed before. For polymeric materials the first study was by Nitschmann and Schrade [99] who showed by nitrocellulose that the elongational viscosity of the viscoelastic fluid increases with elongation rate and this phenomena stabilizes the filaments under extension. Then after the mid 1960's there were several investigators who measured the elongational viscosity of polymer melts under various experimental conditions. It was a difficult task to measure the elongational viscosity of polymer melts under controlled kinematics.

Researchers beginning with Ballman [6], Cogswell [26, 27,28], Meissner [82,83,84], and Vinogradov and his co-workers [143,144,145] developed extensional viscometers to achieve ideal extensional flow of constant extension rate or constant stress. There are also other methods of measuring the extensional properties. A weight dropping experiment developed by Hagler in this department approximates a constant force condition and has been used by Chen, Hagler, Abbott, Bogue, and White [25] and Takaki and Bogue [132].

The condition of constant deformation rate is ideal to study the viscoelastic fluid because stress depends upon not only instantaneous deformation rate but also on deformation history. Under the conditions of constant elongation rate, Ballman [6] first observed the transient stress buildup for a polystyrene melt. Although the shear viscosity decreased with shear rate, the elongational viscosity remained constant (around three times the zero shear viscosity) at relatively low deformation rates. Meissner [82,83, 84] studied the elongational deformation of low density and high density polyethylenes at constant elongation rate using his novel rotational clamp tensile machine. He observed slow buildup of stress to a steady state value at low elongation rate. At high stretch rates, the low density polyethylene showed unbounded stress growth but high density polyethylene did not. Vinogradov et al. [144,145], Stevenson [129], and Everage and Ballman [39] observed similar behavior in polyisobutylene, polyisoprene, and polystyrene.

Generally, nonlinear viscoelastic constitutive equations are tested using shear experiments as described before. Essentially, the idea of the effective relaxation time is based upon the experimental facts of non-Newtonian viscosity. The question now arises whether such constitutive equations can predict the behaviors in elongational flow. Chang and Lodge [21] however, could apply the Lodge fluid (Eq. (2.43)) to describe the Meissner's transient stress data. They could describe the unbounded stress growth data at least semi-quantitatively using relaxation parameters obtained by fitting a small E experiment.

In more definitive tests, the relaxation parameters should be obtained in a separate experiment. Chen, Hagler, Abbott, Bogue, and White [25] and Takaki and Bogue [132] took this attitude to describe the transient stress. Based upon the material parameters obtained in shear experiments, they could describe the transient stress by using the Bogue-White model, Eqs. (2.21)-(2.23) with ξ taken as zero.

Onogi, Matsumoto, and Kamei [62,106] could apply the time-temperature superposition principle for ultimate properties of narrow molecular weight polystyrene melts. The curves of ultimate stress versus strain rate, as well as ultimate strain versus strain rate taken at various temperatures could be superposed into respective master curves by horizontal shifting. The shift factors are of the WLF type [41,154].

D. Filament Stability

General

The ability of a liquid to become a long continuous thread is called spinnability. It is known that spinnability is not inherent to polymeric materials but also exists in other viscous materials including honey, molten glass, and oils [165]. Maximum thread length, a measure of spinnability, as a function of viscosity and extension speed has been investigated by Ziabicki [165]. The spinnability is limited by three mechanisms of instability: capillarity, ductile failure, and fracture (see Fig. 2.1).

The poor spinnability of low viscosity liquids is due to capillary instability. This surface tension induced instability does not require tensile force and it is a configurational or energetical instability. The result that the thread length increases with the product of viscosity and extension speed for low viscosity liquid can be explained by the capillary instability theory of Rayleigh [114] and Weber [146].

For more viscous liquids such as polymer melts, the capillary instability becomes less important and ductile instability caused by tensile stress concentration becomes the dominant instability. This mechanism of necking failure was apparently investigated in metals by Nadai and Manjoine [93] and Orowan [107]. For polymeric materials, Nitschmann and Schrade [99] called attention to ductile instability

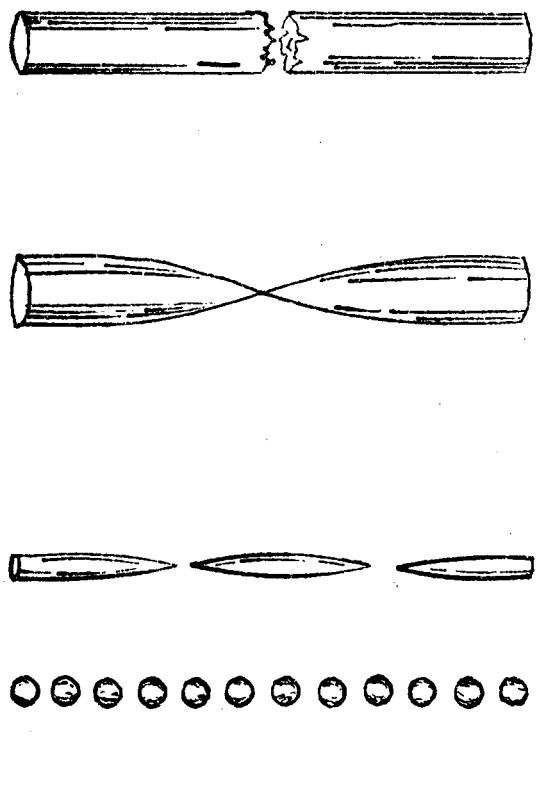


FIGURE 2.1 Mechanisms of filament instability.

and noted that an elongational viscosity which increases with extension rate would lead to stability.

The other mechanism would be cohesive fracture of highly viscous materials at high extension rate. A theoretical treatment of this concept involving initiation by defects was given by Griffith [54] and later modified by Orowan [107]. Cohesive fracture is associated with stored elastic energy and occurs at the moment of deformation, when the elastic energy attains some critical value [115]. The idea seems to have first been presented in general form by Huber in 1904. Reiner, Freudenthal, and Weissenberg [115] modified Huber's idea to give a general view of cohesive fracture of viscoelastic media.

If we consider various polymeric materials and a very wide range of molecular weights, it is apparent that all three mechanisms: a) capillary instability, b) ductile instability, and c) cohesive fracture are important and thus it is necessary to develop a consistent theory which includes all the instabilities. White and Tokita [148,152] and Cogswell and Hubbard [29] have given general discussions of these various types of failure phenomena during polymer processing.

Capillary Instability

Surface tension. Liquid filaments of small diameter possess large external surfaces relative to their volume. Surface tension tends to play a major role in the behavior

of such filaments especially if the liquid possesses a low viscosity and a sharp curvature.

From energetic or mechanical considerations, it can be shown that the elevation of pressure P_γ within a curved surface is described in terms of surface tension γ and radii of curvature R_1 and R_2 [3,14,70,80]

$$P_\gamma = \gamma\left(\frac{1}{R_1} + \frac{1}{R_2}\right) \tag{2.47}$$

Therefore whenever a free surface exists in the interface, the following force balance equation must be satisfied at the surface.

$$\underset{\sim}{\sigma}\cdot\underset{\sim}{n} = -\gamma\left(\frac{1}{R_1} + \frac{1}{R_2}\right)\underset{\sim}{n} \tag{2.48}$$

where $\underset{\sim}{\sigma}$ is the stress tensor and $\underset{\sim}{n}$ is the unit outward normal vector. For a uniform filament of radius R, the surface tension pressure becomes

$$P_\gamma = \gamma/R \tag{2.49}$$

since the radius of curvature along the filament axis is infinite. As we can see from the above expression, the pressure becomes very high for very small diameter filaments.

Surface tension plays a major role in classical fluid statics as described by Clerk Maxwell [80], Boys [14], Adam [3], and Levich [70]. Recently Gains [45] presented values of surface tension of various polymer melts.

Generally organic fluids have values in the range of 20 to 30 dynes/cm independent of molecular weight and decreasing with increasing temperature.

Break up of a capillary column. Study of the surface tension induced instability in a long circular liquid column (a capillary column) was begun in the nineteenth century by Plateau and Rayleigh [114]. Plateau pointed out that the capillary liquid is unstable under surface tension if its length exceeds its circumference and eventually breaks up into droplets.

In 1879, Rayleigh [110,111] analyzed this problem using linear perturbation technique. His analysis, which has been the basis of most subsequent hydrodynamic instability analysis, proceeds as follows. Suppose the radius R of the liquid cylinder is disturbed so that it becomes

$$R = \bar{R} + \xi = \bar{R} + \hat{\xi}(0)\ \exp\{\alpha t + ikz\} \qquad (2.50)$$

The disturbance is assumed periodic along the axis and initially small compared to the radius of the cylinder $\bar{R}$. The column is stable or unstable depending on whether the time coefficient α is negative or positive. Rayleigh showed that all waves with a wavelength greater than the cylinder's circumference have a positive growth rate α and amplify with time. According to "the mode of maximum instability" the wave with the largest growth rate α^* becomes a dominant wave on the cylinder surface and

ultimately breaks it into droplets. Analytically the stability problem reduces to obtaining the relationship between α and k, which is called the characteristic equation. The wave number k^* which gives the largest positive growth rate α^* is the mode of instability.

Rayleigh [112] derived an analytical solution on the stability of viscous liquid in a gaseous media. In terms of the most unstable mode of instability, he noted that in the asymptote of negligible viscosity the column will become droplets of radius approximately $2R$, and if the cylinder is highly viscous liquid, the liquid column would break up at a much longer period. A further study has been made by Tomotika [137] for a viscous liquid cylinder in a second viscous liquid media. There have been several attempts at extension of Rayleigh's analysis including nonlinearity [47,98,157].

In 1936, Tomotika [138] theoretically investigated the capillary instability problem of a viscous liquid thread which is extended by the motion of surrounding viscous fluid. His analysis explains Taylor's experiment [134] that an extending thread does not immediately break up into drops, but remains cylindrical until it has extended sufficiently. Tomotika's work implies that disturbances with very short wavelengths which are initially stable become unstable by the extending motion and eventually achieve very high magnification. However, his analysis does not include

ductile instability because the area is not appropriately integrated in the force balance equation.

According to Rayleigh [112], the characteristic equation for the instability of viscous cylinder in a gaseous media is given by

$$\alpha^2 + \frac{2\eta k^2}{\rho I_0(kR)}\left[I_1'(kR) - \frac{2k\ell I_1(kR)}{(k^2+\ell^2)I_1(\ell R)}\right]\alpha - \frac{\gamma k(1-k^2R^2)}{\rho R^2}\frac{I_1(kR)(\ell^2-k^2)}{I_0(kR)(\ell^2+k^2)} = 0 \qquad (2.51)$$

where γ and ρ are the liquid's surface tension and density, I_0, I_1, and I_1' are modified Bessel functions and its derivative and ℓ is defined by $\ell^2 = k^2 + \rho\alpha/\eta$. It has been shown that the value of kR which gives the maximum growth rate is very close to zero. The Bessel fucntions in the above equation can be approximated by their limiting values, which allows the characteristic equation to be simplified to

$$\alpha^2 + \frac{3\eta k^2}{\rho}\alpha - \frac{\gamma k^2(1-k^2R^2)}{2\rho R} = 0 \qquad (2.52)$$

One can solve for α as a function of k and find the maximum growth rate α^* and the corresponding wave number k^*. The results are

$$\alpha^* = \sqrt{\frac{\gamma}{2\rho R^3}} \Big/ \left(2+3\eta\sqrt{\frac{2}{\rho R\gamma}}\right) \qquad (2.53a)$$

and

$$k^* = 1 \Big/ \sqrt{\eta R \sqrt{\frac{R}{2\rho\gamma}} + 2R^2} \qquad (2.53b)$$

The asymptotes of zero and infinite viscosity are

$$\alpha^* \to \frac{1}{2R}\sqrt{\frac{\gamma}{2\rho R}} \quad , \quad k^* \to 0.7\,\frac{1}{R} \qquad (\frac{\rho}{\eta} \to \infty) \qquad (2.54a)$$

$$\alpha^* \to \frac{\gamma}{6\eta R} \to 0 \quad , \quad k^* \to 0 \qquad (\frac{\rho}{\eta} \to 0) \qquad (2.54b)$$

We see that as viscosity increases the wave number which gives the maximum growth rate decreases and the wavelength $(2\pi/k^*)$ increases implying that the filament will break up at longer period. Furthermore, the rate of disturbance growth is reduced by the higher viscosity and longer times will be required for the filament to break up.

The capillary instability theory has been successfully applied to liquid injection problems determining jet break up length. The application to jets was also realized by Rayleigh [113] and formulated by Weber [14]. Weber used a method of obtaining asymptotic solution of small kR valid for viscous liquid and applied it to jet break up length by simply multiplying jet velocity and break up time. As a criterion for the break up time, Weber uses the time required for the disturbance to become equal in size to jet radius:

$$\hat{\xi}(t_B) = \hat{\xi}(0)e^{\alpha^* t_B} = \bar{R} \qquad (2.55)$$

Then the break up length $L(t_B)$ is obtained by simply multiplying jet velocity V and break up time t_B :

$$L(t_B) = Vt_B = \frac{V}{\alpha^*} \ln\frac{R}{\xi(0)} \qquad (2.56)$$

Substitution of Eq. (2.53a) into Eq. (2.55) gives the well known Weber result for the break up length of liquid jets.

$$\frac{L}{2R} = \ln\frac{R}{\xi(0)}\left[\sqrt{\frac{2\rho V^2 R}{\gamma}} + \frac{3\eta V}{\gamma}\right] = \ln\frac{R}{\xi(0)}\left[\sqrt{N_{Web}} + 3\frac{N_{Web}}{N_{Re}}\right] \qquad (2.57)$$

where $N_{Web} = 2\rho V^2 R/\gamma$ is the Weber number, $N_{Re} = 2RV\rho/\eta$ is the Reynolds number.

The agreement between experimental results and theoretical solutions have been good as long as the jet velocity is low [67,113]. However, when the jet velocity is considerably increased, the resistance of air plays an important role [40].

Middleman [86] considered the stability of viscoelastic jets using a linear Maxwell model. His analysis predicts that the effect of viscoelasticity is to destabilize the jet. Kroesser and Middleman [67] report that at the same levels of Weber number and Reynolds number the break up length decreases with elasticity. Goldin et al. [48] reduced the stability problem of a linear viscoelastic fluid to an analogous form of the Newtonian fluid by application of Laplace transformation techniques. Their analysis also shows that linear viscoelastic fluids exhibit more rapid growth of disturbance waves than Newtonian fluids

of the same zero shear viscosity.

In the experiments by Yerushelm, Shinnar, and their co-workers [48], polymer solutions show an earlier appearance of waves than Newtonian fluids; but the growth of the wave is arrested before break up and a series of droplets connected by random lengths of thin threads is formed. They attributed the phenomena to enhanced elongational viscosity of the non-linear viscoelasticity. The threads thin down with time and eventually lead to jet break up at much later time. They also observed that the wave length increased with distance, suggesting tensile stress in the threads. Several years later, they [50] investigated the jet stability problem under externally controlled disturbances. Newtonian fluid behavior was the same as predicted by the Rayleigh-Weber theory. However, viscoelastic fluids again showed a ligament-droplet configuration which undergoes a stretching motion.

Tensile Failure of Materials

For high viscosity filaments, the surface tension induced failure will be very slow and consideration must be given to instabilities due to stretching. Extension of filaments containing defects generally gives rise to instabilities such as ductile instability or fracture.

The problem of ductile instability, i.e., growth of a neck due to stress concentration, was first considered by metallurgists investigating the ductile failure of steel and

other metals. The concept is implicit in much of the early literature [93,94] but the first specific quantitative development is due to Nadai and Manjoine [93]. They presented a theory of necking or ductile failure with experimental results for metals over very wide range of deformation rates at various temperatures. The necking theory, that is the consideration of the variation in local deformation due to a constant force along a filament of varying cross-section, was later reformulated and elaborated on by Orowan [107]. The consideration was given to Newtonian, power law, and Bingham plastic fluids. It was also implied that necking does not occur for strain hardening materials. Nitschmann and Schrade [99] considered the strain hardening effect to be an essential condition for the tensile stability.

Recently Chang and Lodge [22], using the necked model, explained the enhanced stable elongation phenomena of viscoelastic fluids. The cross-sectional areas of necked and unnecked regions were numerically calculated as a function of time when a constant force was applied. For a Newtonian fluid, the area ratio grows without limit, whereas, for a viscoelastic fluid described by the Lodge model, the area ratio levels off after an initial jump. This demonstrates the characteristic difference between Newtonian fluids and viscoelastic liquids. Due to the fact that the analysis is numerical using the particular material parameters, the solution is not general in the sense that it can not be used

for every viscoelastic fluid (which include Newtonian fluids and elastic solids as asymptotes). A careful discussion of necking in solid polymers was given by Vincent [142], and the detail stress analyses in this region described by a Von Mises Criterion have been given by Bridgman [15].

Numerous theories of cohesive fracture have been proposed through the years based upon critical stress, strains, and distortional energies. The situation is, however, complex due to the presence of microscopic defects and also the combined effect of ductile instability. Griffith [54] proposed a crack theory based upon energy considerations. Orowan [107] extended the Griffith brittle fracture theory, considering plastic deformation energy instead of surface energy. Rivlin and Thomas [116] and Greensmith et al. [53] developed a theory of tearing vulcanized rubber based upon energy considerations. A viscoelastic fluid will deform indefinitely when deformed at small rates and will fracture only with rapid deformations.

Reiner, Freudenthal, and Weissenberg [115] view this in terms of the stored strain energy and propose that we must separate the energy of deformation or stress work into dissipative and stored parts, and that only the stored strain energy contributes to failure. The concept of stored energy is closely related to the stress in the viscoelastic material as shown by Bernstein, Kearsley, and Zapas [8], so that the critical strain energy criteria might take a form of critical stress criteria.

Experimental investigation of the tensile strength and failure properties of solid polymers are very important aspects of engineering design. Smith [121,122,123] investigated the dependence of the tensile strength of vulcanized rubber upon stretch rate and temperature and correlated them in "failure envelope." The fracture of polymers was reviewed by Landel and Fedors [68] and Andrews [4].

Failure studies of polymer melts are relatively scarce. Recently Onogi, Matsumoto, and Kamei [62,106] studied the failure characteristics of narrow molecular weight polystyrene melts at various conditions. Their extensive investigation includes the effects of temperature, stretching speed, and molecular weight. They suggested the existence of various failure mechanisms and showed the validity of time-temperature superposition principle. Chen, Hagler, Abbott, Bogue, and White [25] demonstrated the characteristic difference between low and high density polyethylenes with high density polyethylene failing by ductile instability. Takaki and Bogue [132] investigated the effect of molecular weight distribution and found that the narrow molecular weight polystyrene failed with minimal stretching in the weight dropping experiment.

CHAPTER III

UNIAXIAL STRETCHING OF POLYMER MELTS

A. Experimental

Materials

In order to study the elongational properties of polymer melts, a wide variety of thermoplastics were selected. These are shown in Table II. The series of polymers were chosen as to represent a wide range of molecular weights and rheological properties.

Several of these polymers have been rheologically characterized by researchers in this department in steady shear flow and the value of zero shear viscosity and references to their work are listed in the table. As will be described later, the tensile stress could be measured only for the relatively high viscosity materials listed in the table.

Apparatus

The apparatus used in this experiment was specially designed to stretch a filament at constant rate and also permit the observation of the mode of failure. The essential idea of constant rate stretching is due to Meissner [82,83, 84] who used rotational clamps consisting of two pairs of gripping gears. The apparatus designed here consists of only one drum which wraps up the filament at a fixed position.

TABLE II

MATERIALS USED IN THE EXPERIMENTS

Material	Melt Index (MI) or Molecular Weight	Zero Shear Viscosity [poise]	Reference	Temp.
A. Low Density Polyethylene				
Union Carbide DYDT	MI>2000 (polymer wax)			86 °C
Union Carbide DNDA 0455	MI=60			110 °C
Union Carbide DADA 0917	MI=23	8×10^3 (180 °C)	Minagawa & White [91]	120 °C
Dow DYON 610 M	MI=5.0	9×10^4 (180 °C)	White & Roman [117,151]	140 °C
Dow DYON 560 E	MI=2.1	9×10^4 (160 °C)	Acierno et. al. [2]	140 °C
Tennessee Eastmen Tenite 800	MI=1.7 M_1=25,800	2.6×10^5 (160 °C)	Chen & Bogue [23,24]	160 °C
B. High Density Polyethylene				
Phillips Marlex EMB 6050	MI=5.0	7.5×10^4 (180 °C)	White & Roman [117,151]	145 °C
Tennessee Eastman Tenite 3340	MI=2.6 M_1=49,000	1.65×10^5 (160 °C)	Chen & Bogue [23,24]	150 °C
Phillips Marlex EHM 6001	MI=0.1	2.0×10^6 (180 °C)	Minagawa & White [91]	180 °C

TABLE II (continued)

Material	Melt Index (MI) or Molecular Weight	Zero Shear Viscosity [poise]	Reference	Temp.
C. Polystyrene				
Dow STYRON 678 U	M_w=240,000 M_n=80,000	1.8×10^5(180°C)	White & Roman [117,151]	200°C
Shell TC3-30	M_w=280,000 M_n=61,000	3.1×10^6(160°C)	Takaki & Bogue [131, 132]	220°C
D. Polypropylene				
Hercules PROFAX 6423	MI=6.6 M_i=2.77×10^5		Nadella [95]	180°C
Hercules PROFAX 6823	MI=0.42 M_i=4.3×10^5		Nadella [95]	180°C
E. Polymethyl Methacrylate				
Dupont Lucite 147				220°C

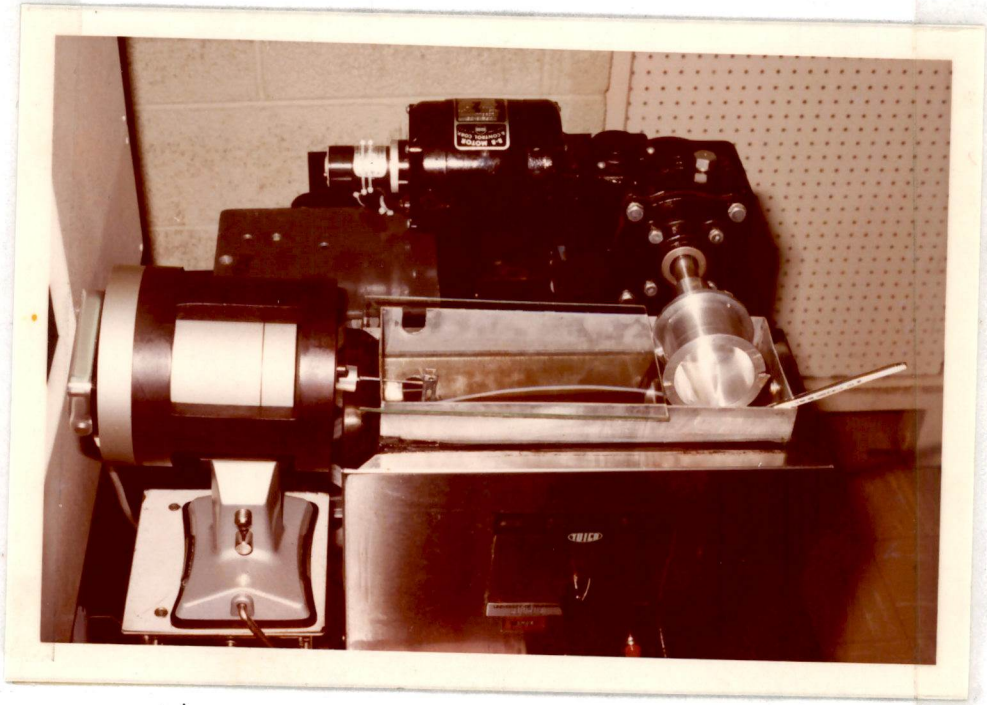
The other end of the filament is clamped stationary to a load cell laid horizontally. This design makes the system much more simplified and easy to construct. This is similar to that used for constant elongational rate experiments in the Mechanical Spectrometer [39].

The experimental set up of the apparatus is shown in Fig. 3.1. The polymer filament is supported and also thermally controlled by silicone oil (G. E. type SF-96: viscosity 100 centistokes, $\rho = 0.968$ g/cm^3 at 25°C). One end of the molten filament is clamped to the rim of the take up drum (See Fig. 3.2). The oil bath is about 30 cm long, 11 cm wide and the oil is 11 cm deep. The temperature is controlled within ±1°C by the thermostat of a Halikainen tube block heater (Model 100) which is fully insulated and enclosed in a stainless steel jacket. This unit was connected to a variac and the voltage was adjusted so that heat loss and input heat are equalized at the desired temperature. By this method the thermostat plays the role of secondary controller which guarantees the temperature within ±1°C and the actual temperature control may be better than this precision. A lid to cover up the take up roll and whole bath was prepared, but it was not useful to observe failure mode and thus was not used all the time. During a stretch, a glass cover seemed to be good enough to insulate and observe the sample failure.

The deformation length between the clamps was 21.5 cm throughout the experiments. The rotation speed of the take up drum can be continuously varied giving a wide range of



a) Overall view of the apparatus



b) Close up view of the sample clamp and the take up roll

FIGURE 3.1 Experimental set up for constant rate stretching.

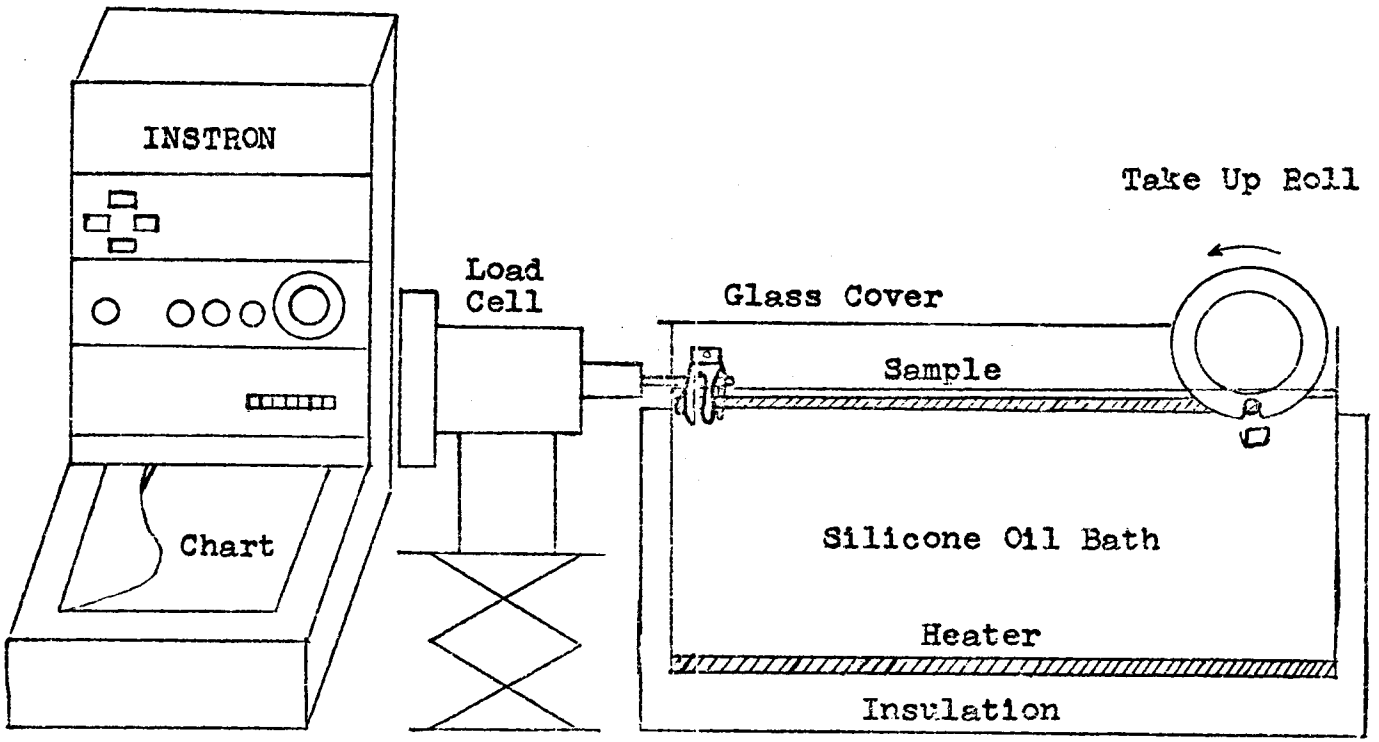


FIGURE 3.2 Schematic diagram of the experimental apparatus

possible stretch rates. Two motors were used to attain as wide a rate as possible: one (1/15 Hp B & B motor, 12 rpm max.) for low speed , and one (1/20 Hp Bodine Electric Company motor, 173 rpm max.) for high speed. With the low speed motor, stretch rates of 0.005 1/sec to 0.2 1/sec were obtained using a 6.35 cm diameter take up drum. With the high speed motor, a stretch rate as high as 1.5 1/sec was attained using the 3.18 cm diameter roll. The motor speed was carefully controlled (within 1%) by the B & B controller type ST-12 with respect to load and voltage fluctuations. The power of the motors were sufficiently larger than the load (at most 100 gw).

Uniaxial Stretching

Procedure. The polymer filaments were prepared by extrusion in the Instron capillary rheometer of barrel diameter 9.53 mm using diameter 2.11 mm (L/D = 30) die. The extrusion speed is usually at 1 inch/min and the simi-solidified filament is taken up by the same take up device used in the tensile stretching experiments. The extrusion temperature for every polymer was chosen so as to obtain semi-solidified filaments just before take up to retain the perfect cylindrical shape. The extrusion temperatures are shown in Table II, pages 42 and 43. The take up speed is approximately the same speed as extrusion speed at the die exit to avoid stretching the filament. Care was taken so as to reduce the residual

stress in the sample as much as possible.

The wound up filament of glassy polymers such as polystyrene and polymethyl methacrylate were re-melted in the oil bath in order to obtain straight filaments. The weight of the molten filament itself causes it to straighten when it is pulled up from the oil bath. For all polymers, shrinkage of filaments in the bath was unavoidable, so that calibration of the dimensions (as a taken up filament and a filament after equilibrium in the oil bath) was necessary. The wound up filaments were cut by scissors according to the calibration so as to become the desired length (23 cm total, 21.5 cm effective length) after equilibrium is attained. The diameter of the annealed filament was measured by a micrometer in the solid state. The diameter differs from polymer to polymer but is in the range of 2 mm to 3 mm.

Before each measurement, the load cell was calibrated by hanging a 10 gram weight with similar set up as in the actual measurements. Experiments were carried out at 160°C for (low and high density) polyethylenes and polystyrenes, and at 180°C for polypropylene and polymethyl methacrylate. Increasing the temperature above 200°C caused rapid evaporation of the silicone oil filling the atmosphere with obnoxious fumes.

Temperature and residual stress equilibrium were usually attained in 3 to 10 minutes depending upon the polymer. The filament was stretched at constant rate and the force

response was recorded in the Instron chart. The force was detected by 2000 gram Instron load cell utilizing mainly the highest sensitivity range (10 gram full scale). The chart speed could be varied instantaneously from 1000 mm/min at the beginning of an experiment to slower speed (as slow as 20 mm/min) at a later stage. The duration of stretching a filament ranged from a few seconds at stretch rate $E = 1.5$ 1/sec to about 20 minutes at $E = 0.005$ 1/sec . This range was chosen as wide as possible and attempts to extend this range would probably be experimentally difficult.

Data processing. The deformation rate E is defined by

$$E = \frac{1}{L}\frac{dL}{dt} = \frac{V_L}{L} \tag{3.1}$$

In the present experiment, deformation length L and rotor speed V_L remain constant with time providing constant stretch rate consitions. As long as the filament deforms uniformly, the tensile stress $\sigma_{11}(t)$ and the (apparent) elongational viscosity $\chi(t)$ can be computed by

$$\sigma_{11}(t) = \frac{4F(t)}{\pi d_0^2} e^{Et} \tag{3.2}$$

$$\chi(t) = \frac{\sigma_{11}(t)}{E} \tag{3.3}$$

where $F(t)$ is the total force and d_0 is the diameter before stretching. We only need to measure total force

$F(t)$ as a function of time t for various stretch rates E. As an example, such raw data is shown in Fig. 3.3 for a low density polyethylene.

Diameter increase due to thermal expansion and crystal melting was estimated by density ratios as noted, for example, by Mendelson, Finger, and Bagley [85]. The ratio of cross-sectional area at experimental temperature and at room temperature was estimated to be 1.16 for HDPE, 1.12 for LDPE, and 1.05 for PS. The ratio for PP and PMMA was taken as 1.16 and 1.05, considering the former to be a crystalline polymer like HDPE and the latter to be a glassy polymer like PS.

The viscous resistance of silicone oil was estimated using the theory of Bachelor [5]. He analized the flow problem when a solid cylinder was suddenly pulled along its length in an infinite sea. With a slight modification for our case, a cylinder fixed at one end and pulled at the other end, the total viscous resistance may be given by

$$F_f = 2\pi\eta C_f \int_0^L V(x)dx = \pi\eta C_f V_L L \qquad (3.4)$$

where η is the viscosity of the silicone oil. The friction coefficient C_f at large momentum diffusion T $(=\eta t/\rho R^2)$ is given by

$$C_f(T) = \frac{2}{\ln(4T)-2\gamma} - \frac{2\gamma}{[\ln(4T)-2\gamma]^2} + \cdots \qquad (3.5)$$

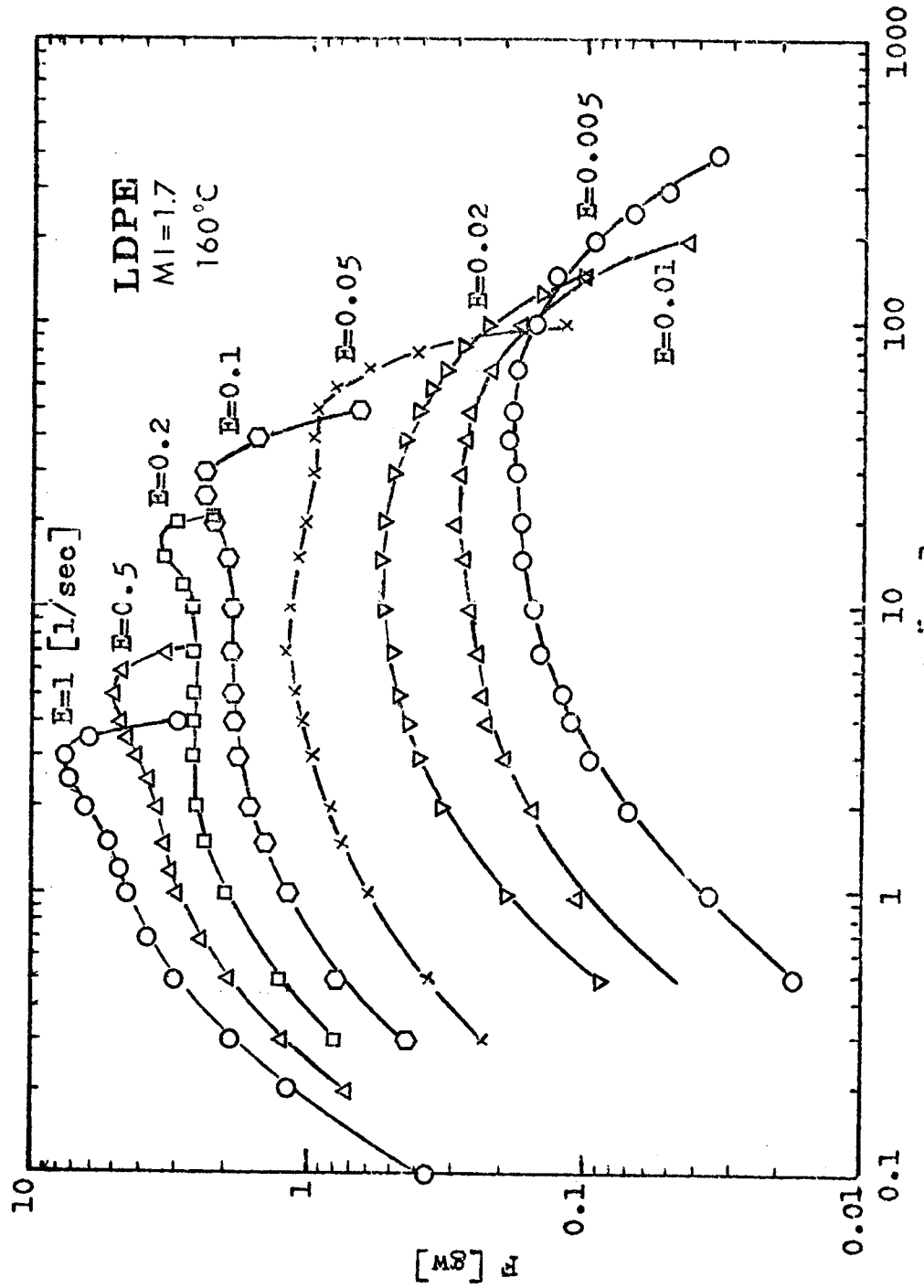


FIGURE 3.3 Load-time curve for a low density polyethylene

where $\gamma=0.577$ is the Euler constant. C_f is usually in the neighborhood of 0.1 to 1 .

Using the above expressions, the viscous resistance is extimated to be a few percent of the tatal force for LDPE (MI=5.0) or HDPE (MI=2.6) whose zero shear viscosities are of the order of 10^5[poise]. For higher viscosity filaments than this value, the viscous resistance is negligible. But for lower viscosity ones, the tension varies along the length due to the viscous resistance and a uniform stretch rate cannot be provided. Besides, natural convection currents in the bath carry the filament away from the center and the experiments were not successful for such low viscosity filaments.

Stress Relaxation

Procedure. Stress relaxation experiments were performed using the same experimental set us as the stress development experiment. In this experiment, the deformation was suddenly stopped and the stress was allowed to decay with time. In order to trace the stress for a long time, very large samples (diameter 4 to 5 mm) of high viscosity materials were initially stretched at a high rate (E=1 [1/sec]). After 50 to 100% strain, the deformation was suddenly stopped and a decay of the stress was recorded.

Data processing. The relaxation function G(t) represented by a series of multi-relaxation parameters G_i and λ_i were first calculated using the rubber elasticity

equation:

$$G(t) = \sum_i G_i e^{-t/\lambda_i} = \frac{\sigma(t_1)}{e^{2Et_1} - e^{-Et_1}} \qquad (3.6)$$

where $\sigma(t_1) = \sum_i \sigma_i(t_1)$ is the total stress at the time of stopping (the stretching) t_1, and E is the stretch rate. The relaxation function $G(t)$ is plotted against time in a semilogarithmic graph. As an illustration of the procedure, the plot for LDPE (MI=1.7) is shown in Fig. 3.4. A straight line is obtained (curve (1)) at long time asymptote. This indicates that the terms of short relaxation time in Eq. (3.6) have damped out and the relaxation mechanism is dominated by one function with the longest relaxation time. The slope of the straight line gives the longest relaxation time λ_1 and the intercept gives its modulus G_1. After representing the long time relaxation data by G_1 and λ_1, one seeks to represent the next long time data by a term of $G(t)$. This is done by plotting $\log(G(t)-G_1e^{-t/\lambda_1})$ versus time. This gives second longest relaxation time λ_2 and its modulus G_2 (see curve (2)). This procedure is repeated until all relaxation data is preresented by the series of Eq. (3.6) (see curves (3) and (4)). This method of obtaining relaxation functions G_i, λ_i is the "procedure X" of Tobolsky and Murakami[135].

The above procedure utilizing rubber elasticity theory (in Eq. (3.6)) is valid as long as the relaxation times are considerably higher than time scale of the experiment and

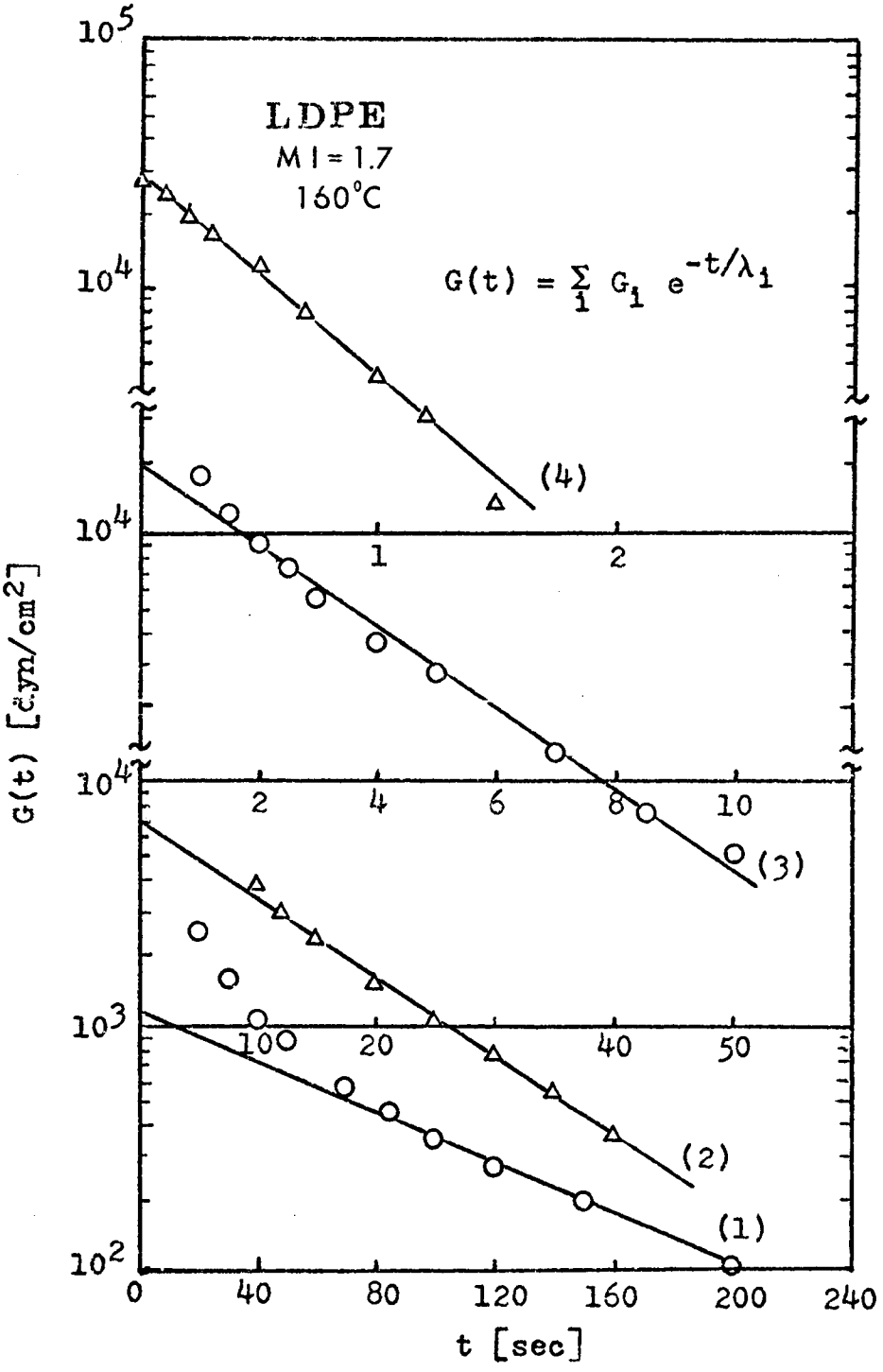


Figure 3.4 An illustration of procedure X.

the Finger strain measure properly represents non-linear effects. In the present case, one of the highest stretch rates of $E = 1$ [1/sec] is used throughout the experiment. However the moduli of short relaxation times might be calculated to be lower than the actual values.

Let us look in more detail at at the comments of the above paragraph. The stress level at the start of relaxation ($t = t_1$) for a constitutive equation such as Lodge fluid is

$$\sigma(t_1) = \sum_i \left\{ \frac{2G_i\lambda_i E}{2\lambda_i E-1}\left[1-e^{(2\lambda_i E-1)t_1/\lambda_i}\right] + \frac{G_i\lambda_i E}{\lambda_i E+1}\left[1-e^{-(\lambda_i E+1)t_1/\lambda_i}\right]\right\} \qquad (3.7)$$

Only when $\lambda_1 E \gg 1$, can we write

$$\sigma(t_1) = \sum_i G_i\left(e^{2Et_1}-e^{-Et_1}\right) \qquad (3.8)$$

If we compare Eq. (3.7) and Eq. (3.8), we see that Eq. (3.8) is larger than Eq. (3.7) and the difference is caused by the terms of small relaxation times. The correction due to viscoelasticity as opposed to rubber elasticity is made for the moduli of short relaxation times.

After the corrections mentioned above are made, all moduli are multiplied by a factor so that the theoretical curve could fit the small stretch rate data. The relaxation functions obtained in this manner are shown in Table III.

TABLE III

MATERIAL PARAMETERS DETERMINED BY RELAXATION EXPERIMENT

LDPE (MI = 1.7)	$\eta_0 = 3.27 \times 10^5$ [pcise]					
G_i [dyn/cm^2]	1.35×10^3	7.89×10^3	2.60×10^4	5.21×10^4		
λ_i [sec]	82.6	13.5	2.60	0.789		
HDPE (MI = 0.1)	$\eta_0 = 4.93 \times 10^6$ [pcise]					
G_i [dyn/cm^2]	6.10×10^3	5.53×10^3	1.36×10^4	4.55×10^4	1.10×10^5	1.93×10^5
λ_i [sec]	568	109	27.4	5.81	1.30	0.409
PS (M_w = 240,000)	$\eta_0 = 1.17 \times 10^6$ [pcise]					
G_i [dyn/cm^2]	3.14×10^4	5.43×10^4	1.41×10^5	1.33×10^5		
λ_i [sec]	23.2	4.09	1.14	0.434		
PP (MI = 0.42)	$\eta_0 = 1.25 \times 10^6$ [pcise]					
G_i [dyn/cm^2]	4.40×10^3	6.38×10^3	1.18×10^4	4.31×10^4	1.98×10^5	
λ_i [sec]	140	32.7	8.88	2.82	0.730	

One notes the distribution of relaxation times for the polystyrene is rather narrow compared to other polymers. This distribution of relaxation times can indicate the molecular weight distribution to a certain extent.

B. Stress Development in Elongational Flow

Results

In this section, the apparent elongational viscosity developments for a wide variety of polymers of different molecular weights are presented. Due to the fact that the elongational viscosities computed by Eq. (3.3) have not reached steady state, the viscosities are by all means apparent ones and should be interpreted as reduced stresses (to viscosity level). The data include the points after local deformation (necking) has started to indicate failure point. This would be seen as a decrease in the viscosity. The actual breaking point, when the material separated into two pieces, is usually a few seconds after the last data point and is not shown in the figures. The temperatures of the measurements are 160°C except polypropylene and polymethyl methacrylate which are at 180°C. The melt densities of the polystyrene and polymethyl methacrylate are greater than silicone oil at the experimental temperatures, so that these materials tend to sink in the oil.

Low density polyethylene (LDPE). The apparent elongational viscosities of LDPE (MI=1.7) are plotted in

Fig. 3.5 as a function of time. The position of three times the zero shear viscosity known as Trouton viscosity is also shown in the figure. The zero shear viscosity was obtained in the Weissenberg rheogoniometer by Chen [23] for the same material at the same temperature. As one can see in the figure, as long as stretch rates are low (less than 0.01 [1/sec]), the behavior is linear viscoelastic as indicated by Eq. (2.39). In this case, elongational viscosity monotonically increases to a steady state value of Trouton viscosity and the true elongational viscosity may be obtained. As the stretch rate increases, the viscosity starts to deviate from the linear curve and increases exponentially with time. In this case, the long time asymptote of the elongational viscosity does not exist, and fracture of the material occurs. As the stretch rate increases, the deviation from linear behavior occurs earlier.

The elongational viscosities of a lower molecular weight LDPE (MI=5.0) are shown in Fig. 3.6. Essentially the same features as the higher molecular weight LDPE (MI=1.7) are observed. At low stretch rates the time to reach steady state is shorter (about 15 seconds as opposed to 50 seconds for MI=1.7), and the value of Trouton viscosity is lower (about 3×10^5 poise as opposed to 10×10^5 poise for MI=1.7). These observations are simply explained by the lower relaxation times at this lower molecular weight polymer possesses.

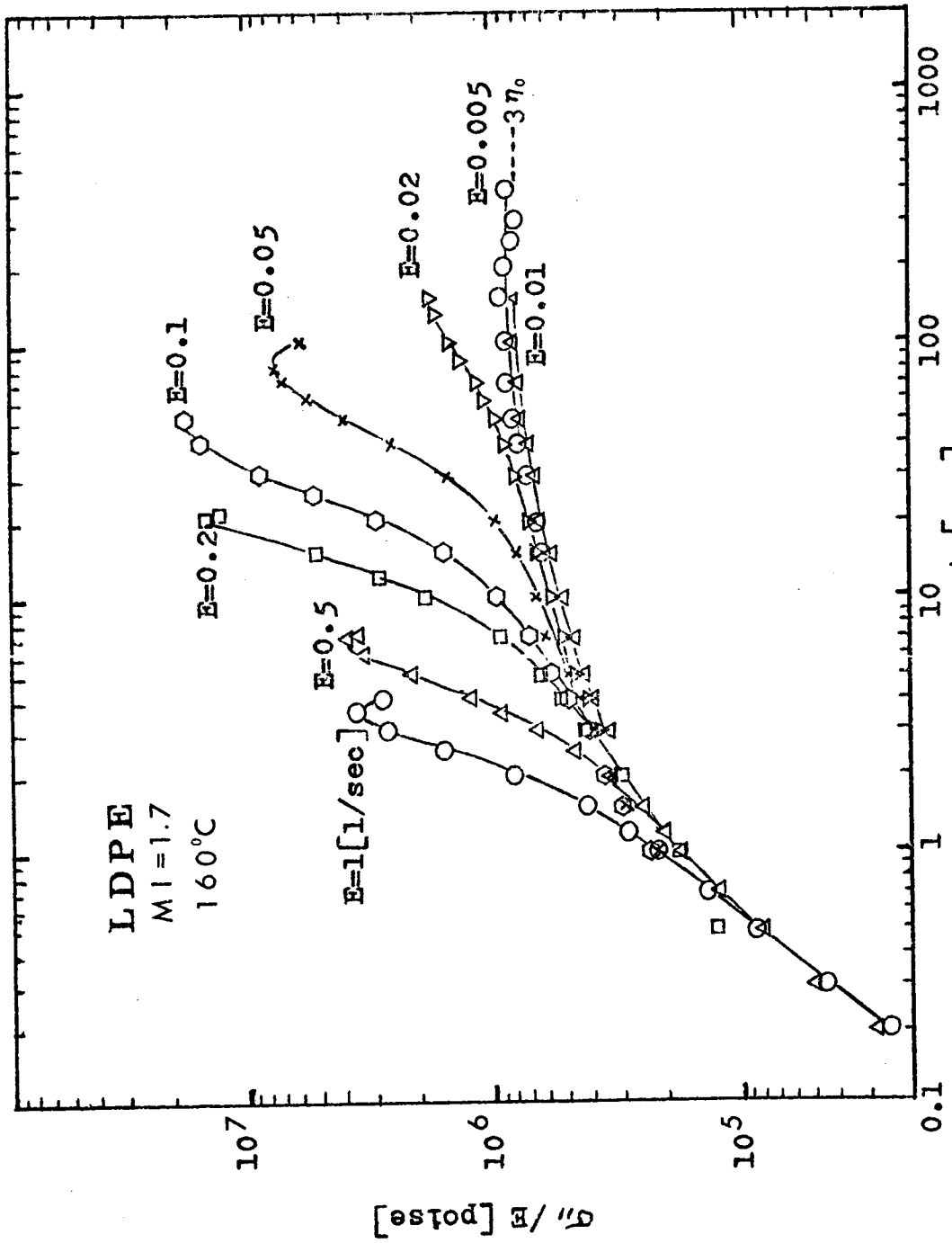


FIGURE 3.5 Stress developments at various stretch rates for LDPE (MI = 1.7).

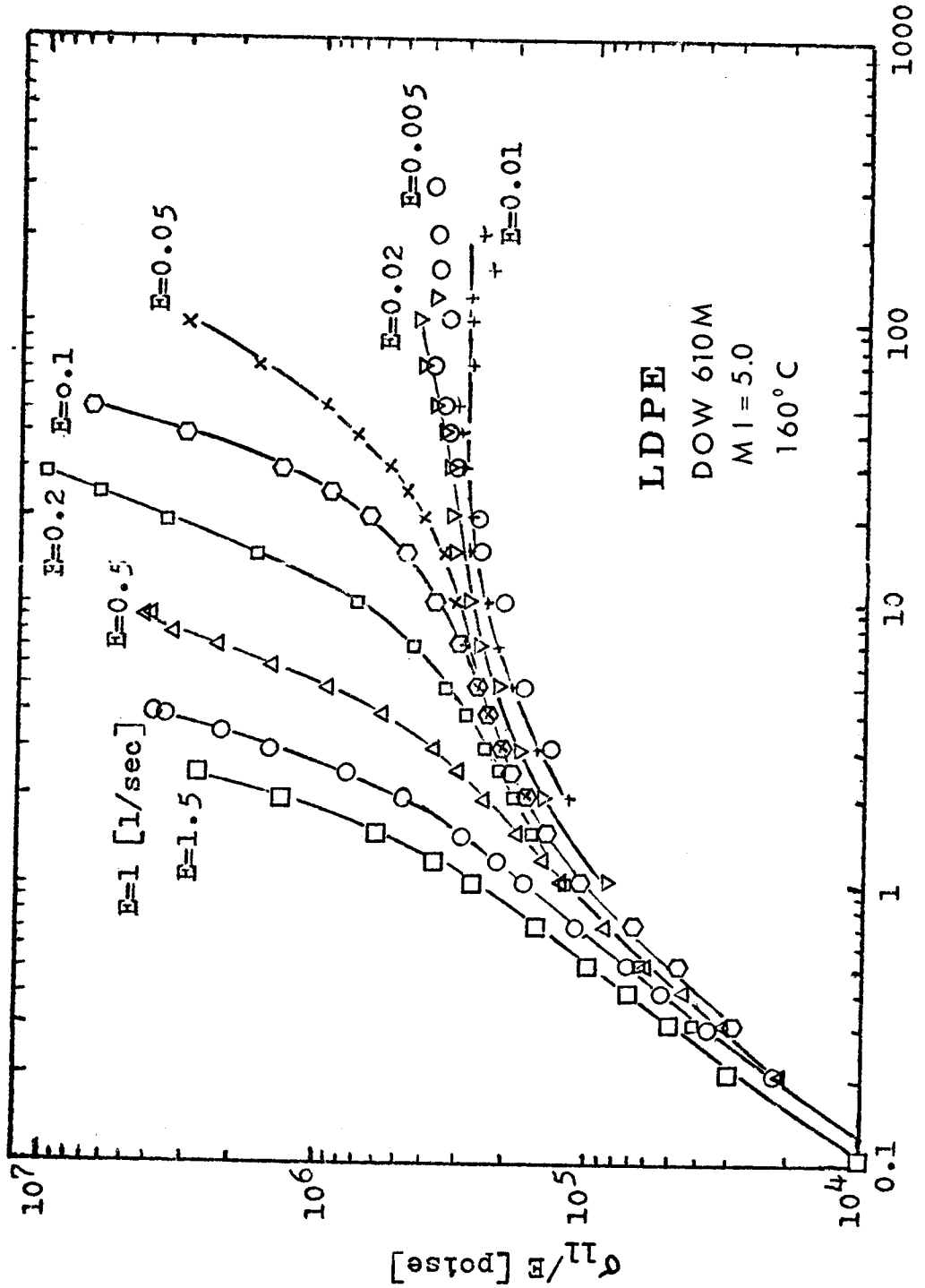


FIGURE 3.6 Stress development at various stretch rates for LDPE (MI = 5.0).

High density polyethylene (HDPE). The elongational viscosity developments of very high molecular weight HDPE (MI = 0.1) are shown in Fig. 3.7. The value of the Trouton viscosity was obtained by the stress relaxation experiments. The relaxation times are rather high so that the linear behavior can not be obtained even at the lowest stretch rate ($\dot{E}$ = 0.005 1/sec). Deviations from linear viscoelastic behavior are also observed for this material, but the growth rates after the "take off" are much smaller than LDPE's. The growth of the stresses (as reduced to elongational viscosity) after the "take off" are more linear with time especially at high stretch rates as contrasted with exponential growths for LDPE's. One observes that the maximum elongational viscosities attained at high stretch rates are lower than the Trouton value, although they reach higher values at low rates. For LDPE's on the other hand, the elongational viscosities could reach more than twenty times the Trouton value at high stretch rates as will be seen later (page 72).

The elongational viscosity developments of the lower molecular weight HDPE (MI = 2.6) are shown in Fig. 3.8. The Trouton viscosity calculated from Chen's [23] dynamic oscillation data is also shown in the figure. At low stretch rates, monotonic increases approaching the Trouton viscosity are observed. At high stretch rates, the growth rates of the viscosity after the take off are again small

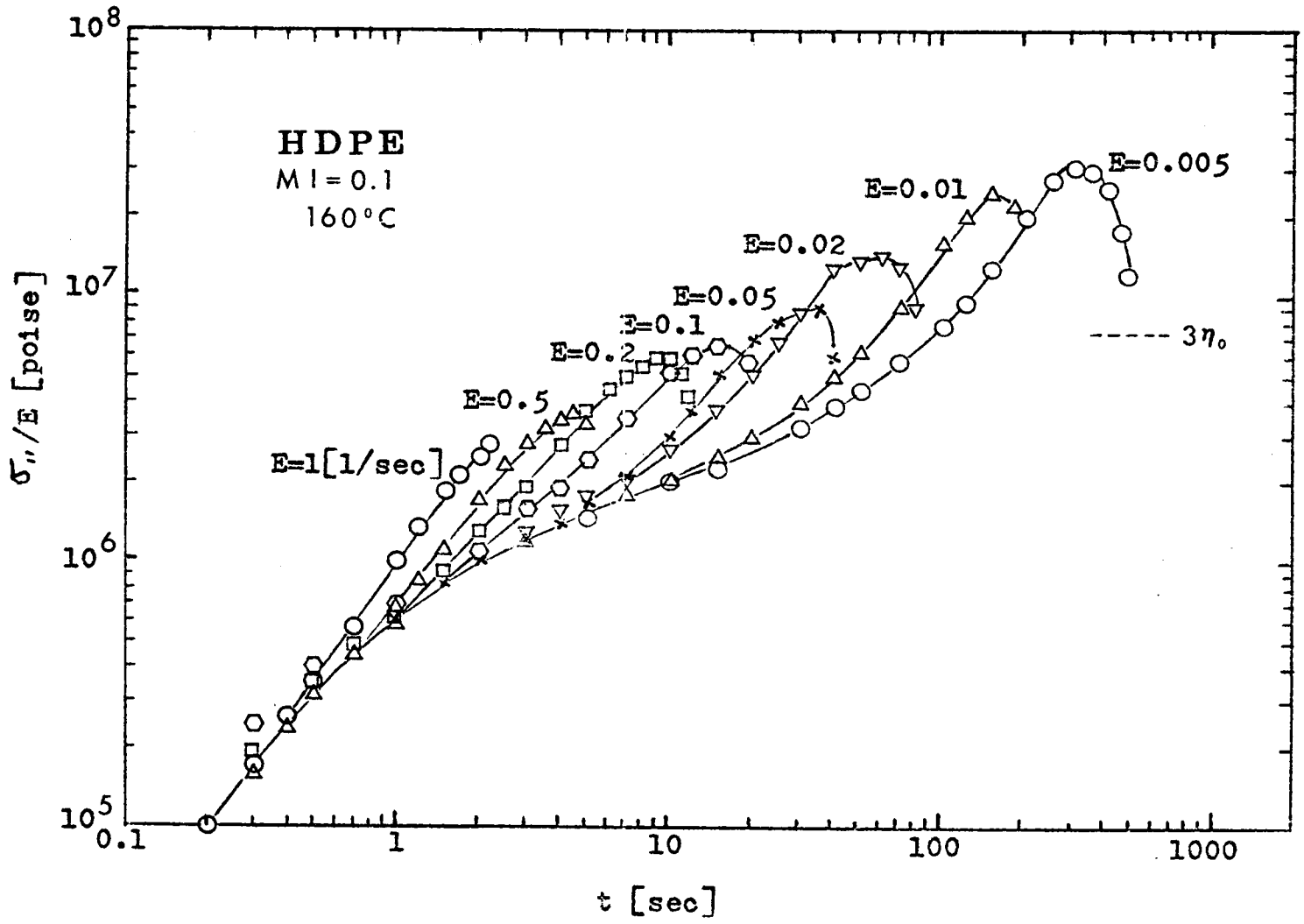


FIGURE 3.7 Stress developments at various stretch rates for HDPE (MI = 0.1).

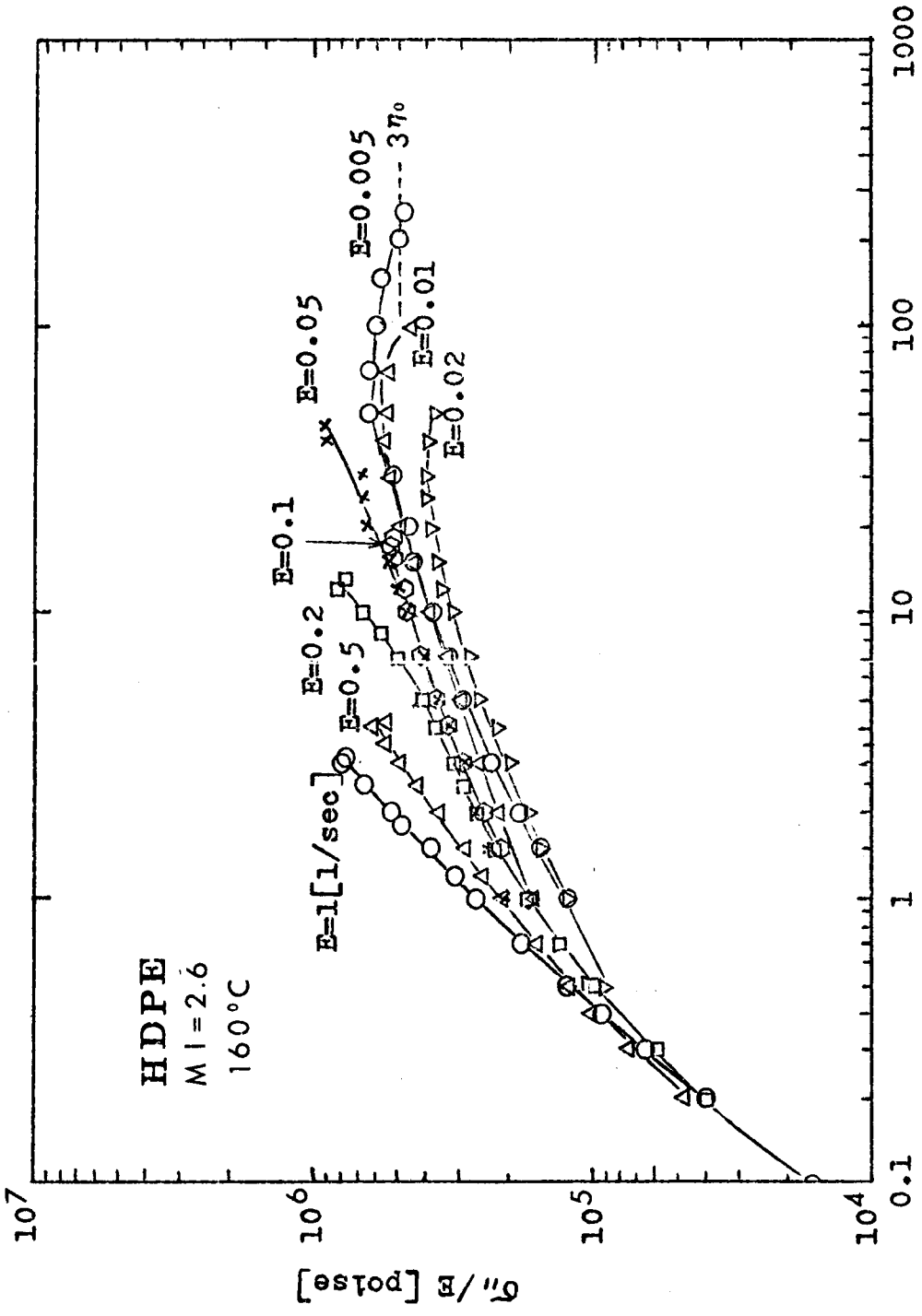


FIGURE 3.8 Stress developments at various stretch rates for HDPE (MI = 2.6).

and more linear growths are observed. The maximum elongational viscosity attained was at most twice the Trouton viscosity.

Polystyrene (PS). Stress developments as reduced to the viscosity level for a PS (Shell TC3-30, M_w = 283,000) are shown in in Fig. 3.9. This polymer had been previously studied by Takaki and Bogue [131,132]. The Trouton viscosity computed from the shear data of Takaki [131] is also indicated in the figure. The character of the growth for the PS is similar to that of LDPE's but is not as sharp as them. A complete leveling off to the Trouton viscosity is not seen but such a trend is clear at low stretch rates.

Fig. 3.10 shows the viscosity developments for a lower molecular weight PS (Dow Styron 678 U, M_w = 240,000). Here the steady states are attained at low stretch rates. The growth rate of the viscosity after the take off is not as sharp as LDPE's but not as slow as HDPE's. The growth rate of this polystyrene (Dow Styron 678 U) seems not as sharp as that of Shell TC3-30 polystyrene. Dow Styron 678 U has sharper molecular weight distribution than Shell TC3-30 as indicated by the polydispersity ratio being 3.0 as opposed to 4.6 of Shell TC3-30.

Polypropylene (PP). The curves for PP (MI = 0.42) are shown in Fig. 3.11. The zero shear viscosity was measured in the stress relaxation experiment described earlier. The behavior is very similar to that of HDPE.

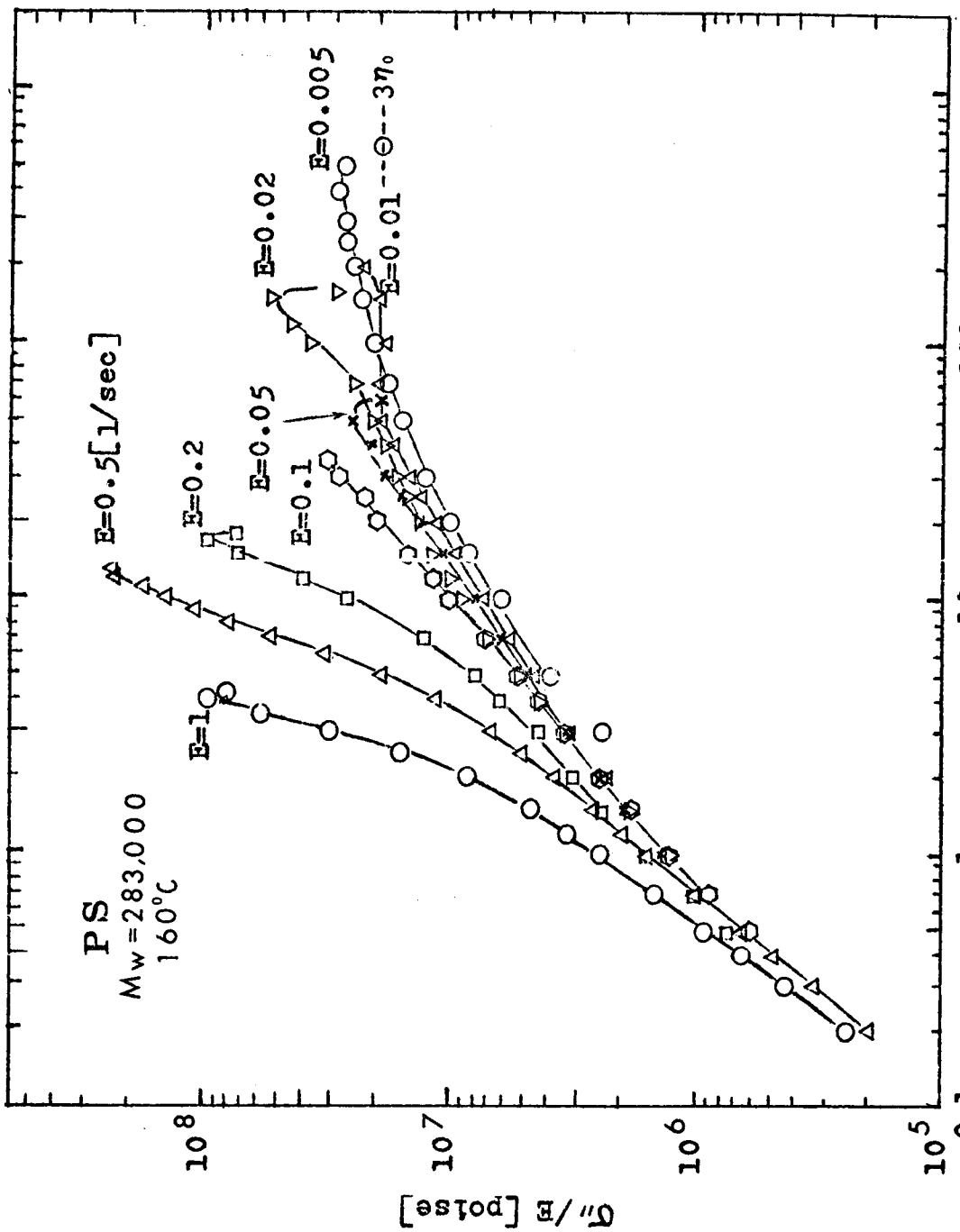


FIGURE 3.9 Stress developments at various stretch rates for PS (Shell TC3-30).

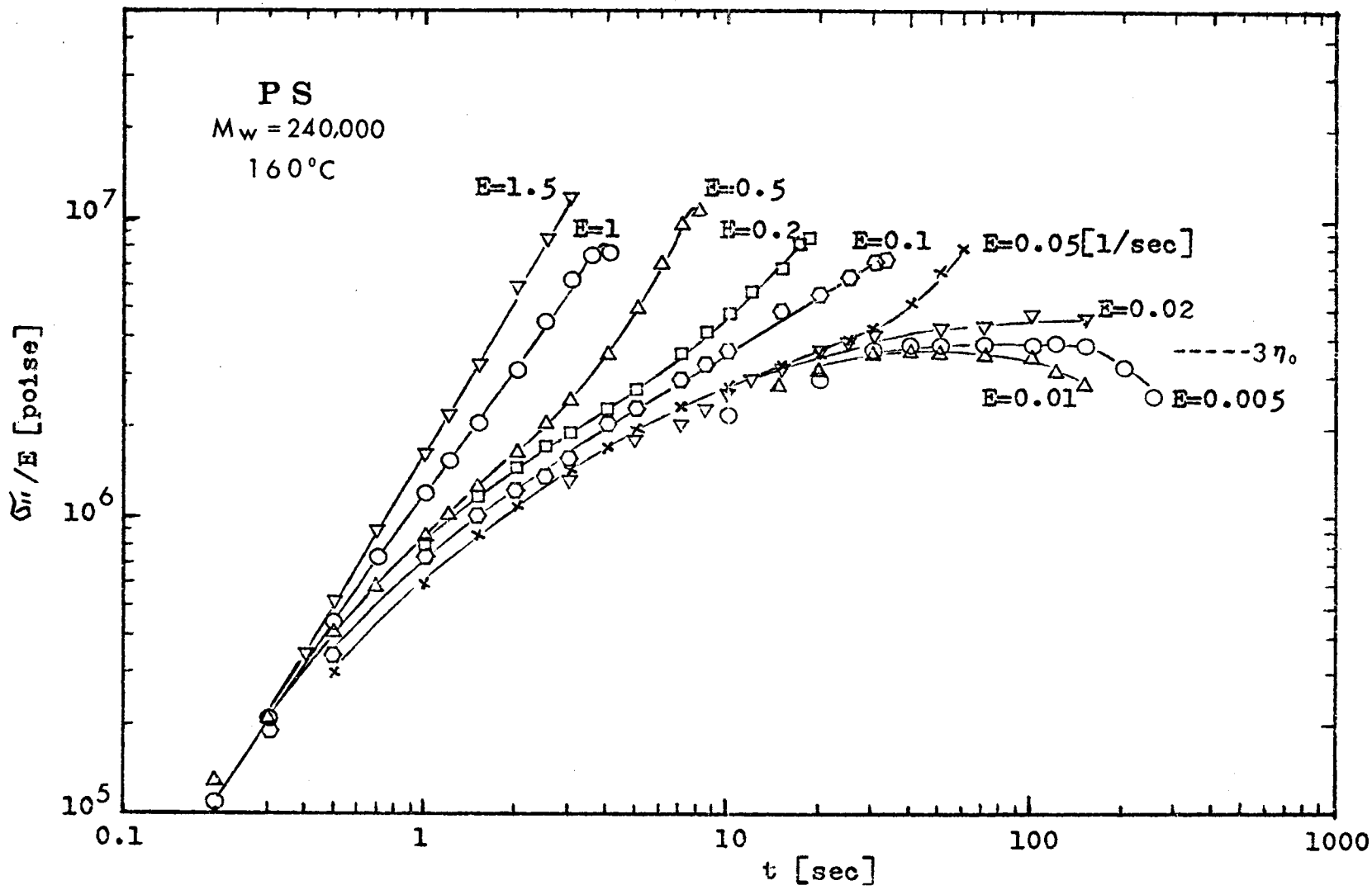


FIGURE 3.10 Stress developments at various stretch rates for PS (Dow Styron 678 U).

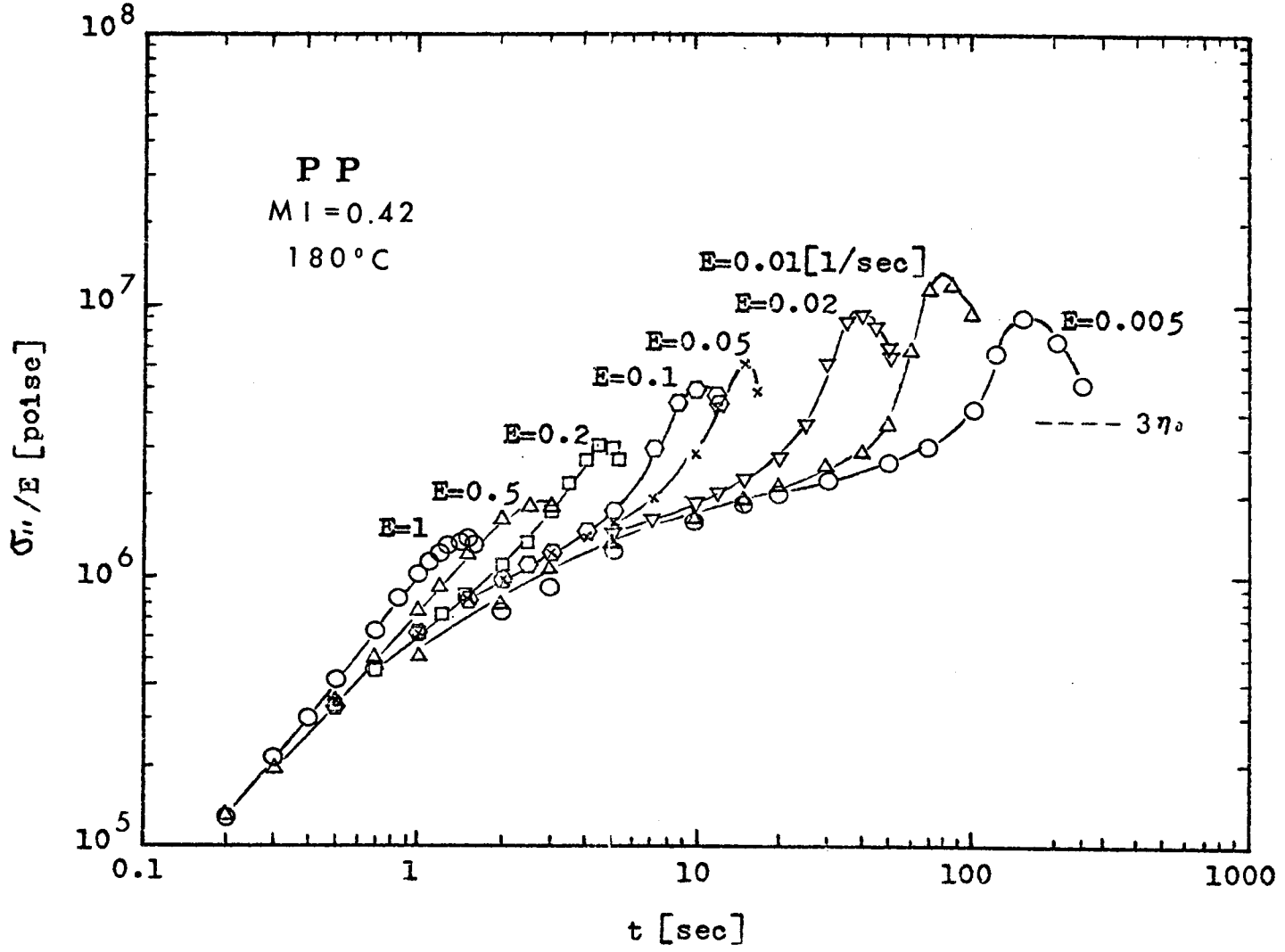


FIGURE 3.11 Stress developments at various stretch rates for PP (MI = 0.42).

At low stretch rates, the viscosity increases very rapidly and decreases after a maximum. At high stretch rates the viscosity is always below the Trouton value.

The stress developments for lower molecular weight PP (MI = 6.6) are shown in Fig. 3.12. The relationship of molecular weight is similar to that of HDPE. At high stretch rates, the viscosity exceeds the Trouton value but is at most three times the Trouton viscosity.

Polymethyl methacrylate (PMMA). This material (Dupont Lucite 147) was found to be rather difficult to handle, probably because it tends to absorb moisture. Pellets of this material were dried in an oven at around 100 °C overnight. Without this process, the material generates many gas bubbles when heated in the Instron barrel. Even after the cylindrical samples were prepared, they were dried again just before use. Otherwise gas bubbles are generated in the samples when they are placed in the oil bath.

With these difficulties, the elongational stress developments of the PMMA were measured at 180 °C. This is shown in Fig. 3.13 in the form of elongational viscosity versus time. Superposition of curves in the linear range is very good except the curves of low stretch rates (E = 0.01, E = 0.005 [1/sec]). This trend is seen for each plot of the various polymers. This is probably due to bad calibration of speed setting at such low speeds and is presumed to be an experimental error.

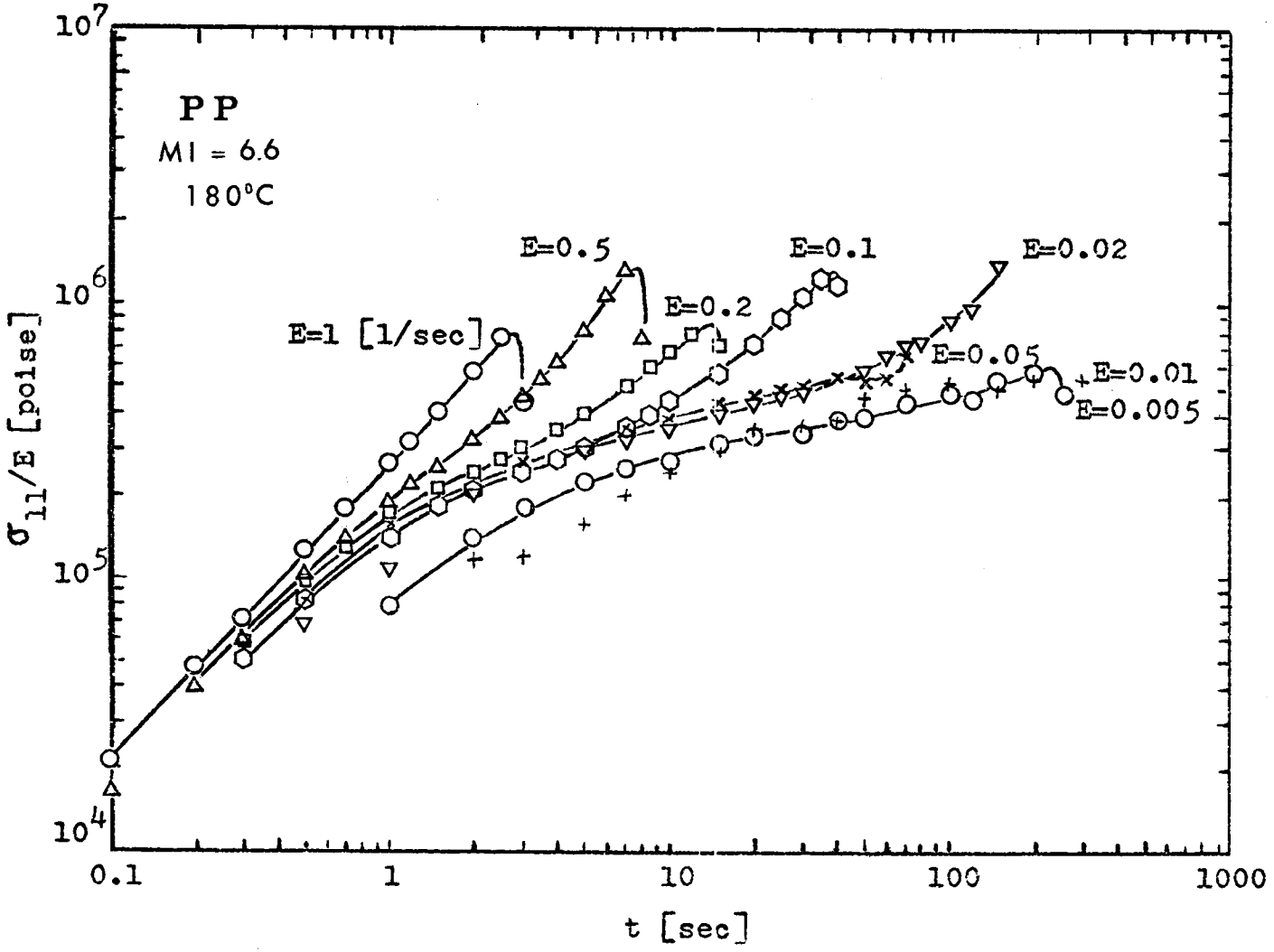


FIGURE 3.12 Stress development at various stretch rates for PP (MI=6.6).

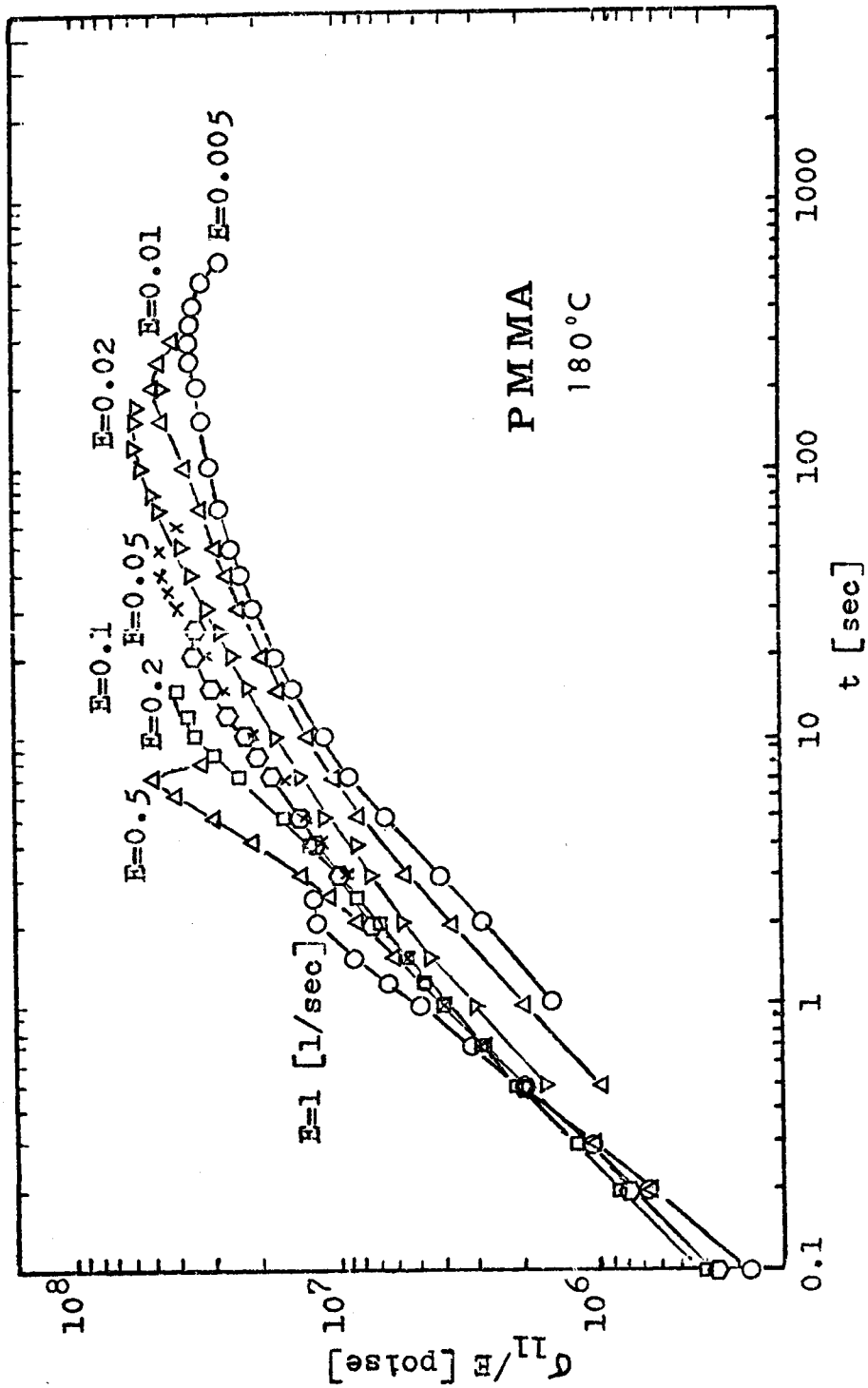


FIGURE 3.13 Stress development at various stretch rates for PMMA.

As far as my experiences with this polymer are concerned, it behaved similar to a polystyrene. However the stress development curves are more similar to HDPE's. In this plot, however, one should realize that the Trouton viscosity is as high as the level of fracture stress of high stretch rate curves (about 2 to 3×10^7 dyn/cm^2). Besides, the experimental fracture stress may have been lowered due to the small gas bubbles generated.

Discussion of Elongational Viscosity

It is apparent that the true elongational viscosity of the low density polyethylene (LDPE) and the polystyrene (PS) generally can not be obtained except at low stretch rates because the steady state can not be achieved. However, for the high molecular weight high density polyethylene HDPE, (MI = 0.1) and the polypropylene (PP, MI = 0.42) the apparent elongational viscosity does not grow indefinitely but rather tends to level off at any stretch condition. One must be aware, however, that a local deformation of the material (necking) is taking place at this time. If one assumes the maximum to be a steady state, one may be able to obtain a true (time independent) elongational viscosity for the HDPE (MI = 0.1) and the PP (MI = 0.42). Fig. 3.14 shows the elongational viscosity χ (reduced by Trouton viscosity) as a function of stretch rate E.

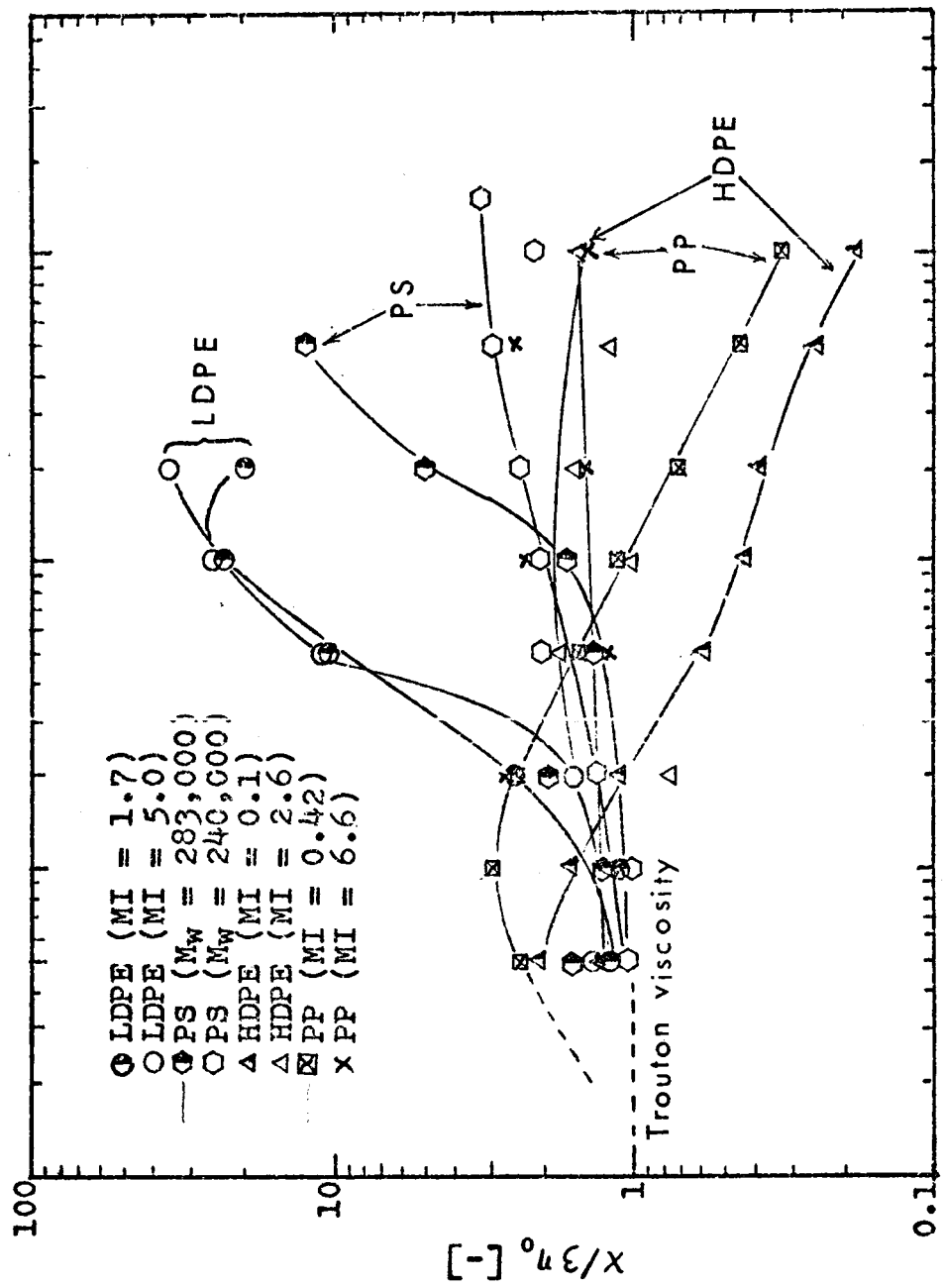


FIGURE 3.14 Maximum attained elongational viscosities for various polymers as a function of elongation rate.

For comparison purposes, the maximum attained elongational viscosities for other polymers, reduced by their Trouton viscosities, are plotted in the same figure. These are not true elongational viscosities because, as is clearly seen in the previous figures, the apparent elongational viscosities are still growing. Due to instabilities such as fracture and ductile failure, the materials failed and the attained elongational viscosities are thus limited. If the materials had not failed, the viscosities would have been much higher and infinite values after steady state should have been possible. The phenomena is further complicated by the distribution of relaxation times. If the maximum relaxation time λ_m of the material satisfies the condition $\lambda_m E > \frac{1}{2}$, the steady state cannot be attained.

At any rate, the figure clearly illustrates the different tensile responses of various materials. The elongational viscosities of LDPE (MI = 1.7 and MI = 5.0) sharply increase with stretch rate as various theories predict. An elongational viscosity of as high as 37 times the Trouton viscosity is seen to be attained before the material fractures for LDPE (MI = 5.0). Polystyrenes also show the same trend, but not as sharp as low density polyethylenes. However for high density polyethylenes and polypropylenes, the maximum elongational viscosities do not increase with stretch rate. Intermediate molecular

weight HDPE (MI = 2.6) and PP (MI = 6.6) show almost constant elongational viscosities and the very high molecular weight HDPE (MI = 0.1) and PP (MI = 0.42) show a decrease in the elongational viscosities with stretch rate. The elongational viscosities of these materials are higher than Trouton viscosity at low stretch rates, but lower at high stretch rates. At extremely low stretch rates, however, the viscosity should become equal to the Trouton viscosity. The polypropylene (PP, MI = 0.42) shows such trend at stretch rates lower than $E = 0.01$ [1/sec].

The results shown in Fig. 3.14 are very similar to Cogswell's summary [29] of elongational viscosities of various polymers. It should be emphasized again that the elongational viscosities in the figure are still mostly apparent ones due to instabilities of elongation. It is thus meaningless to compare these apparent ones with the true elongational viscosity predictions such as Eq. (2.45) or Eq. (2.46).

C. Comparison of the Elongational Flow Behavior with Viscoelastic Fluid Theories

Bogue and White Model

Formulation of transient stress for constant rate stretching. The uniaxial stress development of the Bogue and White model, Eqs. (2.21)-(2.23), is considered because of its success for both shear and elongational flows of

polymer melts [24,25,132]. The tensile stress of the Bogue and White model for uniaxial stretching is expressed by (see Eq. (2.35), page 21):

$$\sigma_{11}(t) = \tau_{11}(t) - \tau_{22}(t) \tag{3.9}$$

$$= \int_{-\infty}^{t} \{m_1(t-s)(C_{11}^{-1} - C_{22}^{-1}) - m_2(t-s)(C_{11} - C_{22})\} ds$$

The physical components of the Finger and Cauchy strain tensors, when the stretching of constant rate E is suddenly applied at $s = 0$, are

$$\underset{\sim}{C}^{-1} = \begin{vmatrix} \beta^2 & 0 & 0 \\ 0 & \beta^{-1} & 0 \\ 0 & 0 & \beta^{-1} \end{vmatrix}, \quad \underset{\sim}{C} = \begin{vmatrix} \beta^{-2} & 0 & 0 \\ 0 & \beta & 0 \\ 0 & 0 & \beta \end{vmatrix} \tag{3.10}$$

where $\beta = e^{E(t-s)}$ $(s \geq 0)$ is the stretch ratio. The strain tensors when the material is unstrained $(s < 0)$ remain the same as those at $s = 0$. However they are functions of present time t because the strain tensors are relative configuration tensors whose reference state is present state $(s = t)$.

The average second invariant of the deformation rate tensor (Eq. (2.23b), page 15) becomes (following Middleman [88]):

$$\langle II_d \rangle^{\frac{1}{2}} = \frac{1}{z} \int_0^z II_d^{\frac{1}{2}} ds = \sqrt{3}\, E \quad (s \geq 0 \text{ or } z \leq t) \tag{3.11a}$$

$$\langle II_d \rangle^{\frac{1}{2}} = \frac{1}{z}\int_0^t II_d^{\frac{1}{2}}\,ds + \frac{1}{z}\int_t^z II_d^{\frac{1}{2}}\,ds$$

$$= \sqrt{3}\,E\,\frac{t}{z} \qquad (s<0 \text{ or } z>t) \tag{3.11b}$$

where $z = t-s$ is the back running time from present. The effective relaxation times become

$$\lambda_{ieff} = \frac{\lambda_i}{1+\sqrt{3}\,a\lambda_i E} \qquad (0 \leq z \leq t: \text{ during stretching}) \tag{3.12a}$$

$$\lambda_{ieff} = \frac{\lambda_i}{1+\sqrt{3}\,a\lambda_i E\,\frac{t}{z}} \qquad (t<z<\infty: \text{ before stretching}) \tag{3.12b}$$

Thus the tensile stress Eq. (3.9) is specifically expressed by

$$\sigma_{11}(t) = (1+\frac{\varepsilon}{2})\Big\{\sum_i \int_0^t \frac{G_i}{\lambda_i}(1+\sqrt{3}a\lambda_i E)e^{-\frac{z}{\lambda_i}(1+\sqrt{3}a\lambda_i E)}(e^{2Ez}-e^{-Ez})dz$$

$$+\sum_i \int_t^\infty \frac{G_i}{\lambda_i}(1+\sqrt{3}a\lambda_i E\,\frac{t}{z})\,e^{-\frac{z}{\lambda_i}(1+\sqrt{3}a\lambda_i E\frac{t}{z})}dz\,(e^{2Et}-e^{-Et})\Big\}$$

$$-\frac{\varepsilon}{2}\Big\{\sum_i \int_0^t \frac{G_i}{\lambda_i}(1+\sqrt{3}a\lambda_i E)e^{-\frac{z}{\lambda_i}(1+\sqrt{3}a\lambda_i E)}(e^{Ez}-e^{-2Ez})dz$$

$$+\sum_i \int_t^\infty \frac{G_i}{\lambda_i}(1+\sqrt{3}a\lambda_i E\,\frac{t}{z})\,e^{-\frac{z}{\lambda_i}(1+\sqrt{3}a\lambda_i E\frac{t}{z})}dz\,(e^{Et}-e^{-2Et})\Big\} \tag{3.13}$$

If we evaluate the integration, the following result is obtained.

$$\sigma_{11}(t) = (1+\frac{\epsilon}{2})\Big\{\sum_i \frac{G_i(1+\sqrt{\beta}a\lambda_i E)}{1-(2-\sqrt{\beta}a)\lambda_i E}\Big[1-e^{-\{1-(2-\sqrt{\beta}a)\lambda_i E\}\frac{t}{\lambda_i}}\Big]$$

$$-\sum_i \frac{G_i(1+\sqrt{\beta}a\lambda_i E)}{1+(1+\sqrt{\beta}a)\lambda_i E}\Big[1-e^{-\{1+(1+\sqrt{\beta}a)\lambda_i E\}\frac{t}{\lambda_i}}\Big]$$

$$+\sum_i G_i\Big[e^{-\frac{t}{\lambda_i}} + \sqrt{\beta}aEtEI(\frac{t}{\lambda_i})\Big]\Big[e^{(2-\sqrt{\beta}a)Et} - e^{-(1+\sqrt{\beta}a)Et}\Big]\Big\}$$

$$-\frac{\epsilon}{2}\Big\{\sum_i \frac{G_i(1+\sqrt{\beta}a\lambda_i E)}{1-(1-\sqrt{\beta}a)\lambda_i E}\Big[1-e^{-\{1-(1-\sqrt{\beta}a)\lambda_i E\}\frac{t}{\lambda_i}}\Big]$$

$$-\sum_i \frac{G_i(1+\sqrt{\beta}a\lambda_i E)}{1+(2+\sqrt{\beta}a)\lambda_i E}\Big[1-e^{-\{1+(2+\sqrt{\beta}a)\lambda_i E\}\frac{t}{\lambda_i}}\Big]$$

$$+\sum_i G_i\Big[e^{-\frac{t}{\lambda_i}} + \sqrt{\beta}aEtEI(\frac{t}{\lambda_i})\Big]\Big[e^{(1-\sqrt{\beta}a)Et} - e^{-(2+\sqrt{\beta}a)Et}\Big]\Big\} \qquad (3.14)$$

where $EI(x)$ is the exponential integral function defined by

$$EI(x) = \int_x^\infty \frac{e^{-u}}{u}\,du \qquad (3.15)$$

which is a steep decreasing function of x from infinity to zero. If we set $\epsilon = 0$ and $a = 0$, we obtain the Lodge fluid prediction, (Eq. (2.43), page 24).

Let us clarify the difference of viscosity predictions between constant rate stretching and constant rate shearing. For the constant rate stretching, one notes the form of the strain tensor (Eq. (3.10)) being exponential. This is a striking contrast with the kinematics of constant rate shearing whose strain increases linearly with time. We know that the relaxation function is exponential with time, so that for the case of shear flow, the relaxation mechanism always catches up with the straining mechanism. However for the case of constant rate stretching, both relaxing and straining mechanisms are exponential, so that competition between both mechanisms in the stress field is always present. If the relaxation mechanism dominates, the stress reaches a steady state, and if the straining mechanism dominates, the stress continuously rises. Even if the relaxation mechanism dominates the stress field, the level of steady state depends upon the strength of the mechanism. This is the reason elongational viscosity increases with elongation rate when the model predicts constant shear viscosity. We should realize the difference in kinematics, especially the form of the strain tensor to understand the different viscosity features.

If we apply the same argument for the constant rate elongation of the Bogue and White model, we find that the straining rate is $\exp(2Et)$ and the relaxation rate is $\exp(-t/\lambda_{1eff})$ for the Finger strain measure. Therefore

only when $2E > (\lambda_{meff})^{-1}$ (effective maximum relaxation time) will the stress grow exponentially with time. This condition develops in Eq. (3.14) only when

$$(2-\sqrt{3}a)E-\frac{1}{\lambda_m}>0 \text{ or } (2-\sqrt{3}a)\lambda_m E>1 \ . \qquad (3.16)$$

However if

$$a \geq \frac{2}{\sqrt{3}} = 1.16 \quad \text{(Finger strain measure)} \qquad (3.17)$$

Eq. (3.16) is never satisfied and the stress never grows exponentially at any stretch condition (as first pointed out by Middleman [88]). The straining rate for the Cauchy strain measure is $\exp(Et)$ and the relaxation rate is $\exp(-t/\lambda_{ieff})$. This gives the critical value $a = 1/\sqrt{3} = 0.58$ for the unbounded stress growth for the Cauchy fluid.

It is found that the straining mechanism of Finger measure is much more severe than that of Cauchy measure (specifically $(L/L_0)^2$ versus L/L_0, where L/L_0 is the stretch ratio). And also, according to the second normal stress difference data, $\varepsilon/2$ of Eq. (3.14) is small and lies in the neighborhood of -0.1 to -0.3 [69] (see Table I, page 19). Thus it may be found that in the tensile stress of Eq. (3.14), terms multiplied by $\varepsilon/2$ are relatively small compared to the terms based upon Finger strain measure. Therefore in the following section

$\varepsilon/2$ was taken to be zero for simplicity. The influence of neglecting the Cauchy strain measure would be to predict the stress somewhat higher.

Stress growth data and comparisons with the model. This section is meant not only to compare the data with the constitutive equation, but also to present the stress growth data for a wide variety of polymers. Application of the constitutive equation requires that the relaxation functions (G_i and λ_i) of the material be known. Such material parameters of selected polymers have been determined by Chen [23,24] and Takaki [131,132] in a shear oscillation experiment using the Weissenberg rheogoniometer. Using such data we can predict "a priori" the stress developments of the materials. When such data is not available, the material parameters determined by the stress relaxation experiments will be used. In this case a complete a priori prediction is not made because the moduli are determined to fit the low stretch rate curves.

Performing a dynamic experiment in the Weissenberg rheogoniometer, one can obtain a relaxation spectrum. For LDPE (MI = 1.7) and HDPE (MI = 2.6), the relaxation spectrums had been obtained by Chen [23]. Based upon his continuous relaxation spectrum, discrete relaxation functions appropriate to our equation (Eq. (3.14)) are obtained. The relationship is (from Eq. (2.13) and Eq. (2.14), pages 10 and 11)

$$G(0) = \sum_i G_i = \int_{-\infty}^{\infty} H(\lambda) d \ln \lambda = \sum_i H_i \ln \lambda_i \qquad (3.18)$$

When a one decade time interval is chosen ($\ln \lambda_i = 2.303$), then moduli G_i are simply calculated by $G_i = 2.303 H_i$ where H_i is the height of the relaxation spectrum at relaxation time λ_i . The zero shear viscosity is calculated by

$$\eta_0 = \sum_i G_i \lambda_i \qquad (3.19)$$

The results for LDPE (MI = 1.7) and HDPE (MI = 2.6) are shown in Table IV.

Using these material parameters, "a priori" predictions of stress development are possible. Calculations were carried out using an IBM computer (model 360). A FORTRAN program to perform calculation of Eq. (3.14) is attached in Appendix.

Fig. 3.15 shows stress development data for the LDPE (MI = 1.7) together with predictions of the Bogue and White model (Eq. (3.14)). Predistions of only selected stretch rates (E = 1, 0.1, and 0.01 [1/sec]) are shown to avoid crowding. The parameter a indicates the dependence of relaxation times on deformation rate. An excellent agreement between the "a priori" prediction and the experimental data is seen except for E = 1 [1/sec] . At times shorter than one second, disagreement becomes

TABLE IV

MATERIAL CONSTANTS (DATA OF CHEN [23])

LDPE (MI = 1.7)	$\eta_0 = 2.65 \times 10^5$ [poise]					
G_i [dyn/cm^2]	4.19×10^2	1.30×10^4	6.54×10^4	2.11×10^5	5.35×10^5	1.04×10^6
λ_i [sec]	100	10	1	0.1	0.01	0.001
HDPE (MI = 2.6)	$\eta_0 = 1.79 \times 10^5$ [poise]					
G_i [dyn/cm^2]	6.30×10^2	7.60×10^3	4.37×10^4	1.76×10^5	7.48×10^5	3.12×10^6
λ_i [sec]	50	10	1	0.1	0.01	0.001

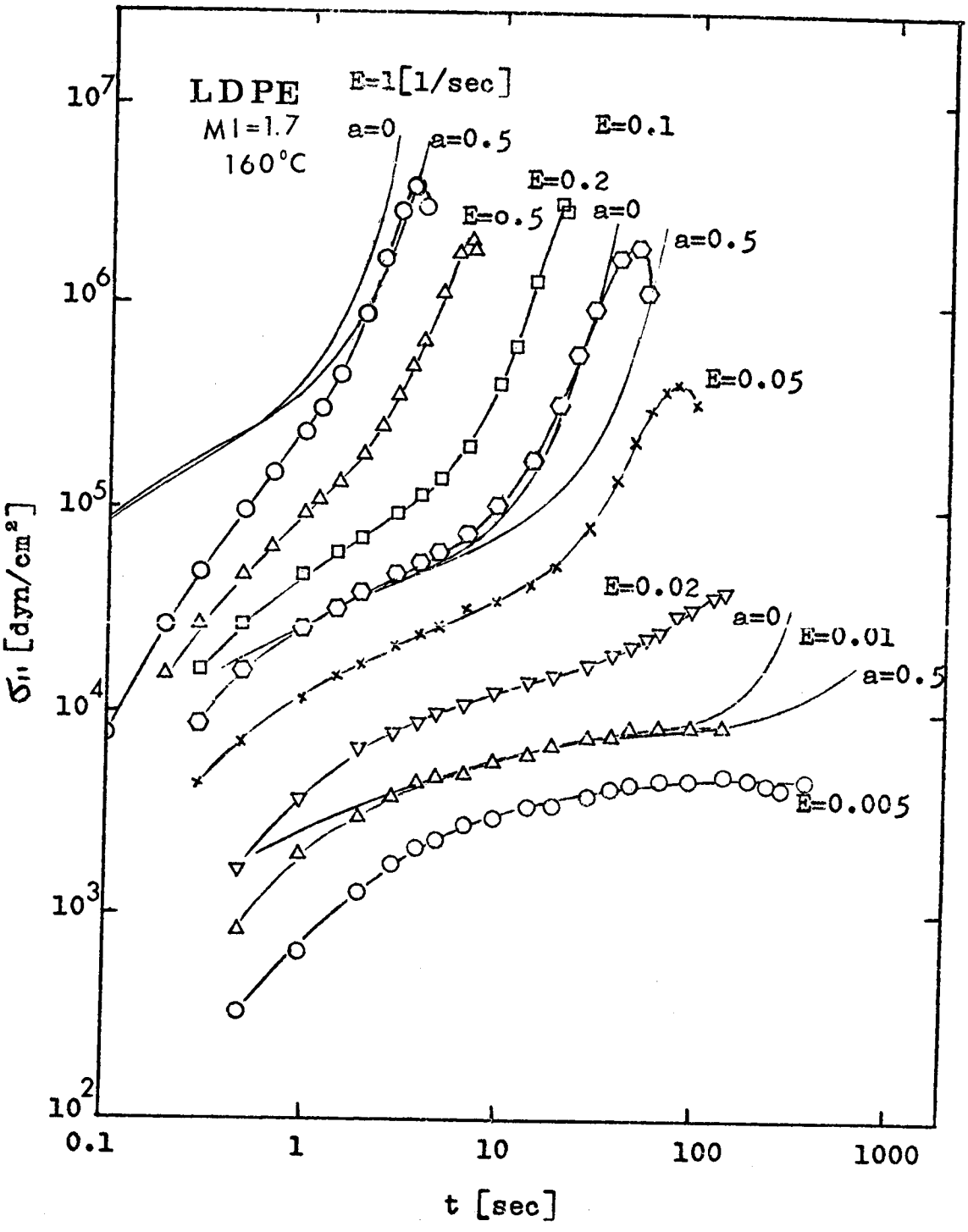


FIGURE 3.15 Stress development data of LDPE (MI = 1.7) and the Bogue and White model prediction based upon Chen oscillation data.

apparent. However data at this period may be expected to contain errors due to experimental difficulties but this discrepancy is not serious, especially if one plots total strain in the abscissa. At the highest stretch rate $E = 1$ [1/sec] the data is considerably lower than the Lodge fluid prediction ($a = 0$). This may be attributed to decrease in the relaxation times at high deformation rates. It is seen that the data points lie closer to the $a = 0$ curve than the $a = 0.5$ curve. One also observes that the difference of the $a = 0$ curve and the $a = 0.5$ curve seems to be larger for $E = 0.1$ [1/sec] case and the $a = 0.5$ curve exceeds $a = 0$ curve at short times of $E = 1$ [1/sec]. This mathematical phenomenon caused by the exponential integral function of the Eq. (3.14) seems not compatible with the physical phenomena.

The stress development data of HDPE (MI = 2.6) and a priori prediction of the Bogue and White model (Eq. (3.14)) for the three stretch rates are shown in Fig. 3.16. If one considers the predicted curves being completely a priori based upon external measurement, very good agreement between theory and experiment is observed. Again the disagreement at less than one second becomes less serious on a stress-strain basis. In terms of the a parameter data points resemble the shape between the $a = 0.5$ curve and the $a = 1.0$ curve. It is estimated that the parameter a has a somewhat higher value than 0.5.

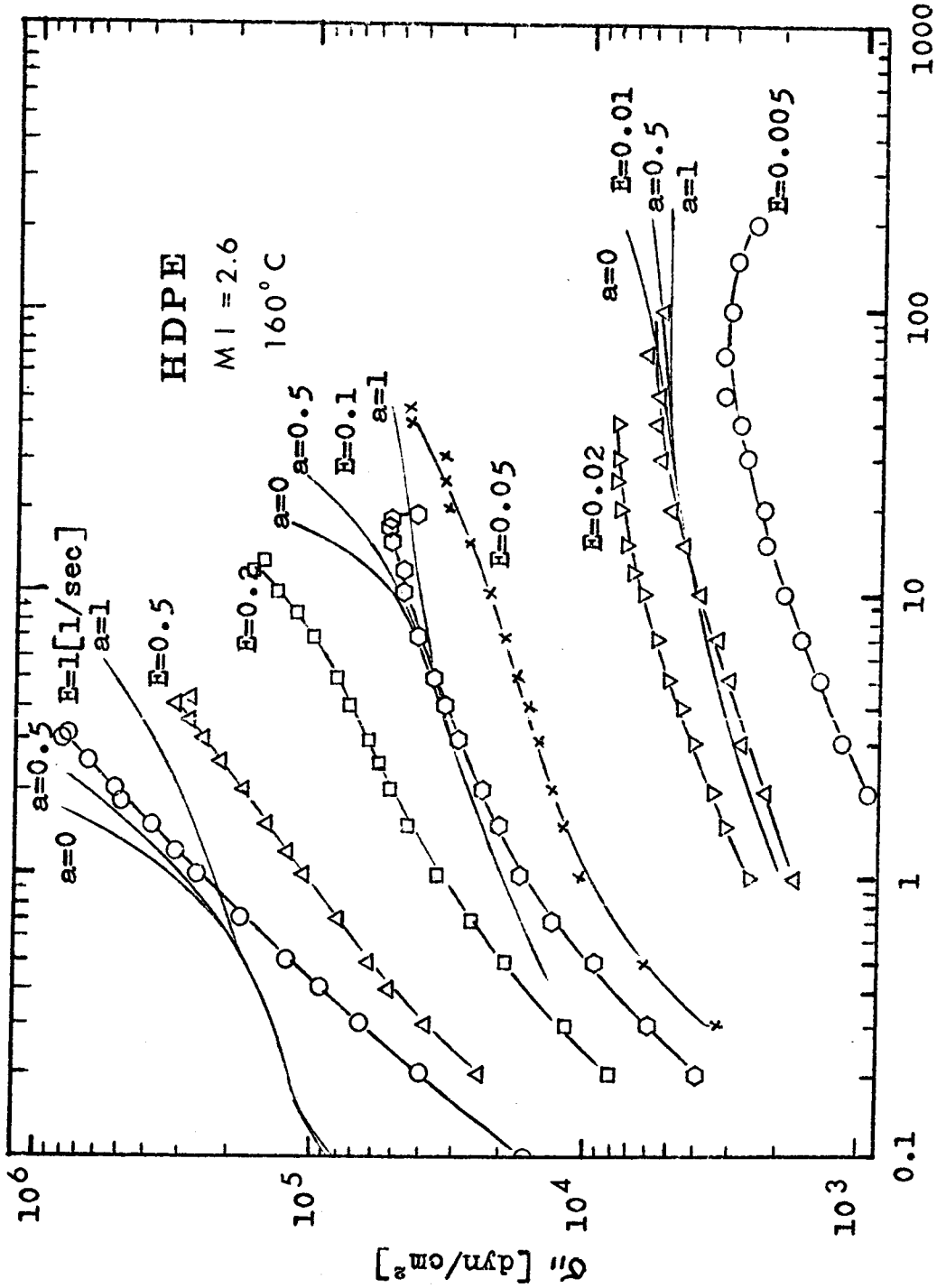


FIGURE 3.16 Stress development data of HDPE (MI = 2.6) and the Bogue and White model prediction based upon Chen oscillation data.

Takaki and Bogue [132] had predicted the stress development for Shell TC3-3C. It was reproduced in Fig. 3.17 together with the data obtained in this work. The value of a parameter of this prediction is $a = 0.29$ because $\sqrt{3}$ is lost in their effective relaxation times. A very good agreement is seen, although the data seems somewhat lower than predicted.

Based upon the material parameters obtained by the stress relaxation experiments (Table IV, page 82), the Bogue and White model prediction (Eq. (3.14)) was calculated for various polymers. Fig 3.18 shows the result for LDPE (MI = 1.7). As compared to the prediction based upon the shear oscillation data, the disagreements at low times are almost completely eliminated. As will be described later, the stress at this period is dominated by low relaxation time components. If we compare the shortest relaxation time for the oscillation data and the relaxation data, we find enormous difference (respectively 10^{-3} seconds and 0.789 seconds). This is the cause of the different predictions at short times. For the oscillation data, we can choose much shorter relaxation times out of the relaxation spectrum. However the contributions of the small relaxation times for the data greater than one second are not important. An excellent agreement between theory and experiment is obtained.

The data and the predictions for HDPE (MI = 0.1), PS (M_w = 240,000), and PP(MI = 0.42) are shown in Fig. 3.19,

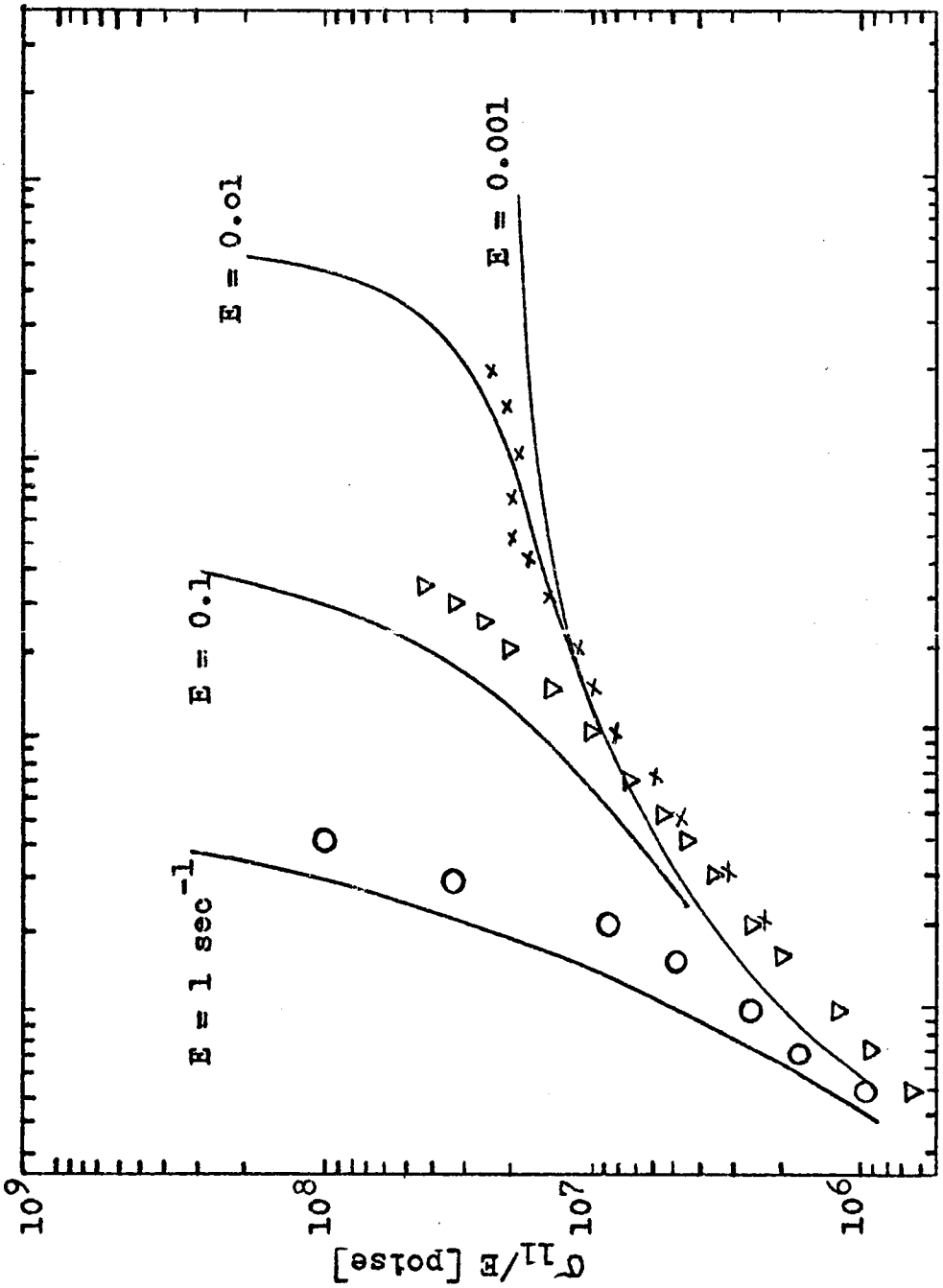


FIGURE 3.17 Predicted tensile stress by Takaki and Bogue and stress development data of Shell TC3-30 at 160°C.

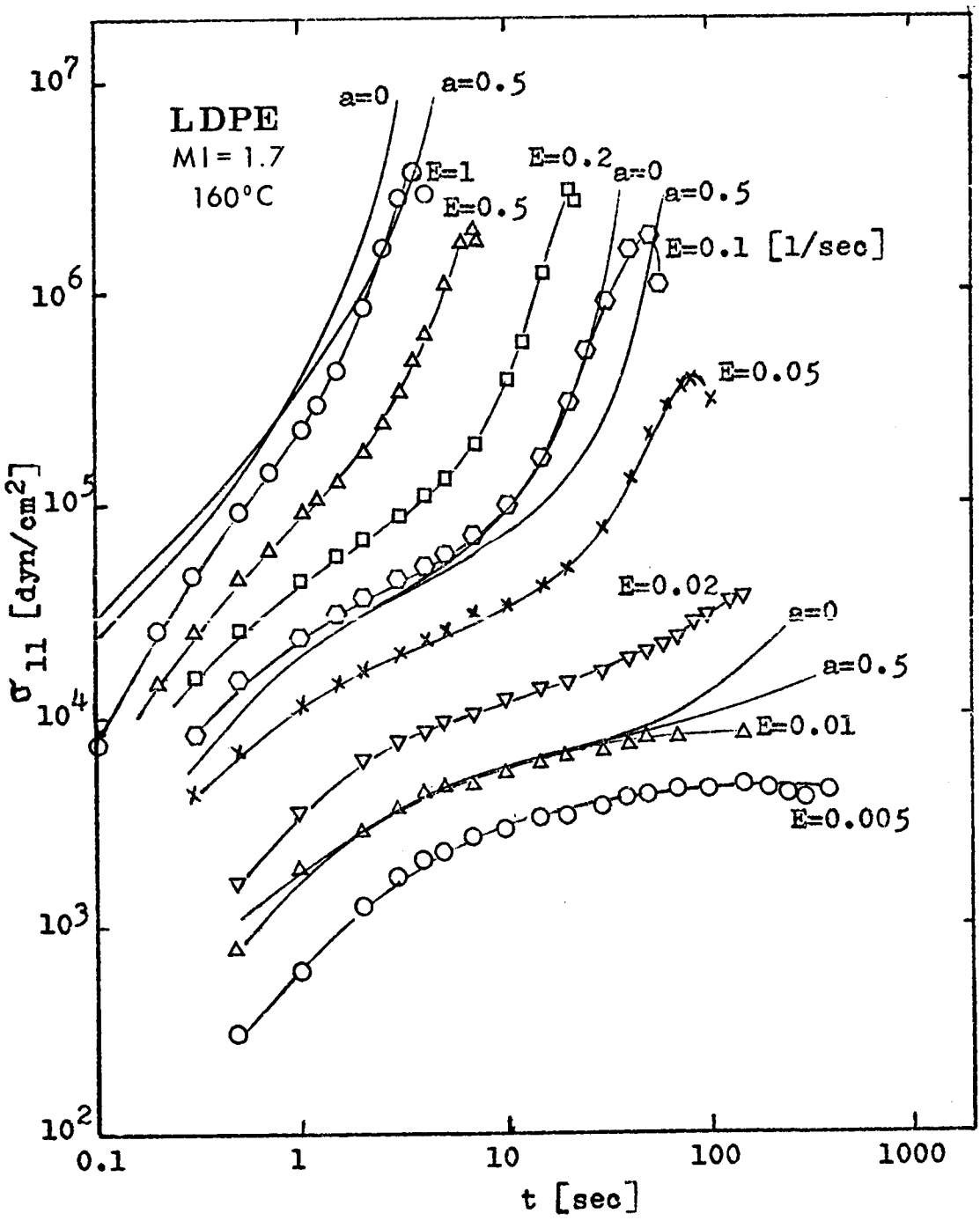


FIGURE 3.18 Stress development data of LDPE (MI = 1.7) and the Bogue and White model based upon stress relaxation data.

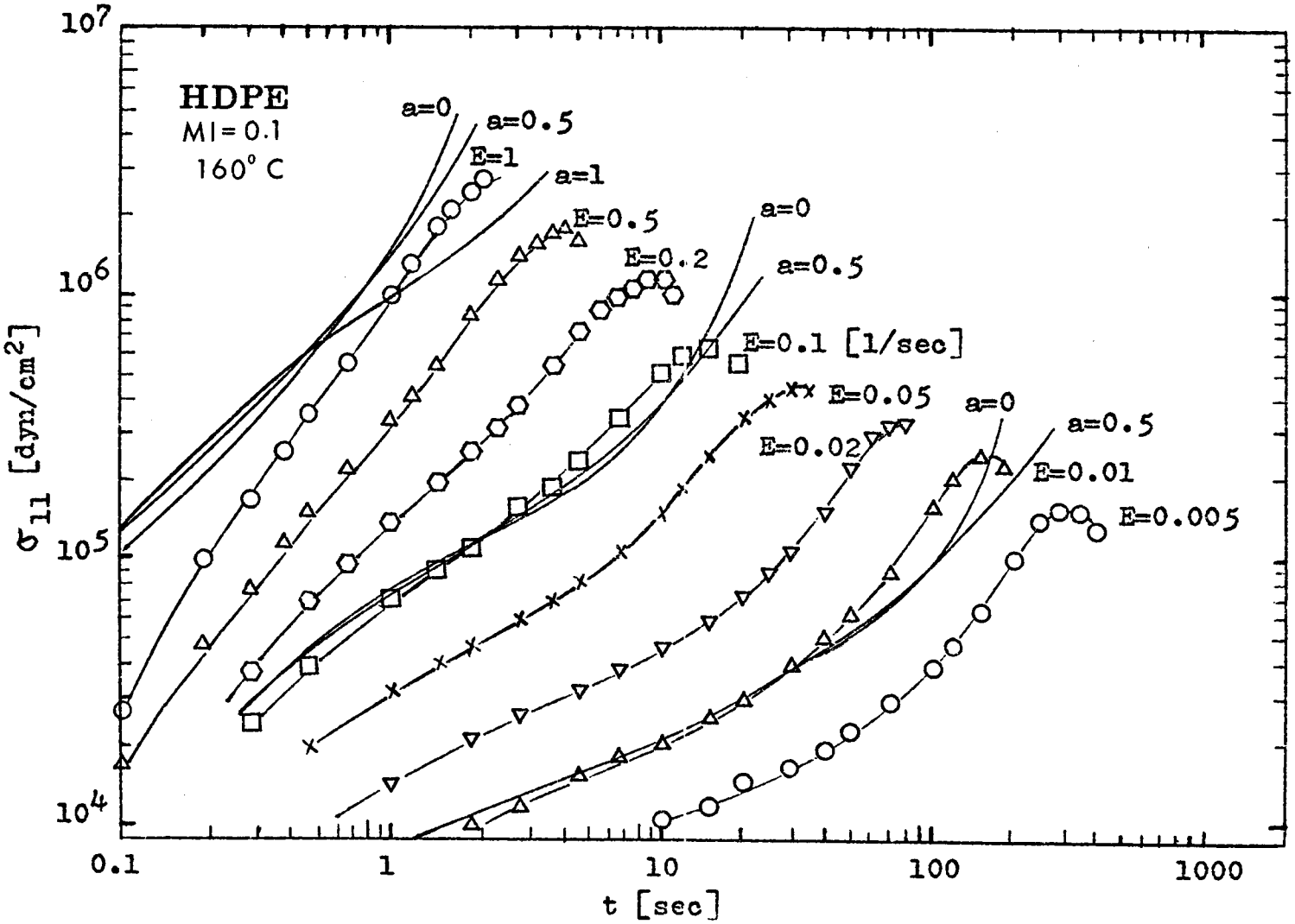


FIGURE 3.19 Stress development data of HDPE (MI = 0.1) and the Bogue and White model based upon stress relaxation data.

Fig. 3.20, and Fig. 3.21, respectively. The agreement between theory and the data for the HDPE and PP is not so good as the others. This, however, does not mean that the theory does not work well for these materials. This is probably caused by rather inaccurate methods, such as procedure X, of determining the relaxation parameters. However the relaxation experiment is a very easy method of determining relaxation times and the data still predicts essential features of the response.

The Bogue and White model was found to represent the transient elongational flow as well as transient shear flow reasonably well. However at early times of constant rate stretching, this model predicts higher stress level than the Lodge model which uses relaxation times unaffected by the deformation rate. For overshoot phenomena in the shear flow, this model gives an earlier peak of overshoot than the data as shown by Chen and Bogue [24]. This problem is probably caused by averaging the deformation rate from present to past when the material is still stationary.

Generalized Maxwell Model

Formulation of the transient stress for constant rate stretching. We shall now look at another model. If we employ the effective relaxation time λ_{eff} as in the Bogue and White model, but take instantaneous deformation rate invariant, the White and Metzner model can be written

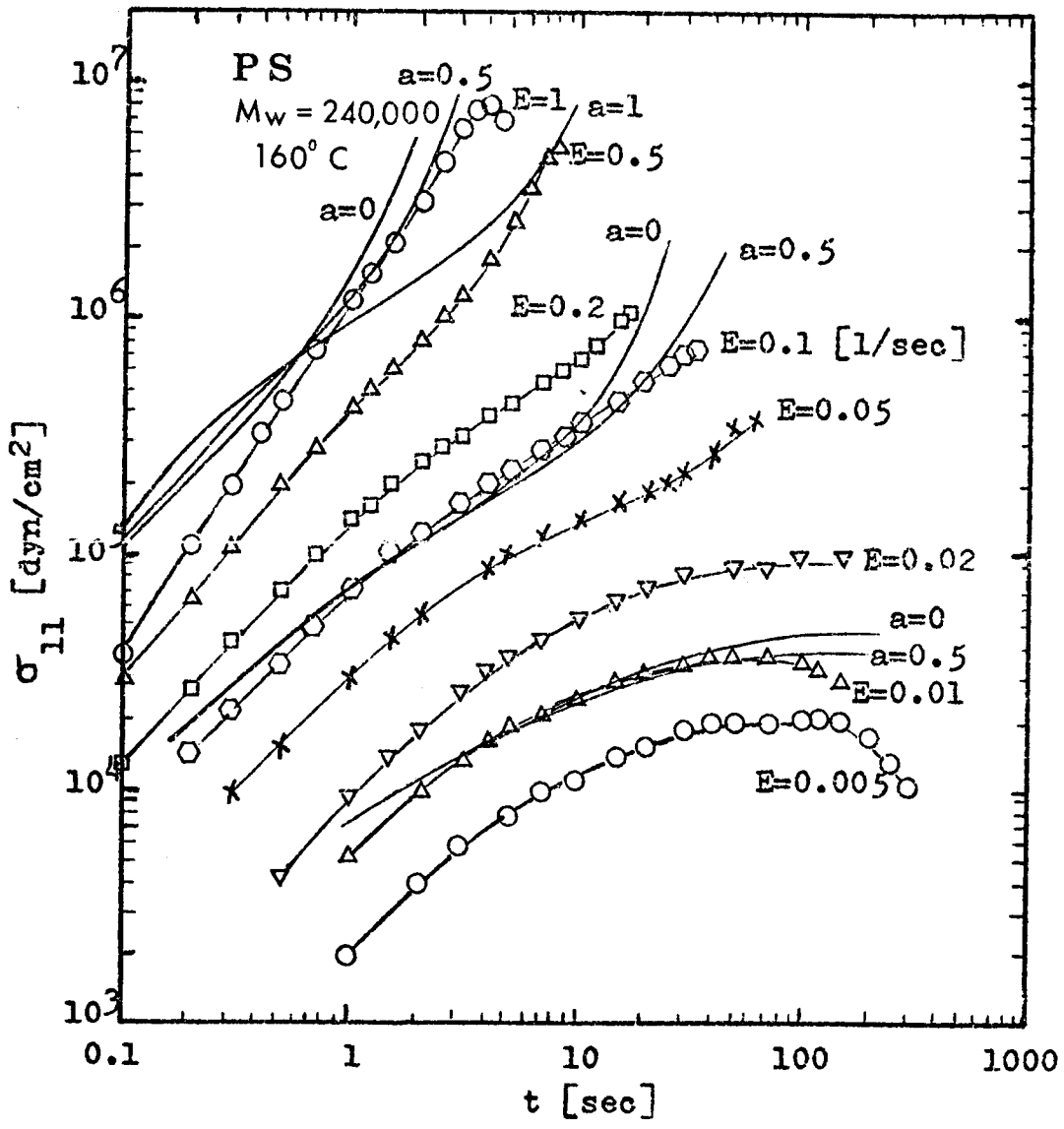


FIGURE 3.20 Stress development data of PS (Dow Styron 678 U) and the Bogue and White Model based upon stress relaxation data.

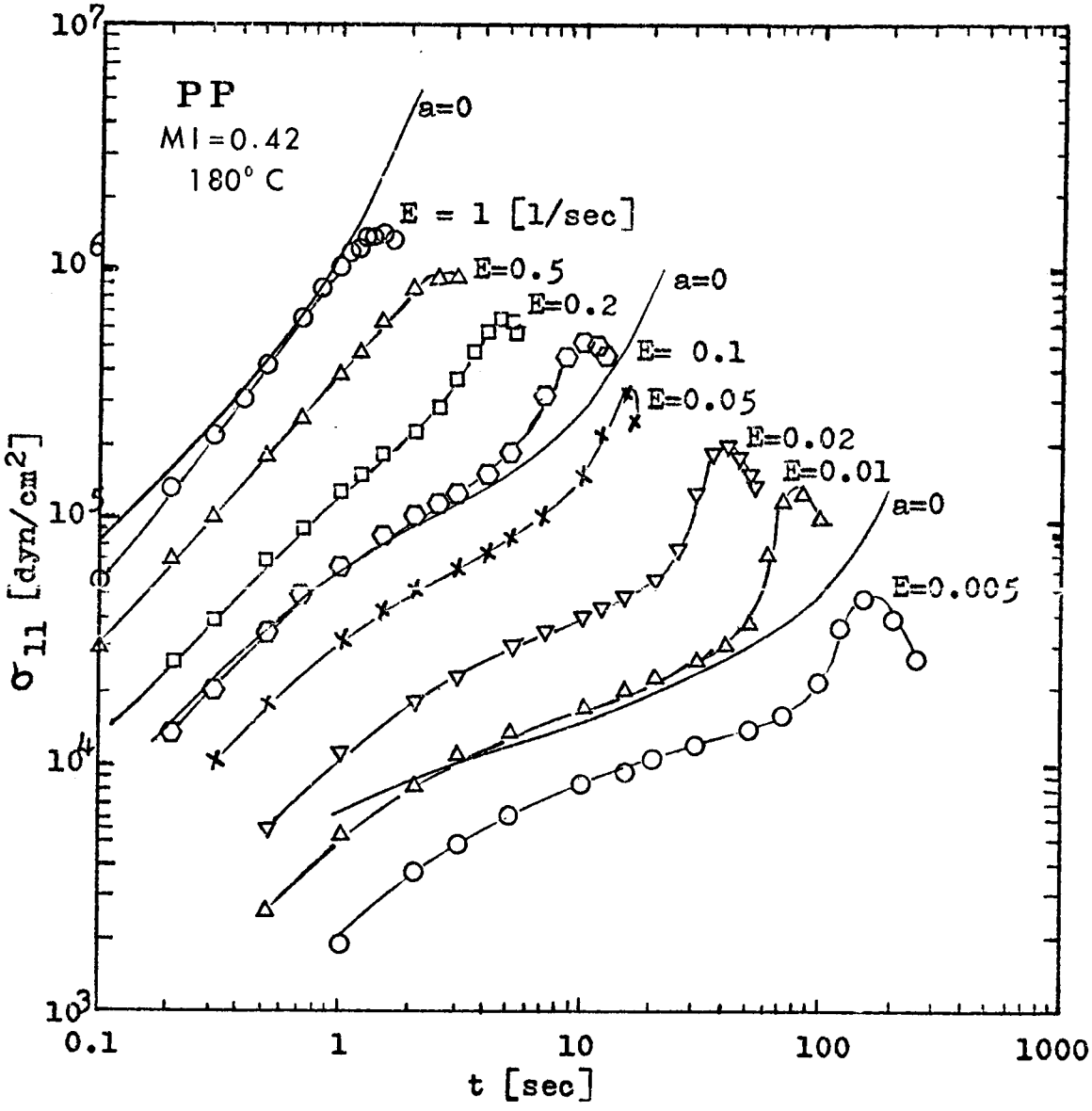


FIGURE 3.21 Stress development data of PP (MI = 0.42) and the Bogue and White model based upon stress relaxation data.

as

$$\underset{\sim}{\tau} + \lambda_{eff} \frac{\delta \underset{\sim}{\tau}}{\delta t} = 2G\lambda_{eff} \underset{\sim}{d} \tag{3.20a}$$

$$\frac{\delta \underset{\sim}{\tau}}{\delta t} = \frac{\partial \underset{\sim}{\tau}}{\partial t} + \underset{\sim}{v}\cdot\nabla\underset{\sim}{\tau} - \nabla\underset{\sim}{v}\cdot\underset{\sim}{\tau} - \underset{\sim}{\tau}\cdot(\nabla\underset{\sim}{v})^{T} \tag{3.20b}$$

$$\lambda_{eff} = \frac{\lambda}{1+a\lambda\sqrt{2II_d}} \tag{3.20c}$$

Employing the second invariant of rate of deformation tensor II_d in the effective relaxation time seems more natural in this differential model than in the integral models, because the rate of deformation tensor $\underset{\sim}{d}$ directly appears in this constitutive equation.

Applying this constitutive equation to the constant rate stretching problem, we obtain the following tensile stress (following Denn and Marrucci [34]):

$$\sigma_{11}(t) = 2GE\int_0^t \exp\left(-\int_s^t \frac{dz}{\lambda_{eff}}\right) \exp(2E(t-s))ds$$

$$+ GE\int_0^t \exp\left(-\int_s^t \frac{dz}{\lambda_{eff}}\right) \exp(-E(t-s))ds \tag{3.21}$$

Substituting

$$\frac{1}{\lambda_{eff}} = \frac{1}{\lambda} + \sqrt{3}\, aE \tag{3.22}$$

gives

$$\sigma_{11}(t) = 2GE\int_0^t e^{(2E-\frac{1}{\lambda})z}\,(e^{-Ez})^{\sqrt{3}a}\,dz$$

$$+ GE\int_0^t e^{-(E+\frac{1}{\lambda})z}\,(e^{-Ez})^{\sqrt{3}a}\,dz \qquad (3.23)$$

The final result is

$$\sigma_{11}(t) = \frac{2G\lambda E(1+\sqrt{3}a\lambda E)}{1-(2-\sqrt{3}a)\lambda E}\left[1-e^{-\{1-(2-\sqrt{3}a)\lambda E\}\frac{t}{\lambda}}\right]$$

$$+ \frac{G\lambda E(1+\sqrt{3}a\lambda E)}{1+(1+\sqrt{3}a)\lambda E}\left[1-e^{-\{1+(1+\sqrt{3}a)\lambda E\}\frac{t}{\lambda}}\right] \qquad (3.24)$$

In this formulation, the idea of average deformation rate suggested by Bogue [9] is naturally incorporated in Eq. (3.21) as a time integral of the effective relaxation time, although the time averaging is somewhat different. Careful examination of Eq. (3.23) suggests that the relaxation time nonlinearity may be interpreted to enter in a form of "strain," since

$$(e^{-Ez})^{\sqrt{3}a} = \left(\frac{L(0)}{L(z)}\right)^{\sqrt{3}a} \qquad (3.25)$$

where $L(z)$ and $L(0)$ represent instantaneous length and original length, respectively. Eq. (3.23) involves a weighted integral of "straining," "relaxation," and a "strain nonlinearity." The criteria of unbounded stress growth is seen to be the same as the Bogue and White model $(a \leq 2/\sqrt{3})$.

One can easily generalize the White and Metzner type Maxwell model employing many relaxation times and moduli (a Wiechert model) as applied by Spearot and Metzner [125]. For the Wiechert model, the tensile stress is written as

$$\sigma_{11}(t) = \sum_i \frac{2G_i\lambda_i E(1+\sqrt{3}a\lambda_i E)}{1-(2-\sqrt{3}a)\lambda_i E}\left[1-e^{-\{1-(2-\sqrt{3}a)\lambda_i E\}\frac{t}{\lambda_i}}\right]$$

$$+\sum_i \frac{G_i\lambda_i E(1+\sqrt{3}a\lambda_i E)}{1+(1+\sqrt{3}a)\lambda_i E}\left[1-e^{-\{1+(1+\sqrt{3}a)\lambda_i E\}\frac{t}{\lambda_i}}\right] \qquad (3.26)$$

This expression gives the same result as the Bogue and White model prediction Eq. (3.14), if ε of Eq. (3.14) is taken zero and the exponential integral function has decayed away.

Comparison. Single relaxation time White and Metzner model will be compared with experimental data first. The best method to obtain single characteristic relaxation time would be from the steady state shear data which includes shear stress σ_{12} and principal normal stress difference $\sigma_{11} - \sigma_{22}$. Using the following relation (see Eq. (2.29), page 18, and Table I, page 19)

$$\lambda_{eff} = \frac{\sigma_{11} - \sigma_{22}}{2\sigma_{12}\dot{\gamma}} \qquad (3.27)$$

the effective relaxation time may be calculated. Fig. 3.22 shows the effective characteristic relaxation times of LDPE (MI = 1.7) and HDPE (MI = 2.6) calculated by

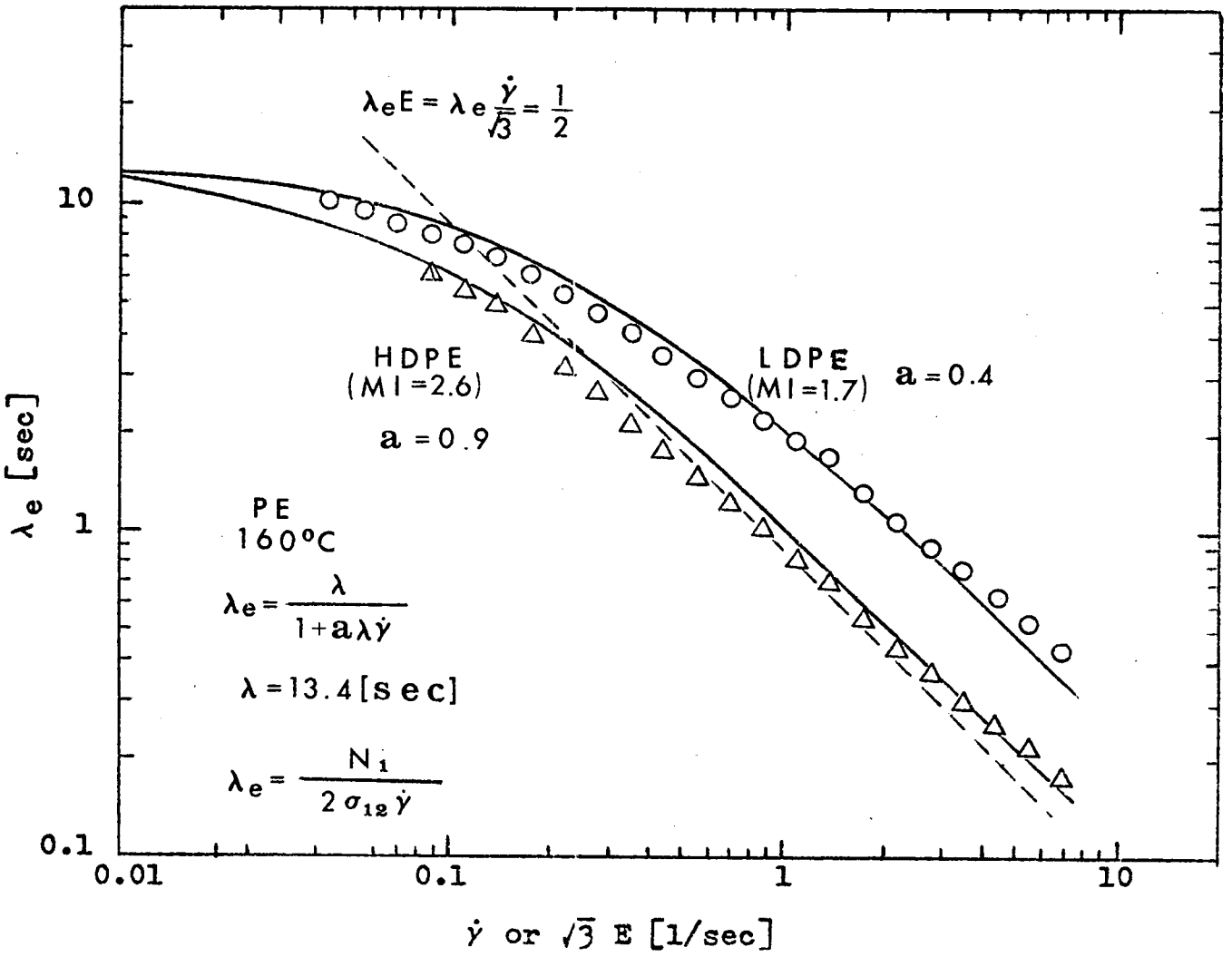


FIGURE 3.22 Deformation rate dependence of the characteristic relaxation time (calculated by steady shear data of Chen).

Chen's shear data [23]. The abscissa is the square root of the second invariant of the rate of deformation tensor. In order to have the same degree of deformation rate in shear and elongation, the numerical value of shear rate should be $\sqrt{3}$ times the elongation rate, for instance $\dot{\gamma} = \sqrt{3}$ 1/sec and $E = 1$ 1/sec are equivalent in degree of deformation rate.

It is seen that the expression of effective relaxation time used in the Bogue and White model closely approximates for the deformation rate dependence of the relaxation time for a reasonably wide range of deformation rates. For the same zero shear relaxation time ($\lambda_0 = 13.4$ sec), the value of relaxation time nonlinear parameter a would be $a = 0.4$ for LDPE (MI = 1.7) and $a = 0.9$ for HDPE (MI = 2.6) to give the best fit. The dotted line represents the critical value for the stress growth, i.e., $\lambda_e E = \frac{1}{2}$, of constant rate stretching if the effective relaxation time is obtained from the shear data. The left lower portion of the line represents the region $\lambda_e E < \frac{1}{2}$ where steady state can be achieved, and the right upper portion represents the unbounded stress growth region $\lambda_e E > \frac{1}{2}$. It may be seen that for very large values of the nonlinear parameter a such as $a > 2/\sqrt{3}$ the product $\lambda_e E$ always remains $\lambda_e E < \frac{1}{2}$.

The modulus may be calculated by

$$G = \eta / \lambda_{eff} \qquad (3.28)$$

where η is the non-Newtonian viscosity. Based upon the single relaxation time and its modulus, the stress prediction of the White and Metzner model can be calculated. As an example, stretching of the LDPE (MI = 1.7) at an intermediate rate $E = 0.1$ [1/sec] will be considered. Fig. 3.23 shows the predicted stress of the single relaxation time White and Metzner model and data points. Although the agreement at long times is very good, the disagreement at short times becomes apparent. It is found to be impossible to represent the data over a wide range of time scale by a single relaxation time.

The generalized form (a Wiechert model) which is a sum of many terms having different relaxation times is considered next. Based upon the relaxation times obtained by the stress relaxation, Eq. (3.26) was calculated for $a = 0$. The contribution of each term having different relaxation time is illustrated in Fig. 3.23. The total stress as a sum of each term can closely represent the data. It is clear that the stress at short times is dominated by terms of short relaxation times and the stress at long times, especially exponentially growing stress, is dominated by the terms of long relaxation times satisfying the condition $\lambda E > \frac{1}{2}$.

A comparison of the generalized Maxwell model Eq. (3.26) with the stress development data of a PS (Shell TC3-30) was made. The material parameters of this material

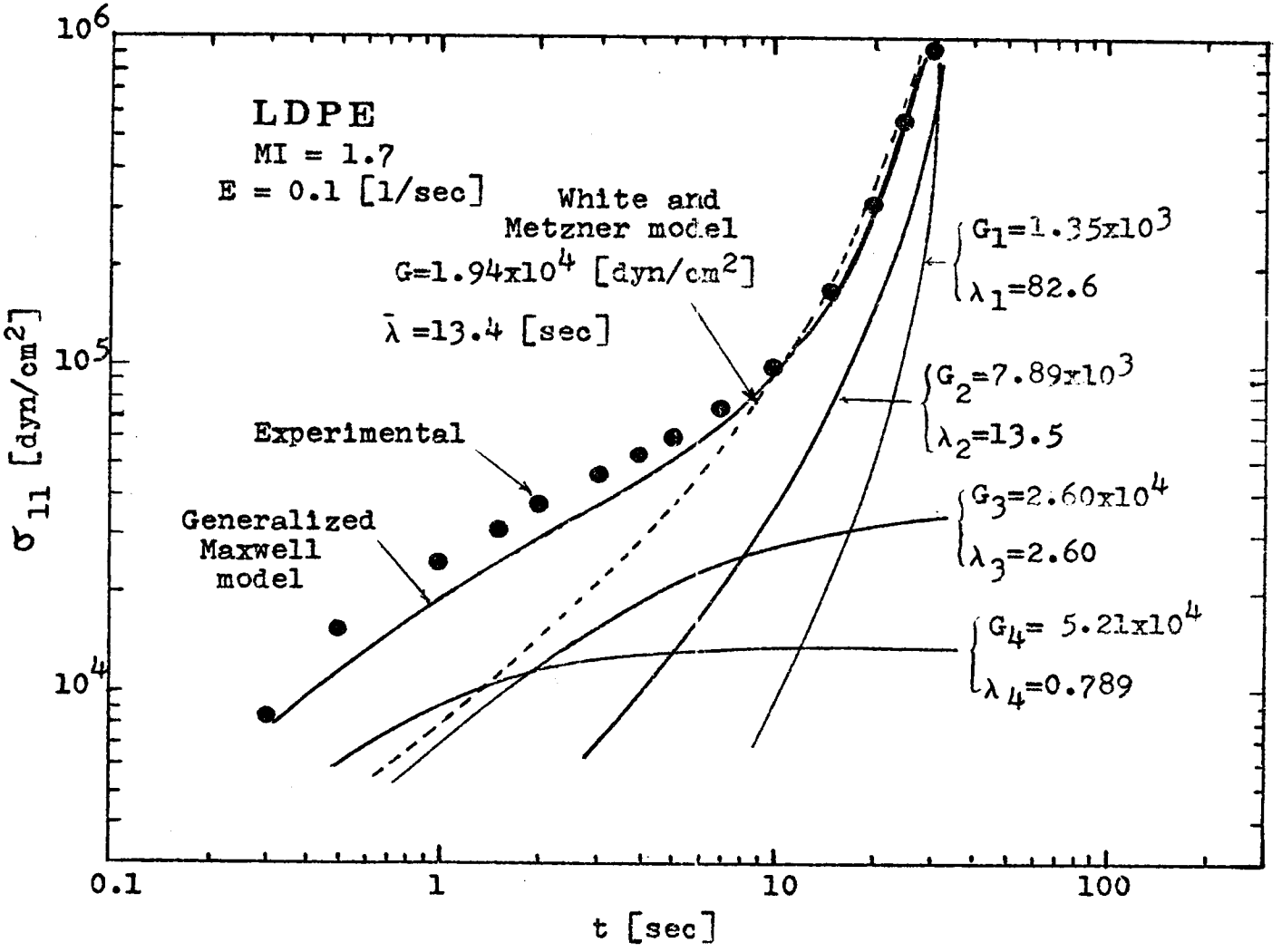


FIGURE 3.23 Comparison of White and Metzner model and Generalized Maxwell model with experimental data.

had been determined by Takaki and Bogue [132]. They tried to develop a connection between the various moduli and a rubbery plateau modulus of the dynamic data, adapting a molecular weight model suggested by Bogue, Masuda, Einaga, and Onogi [10].

This model connects the relaxation function of the Bogue and White model to molecular weight distribution as

$$m_1(t-s) = G^* \sum_{m=1}^{N} \sum_{n=1}^{N} W_m W_n \frac{e^{-(t-s)/\lambda^*_{mn}}}{\lambda^*_{mn}} \qquad (3.29)$$

where W_m is the weight fraction of species having molecular weight M_m, G^* is the elastic modulus of the entanglement (rubbery) regime, and N is the number of molecular weight species. This quadratic blending law model has its relaxation times of the form:

$$\lambda^*_{mn} = \frac{\sqrt{\lambda_m \lambda_n}}{1+\sqrt{3}a\sqrt{\lambda_m \lambda_n}E} \qquad (3.30)$$

Takaki and Bogue [131,132] determined the material parameters of Shell TC3-30 which could fit steady shear data and also a transient elongation data. One can use their values in the generalized Maxwell model Eq. (3.26) simply by replacing the various moduli with combinations of weight fractions as Eq. (3.29). The result computed by the IBM computer is shown in Fig. 3.24. A very good agreement between theory and data can be seen. Best fit seems to be obtained for the curve of a being somewhat

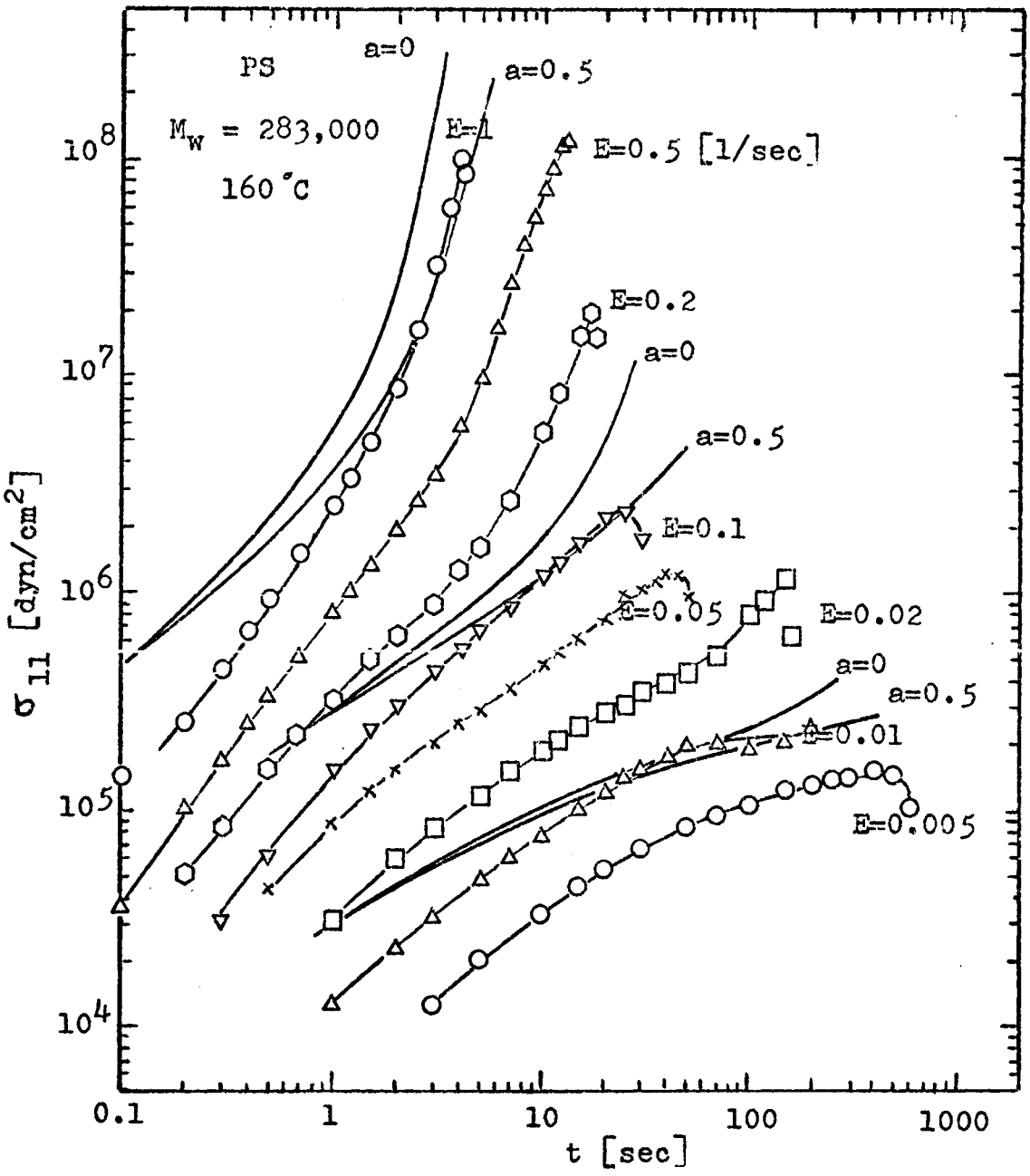


FIGURE 3.24 Stress development data of PS (Shell TC3-30) and the generalized Maxwell model (material parameters were determined by Takaki and Bogue).

smaller than 0.5 .

In this generalized Maxwell model, the curve employing reduced relaxation times such as $a = 0.5$ curve never exceeds the $a = 0$ curve. This seems physically reasonable and gives somewhat better fit to the data.

D. Mechanisms and Elongation to Failure

Qualitative Observations

In an early stage of the research, failure study was made with the equipment shown in Fig. 3.25. But in a later stage, the failure study was carried out together with the stress development study using the apparatus shown in Fig. 3.2, page 46. The low viscosity polymer wax broke up as soon as the material melted after it was immersed in the hot silicone oil. The failure mode was capillary failure induced by surface tension (in this case interfacial tension between oil and the material). A long filament of the polymer wax melted in the bath often shrunk, but a break-up was sometimes observed. If both ends of the filament were fixed, a break up into several pieces took place and semi-spherical droplets were eventually formed.

Observations on a little more viscous LDPE's (MI = 60, MI = 23) were also made. It was found that these materials apparently undergo almost indefinite elongation. However, the viscosities are still too low compared to

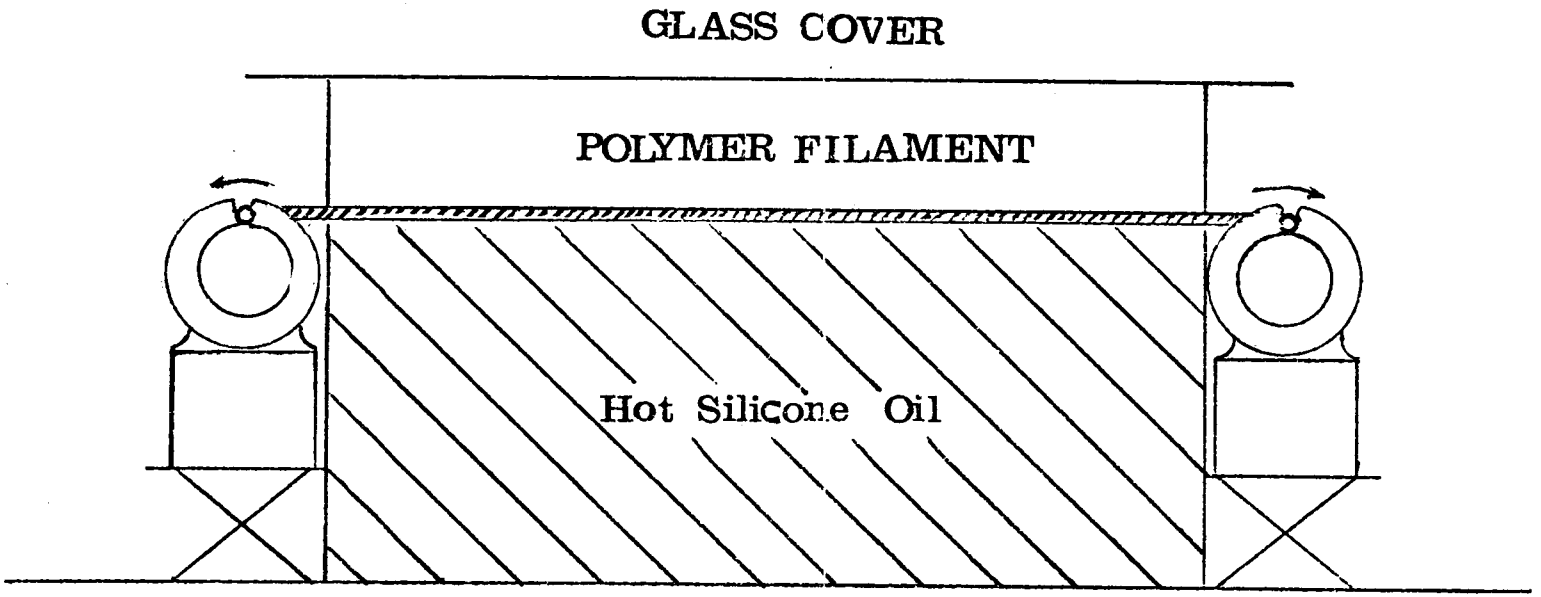


FIGURE 3.25 Experimental apparatus for study of tensile failure of molten polymer filaments.

the viscous resistance of silicone oil and also to the convective current of the oil. Thus the entire tensile force provided by the roller is not felt by the materials. For the relatively high viscosity LDPE's (MI = 1.7, MI = 2.1, and MI = 5.0), almost indefinite elongation seems possible as long as strecth rate is low. However at high stretch rates, the material fractures and the separated pieces snap back very rapidly ending up in a curl.

High density polyethylene, on the other hand, failed in a ductile manner; that is, complete reduction of cross-section in a particular region (neck). The snap back or recovery after the separation was slight. The ductile failure was more severe for higher molecular weight HDPE (MI = 0.1) than lower molecular weight HDPE (MI = 2.6).

Polypropylenes (PP) behaved more like HDPE's. The high molecular weight PP (MI = 0.42) failed in a ductile manner like the HDPE (MI = 0.1) and very small strains were obtained before failure. The intermediate molecular weight PP (MI = 6.6) extended more uniformly and combined dectile-fracture failure was observed after a relatively large elongation.

Polystyrenes (PS) and the polymethyl methacrylate (PMMA) failed more like LDPE's. They fractured at high stretch rates but showed stable elongation at low stretch rates and eventually failed in a ductile manner. The recovery after the separation was not as fast as LDPE's

and the curled end was not seen.

Total Elongation before Failure

The time until the material separates into two pieces may be defined as breaking time t_B . The breaking time was measured by a stop-watch as a function of stretch rate.

Raw data for the LDPE (MI = 1.7) and the LDPE (MI = 5.0) is shown in Fig. 3.26. The solid points were measured together with the stress development study using the apparatus shown in Fig. 3.2, page 46, and are probably more reliable. The rest of the data were measured using the equipment shown in Fig. 3.25. For a wide range of stretch rates, the curves show straight lines of slope -1 indicating the the logarithm of the elongation ratio (or Hencky strain) is constant in this range. A more useful plot of total strain against stretch rate is shown in Fig. 3.27. The data was shown in bands, since the scattering became severe in this plot. Despite the scattering, one can say that the higher viscosity LDPE (MI = 1.7) fails shorter than viscosity LDPE (MI = 5.0). One also notes that the total elongation decreases with increasing stretch rate.

The elongation to break data of the LDPE's at 130°C are shown in Fig. 3.28. These data are taken using the equipment shown in Fig. 3.25. The elongation is seen to be considerably reduced at this low temperature. The

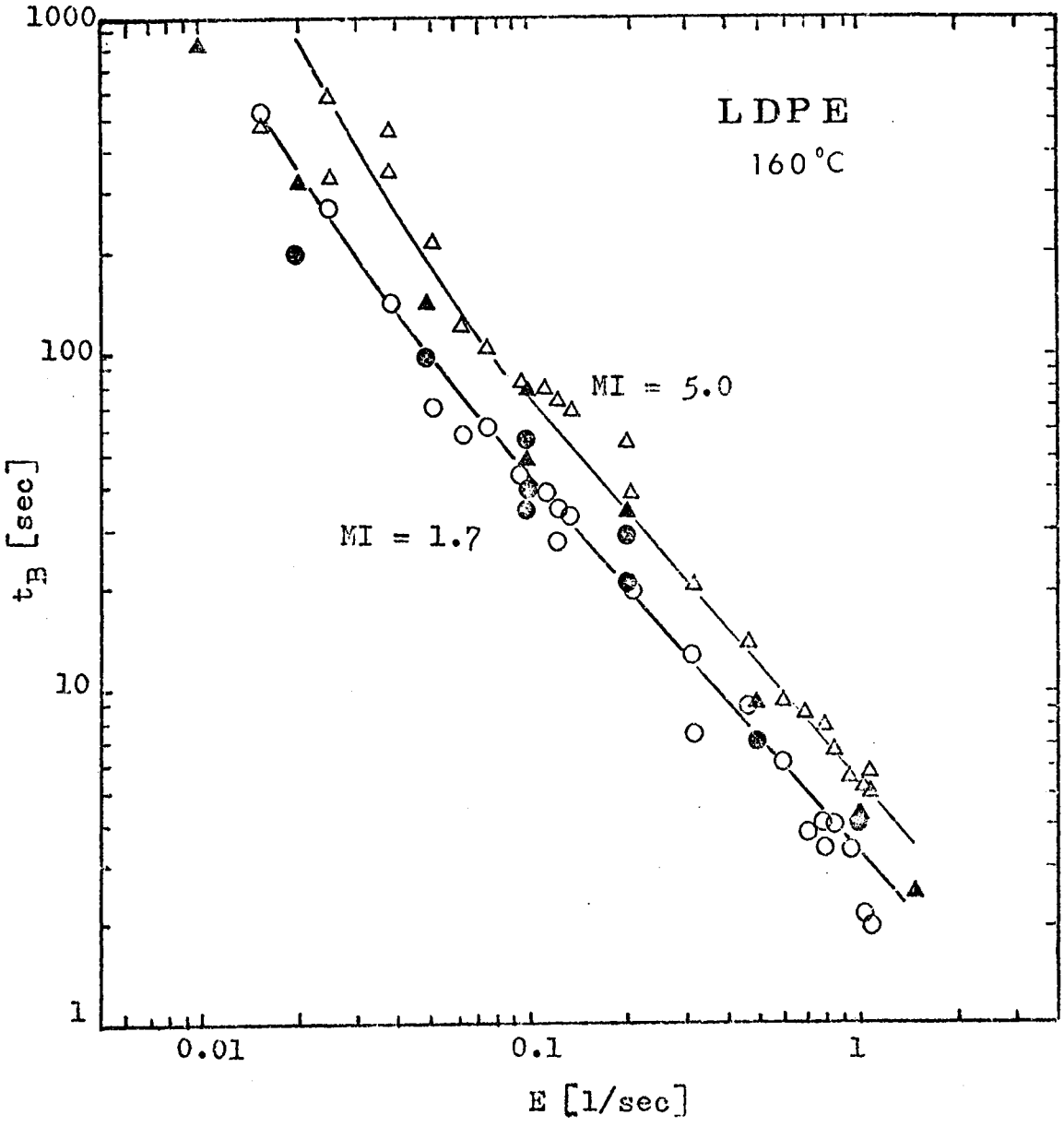


FIGURE 3.26 Time to break as a function of stretch rate at 160 °C.

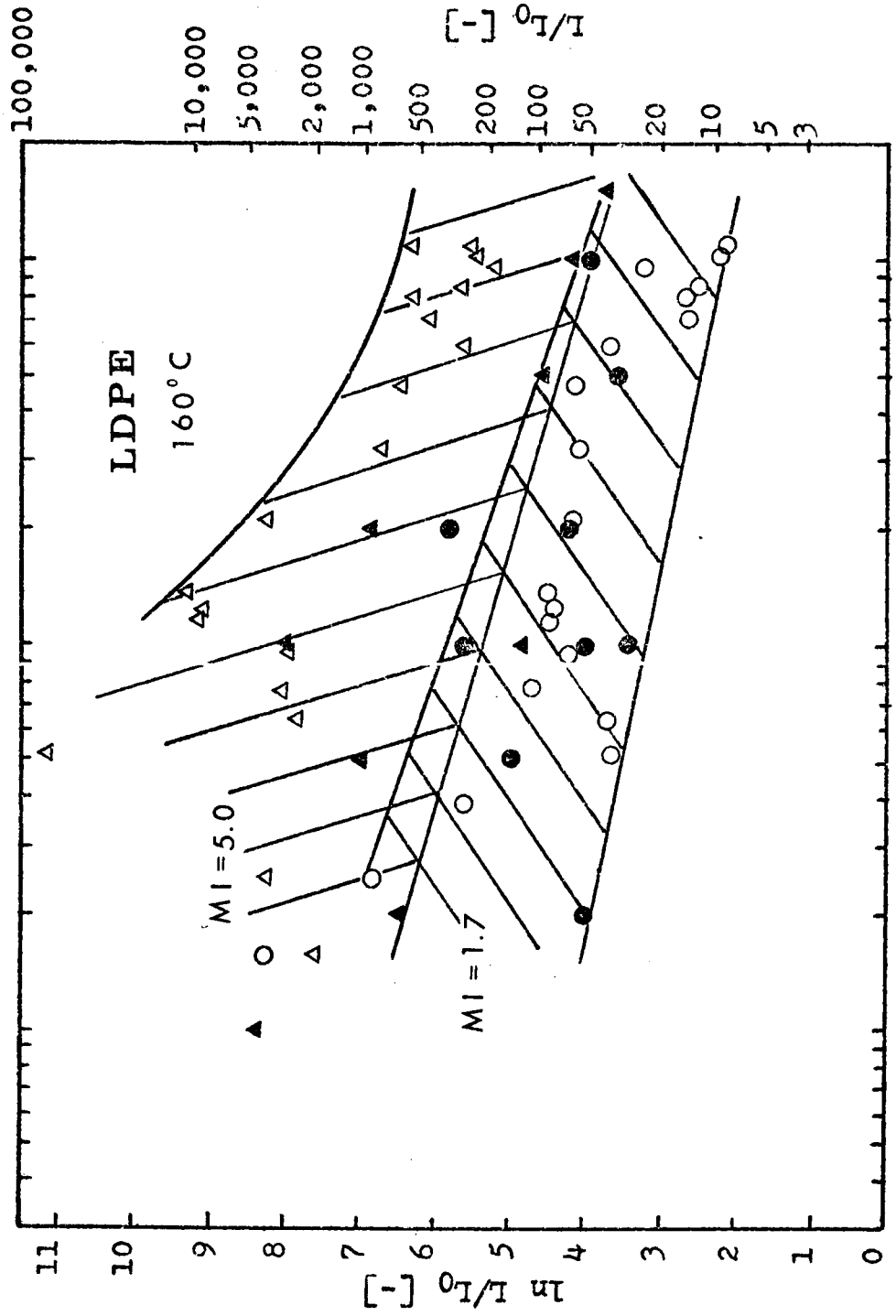


FIGURE 3.27 Total elongation as a function of stretch rate at 160°C.

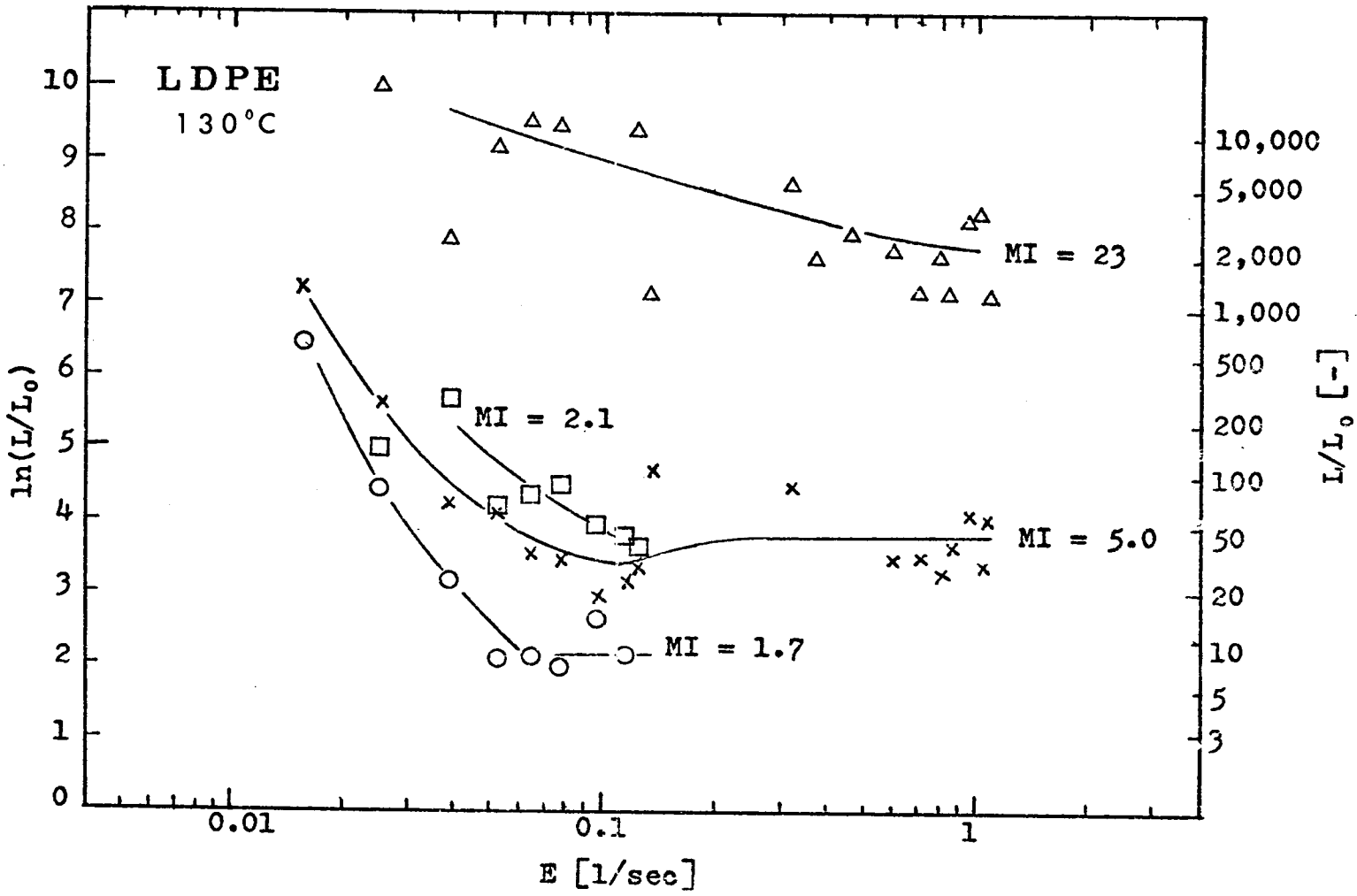


FIGURE 3.28 Total elongation of LDPE as a function of stretch rate at 130°C.

extension of the LDPE (MI = 1.7) is now limited to less than 10 times the original length even at strecth rate E = 0.1 [1/sec] but is seen to increase at lower stretch rates.

These results are consistent with the qualitative observations of the failure modes. The LDPE fails by fracture at high stretch rates but extends almost indefinitely at low stretch rates. As clearly seen in Fig. 3.6, page 60, for LDPE (MI = 5.0) and Fig 3.15, page 83, for LDPE (MI = 1.7); low density polyehtylene fractures at a critical stress around 4×10^6 [dyn/cm^2] . Due to the fracture instability, higher viscosity LDPE extends to a lesser extent.

The data of total elongation for high density polyethylenes (HDPE) are shown in Fig. 3.29. The elongation of HDPE's at 160°C is around 10 to 20 times the original and considerably shorter than LDPE's which is around 20 to 200 times. The elongation is seen to be independent of stretch rates. The failure mode was ductile failure even for the very high viscosity HDPE (MI = 0.1), although total elongation is shorter for this material. Fig. 3.19 also shows no critical stress for the HDPE (MI = 0.1).

The total elongations for various polymers except polyethylenes are summarized in Fig. 3.30. PS and PMMA extend about 20 to 100 times the original length.

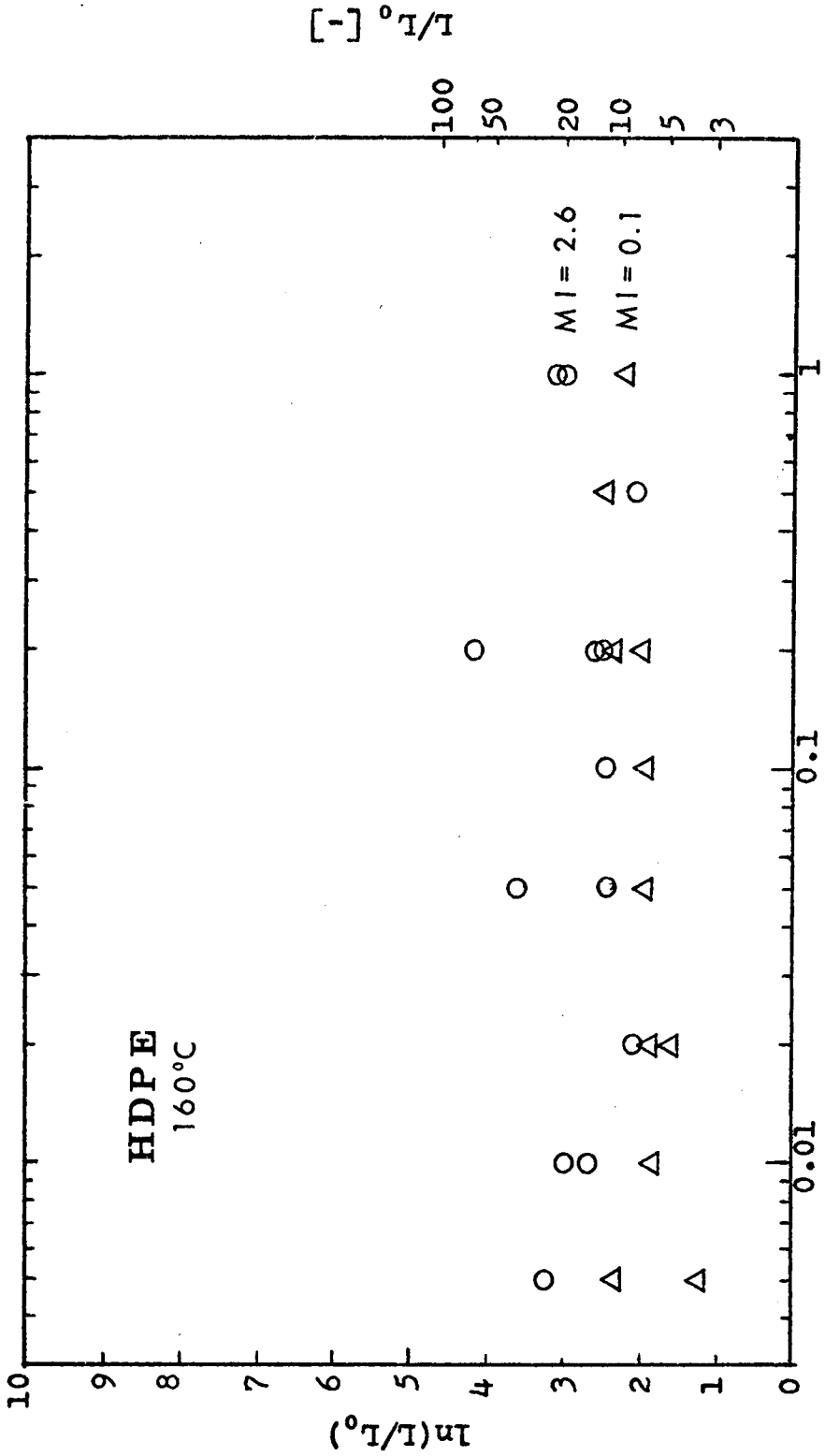


FIGURE 3.29 Total elongation of HDPE at 160°C.

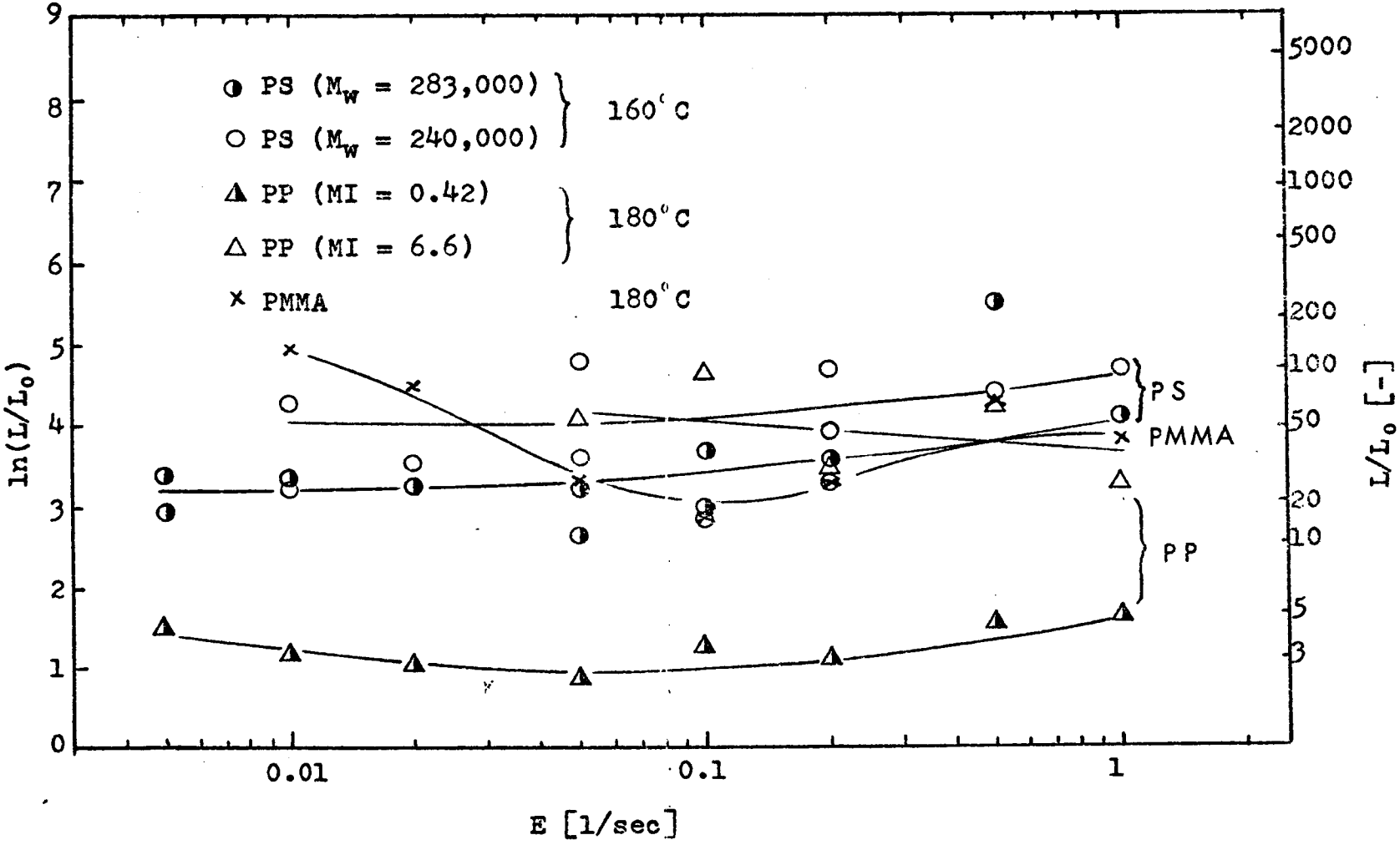


FIGURE 3.30 Total elongation for various polymers plotted against stretch rate.

The lower viscosity PS (Dow Styron 678 U) is seen to extend longer, consistent with fracture failure observation. Fig 3.24 shows the critical stress for the PS (Shell TC3-30) is as high as $1x10^8$ [dyn/cm^2] . This value is of the same order of magnitude as the brittle fracture stress that Onogi, Matsumoto, and Kamei [106] found. The maximum stress attained for the PS (Dow Styron 678 U) is around 10^7 [dyn/cm^2] as seen in Fig. 3.20, but much higher stress seems to be possible at stretch rates higher than $E = 1$ [1/sec] . The observed critical stress of the PMMA was around $3x10^7$ [dyn/cm^2] as seen in Fig. 3.13, page 70.

Interpretation of Failure

The capillary instability of the polymer wax and capillary-ductile combined instability will be theoretically investigated in the next chapter. Ductile failure at low stretch rates and fracture at high stretch rates of LDPE's, PS's, and PMMA will be investigated in a self consistent theory. The ductile failure of HDPE's and PP's is also theoretically interpreted in terms of high nonlinearity of relaxation time in the next chapter.

The fracture failure may not require rigorous theoretical investigation if we hypothesize that the fracture occurs at a critical stress. This failure can be interpreted with the present knowledge and therefore will be discussed in this section in detail.

The critical fracture stresses obtained at the highest stretch rate are in general agreement with the values obtained by Cogswell [29]. According to Cogswell's summary, fracture stresses of polymer melts are of the order of 10^7 to 10^8 [dyn/cm^2] . He showed highly branched and higher molecular weight polyethylenes were more brittle and had lower fracture stresses.

The breaking stresses at intermediate stretch rates of LDPE's and PS's (for example, see Fig 3.15, page 83, and Fig. 3.20, page 91) are lower than the fracture stress at the highest strecth rate. This point seems to be attributable to the distribution of relaxation times. As shown in Fig. 3.23, page 99 , terms of short relaxation times do not contribute to the exponentially growing stress, so that only high relaxation times satisfying the condition $\lambda E > \frac{1}{2}$ are directly responsible to the fracture stress. If one considers the distribution of relaxation time is closely related to the distribution of molecular weight, and further, short relaxation times are due to low molecular weight components and long relaxation times are due to high molecular weight components, only high molecular weight components fracture. When stretch rate is high enough so that all components contribute to the growing stress, the true fracture may occur instantaneously. However, if only parts of the components contribute and each component behaves independently, the breaking stress may be lower and instaneous fracture may not occur.

Fracture is further complicated by the combined effects of ductile instability. Due to the ductile instability, cross-section at a particular portion (neck) of the filament becomes smaller than other portions and a fracture may occur at this portion.

CHAPTER IV

THEORETICAL INVESTIGATION OF THE SPINNABILITY

The ability of fluids to be stretched into thin filaments will be investigated in this chapter. We shall refer to it as the spinnability of the fluid. Three mechanisms; capillary instability, ductile instability, and fracture, which are thought to limit the spinnability will be considered in a self-consistent theory. We will investigate the manner in which the spinnability would vary in a homologous series of organic compounds ranging from low molecular weights to high polymers. We will specifically analyze the stability of a liquid filament in a tensile test using the method of linear stability analysis.

A. Fundamental Equations for a Cylindrical Filament

In the stress field of a filament, the stress appears only in the axial direction as derived earlier (see Eq. (2.35), page 21). This makes the problem one dimensional, and we need consider the force balance only in the axial direction. The axial component of the equation of motion for a cylinder is

$$\rho\left(\frac{\partial V}{\partial t}+V\frac{\partial V}{\partial z}\right)=\frac{\partial \sigma_{zz}}{\partial z}+\frac{1}{r}\frac{\partial}{\partial r}(r\sigma_{rz})+\rho g \qquad (4.1)$$

Presuming a flat velocity profile, we integrate the above force balance equation over the cross section (multiplying by $2\pi r dr$). Then

$$\pi R^2\rho\left(\frac{\partial V}{\partial t}+V\frac{\partial V}{\partial z}\right)=\frac{\partial}{\partial z}(\pi R^2\sigma_{zz})+2\pi R(\sigma_{Rz}-\sigma_{zz}\frac{\partial R}{\partial z})+\pi R^2\rho g \qquad (4.2)$$

Now following Matovich and Pearson [77], we evaluate the shear stress σ_{Rz} at the surface of the cylinder. Continuity of the stress at the free surface requires (see Eq. (2.48), page 31)

$$\sigma_{Rz}n_R+\sigma_{zz}n_z=-\gamma\left(\frac{1}{R}\right)n_z \qquad (4.3)$$

where components of the surface normal vector $\underset{\sim}{n}$ are given by

$$n_R=\left(1+\frac{\partial R}{\partial z}\right)^{-\frac{1}{2}}\ ,\quad n_z=-\frac{\partial R}{\partial z}\left(1+\frac{\partial R}{\partial z}\right)^{-\frac{1}{2}} \qquad (4.4a,b)$$

This gives

$$\sigma_{Rz}=\frac{\partial R}{\partial z}\left(\sigma_{zz}+\frac{\gamma}{R}\right) \qquad (4.5)$$

Therefore the force balance equation for a cylinder is expressed by

$$\pi R^2\rho\left(\frac{\partial V}{\partial t}+V\frac{\partial V}{\partial z}\right)=\frac{\partial}{\partial z}(\pi R^2\sigma_{zz})+2\pi\gamma\frac{\partial R}{\partial z}+\pi R^2\rho g \qquad (4.6)$$

Note that the special case of the above equation where inertia, surface tension, and gravity are neglected is

$$\frac{\partial}{\partial z}(\pi R^2 \sigma_{zz}) = \frac{\partial F}{\partial z} = 0 \qquad (4.7)$$

where F is the tensile force acting on the filament cross-section. This simply states that the force is constant along the length.

The integration of the continuity equation can be carried out in the same manner. The continuity equation for a symmetrically deforming cylinder is

$$\frac{\partial V}{\partial z} + \frac{1}{r}\frac{\partial}{\partial r}(rU) = 0 \qquad (4.8)$$

where V is the axial velocity and U is the velocity in radius direction. Integration over the cross section (multiplying by $2\pi r dr$) gives

$$\frac{\partial V}{\partial z} = -\frac{2}{R} U_R \qquad (4.9)$$

where U_R is the radial velocity at the cylinder surface and is expressed by the substantial derivative of R :

$$U_R = \frac{DR}{Dt} = \frac{\partial V}{\partial t} + V\frac{\partial R}{\partial z} \qquad (4.10)$$

In tensile stretching, where a specimen of radius R and length L is stretched from both ends, the following relations hold.

$$\frac{\partial V}{\partial z} = \frac{1}{L}\frac{dL}{dt}\ , \quad \frac{\partial R}{\partial z} = 0 \qquad (4.11a,b)$$

Then Eq. (4.9) is rearranged to give

$$\frac{d}{dt}(\pi R^2 L) = 0 \qquad (4.12)$$

This simply states the volume of the cylinder remains constant.

B. Stability Analysis of Liquid Filaments

Disturbances and Linearized Disturbance Equations

We presume that the periphery of a filament is perturbed by an amount ξ (see Fig 4.1).

$$R = \bar{R} + \xi \qquad (4.13)$$

which results in the velocity and stress fields being perturbed according to

$$\underset{\sim}{V} = \bar{\underset{\sim}{V}} + \underset{\sim}{V}' \qquad (4.14a)$$

$$\underset{\sim}{\sigma} = \bar{\underset{\sim}{\sigma}} + \underset{\sim}{\sigma}' \qquad (4.14b)$$

where the bar refers to the steady homogeneous deformation and the prime denotes the perturbed value, which is small compared to unperturbed value. These perturbed relations are substituted into the fundamental equations: the force balance equation (Eq. (4.6)) and the continuity equation (Eq. (4.9)). These equations are linearized with respect to first order disturbance (order of ξ^2, $(\underset{\sim}{V}')^2$, and $(\underset{\sim}{\sigma}')^2$ are very small and are neglected) and the equations for the unperturbed deformations (equivalent to Eq. (4.6) and Eq. (4.9)) are subtracted.

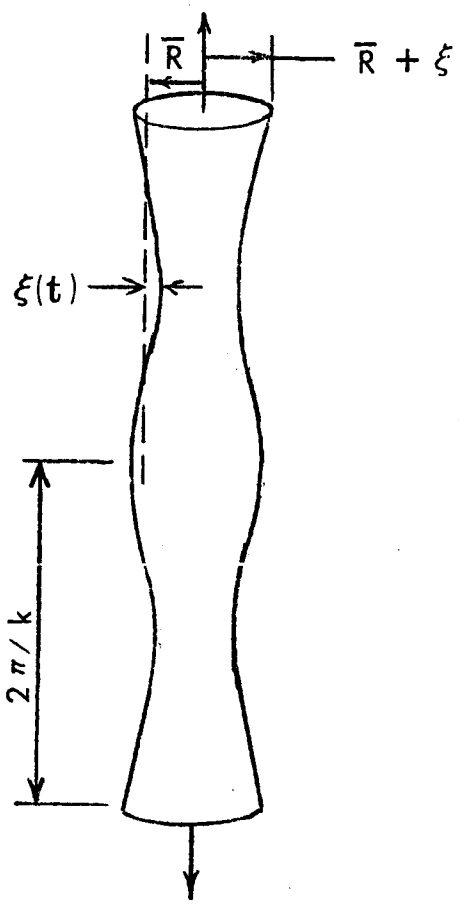


FIGURE 4.1 Filament containing a periodic disturbance in its diameter.

The perturbed force balance equation (Eq. (4.6)) becomes

$$\rho[\pi R^2(\frac{\partial V'}{\partial t} + \bar{V}\frac{\partial V'}{\partial x_1} + V'\frac{\partial \bar{V}}{\partial x_1}) + 2\pi R\xi\bar{V}\frac{\partial \bar{V}}{\partial x_1}]$$

$$= \frac{\partial}{\partial x_1}[\pi R^2(\sigma'_{11} + \frac{2\xi}{R}\bar{\sigma}_{11} + \frac{2\gamma}{R^2}\xi)] \quad (4.15)$$

where subscript 1 refers to axial direction. When inertia can be neglected (which is the practical case), the above force balance equation simplifies to

$$0 = \frac{\partial}{\partial x_1}[R^2(\tau'_{11} - \tau'_{22} - P'_\gamma) + \frac{2\xi}{R}(\bar{\tau}_{11} - \bar{\tau}_{22})] \quad (4.16)$$

The surface tension pressure is given by [70,112]

$$\bar{P}_\gamma = \frac{\gamma}{R}, \quad P'_\gamma = -\gamma(\frac{\xi}{R^2} + \frac{\partial^2 \xi}{\partial x_1^2}) \quad (4.17a,b)$$

Note that $\bar{P}_\gamma$ cancels out if we write in terms of extra stresses τ_{11}, τ_{22}.

The perturbed continuity equation is obtained by Eq. (4.9) as

$$\frac{\partial \bar{V}}{\partial x_1} + \frac{\partial V'}{\partial x_1} = -\frac{2}{R+\xi}[\bar{U}_R + U'_R] \quad (4.18)$$

After linearization, we obtain

$$\frac{\partial \bar{V}}{\partial x_1} = -\frac{2}{R}\bar{U}_R, \quad \frac{\partial V'}{\partial x_1} = -\frac{2}{R}[U'_R - \frac{\bar{U}_R}{R}\xi] \quad (4.19a,b)$$

where

$$\bar{U}_R = \frac{\partial R}{\partial t} , \quad U'_R = \frac{D\xi}{Dt} \qquad (4.20a,b)$$

We will presume that the disturbance ξ varies periodically along the length of the filament, i.e., (see Fig. 4.1)

$$\xi(t,x_1) = \hat{\xi}(t)e^{ikx_1} \qquad (4.21)$$

This makes all other disturbed values such as $\underset{\sim}{V}'$ and $\underset{\sim}{\sigma}'$ vary with length in a similar manner.

$$\underset{\sim}{V}'(t,x_1) = \hat{\underset{\sim}{V}}(t)e^{ikx_1} \qquad (4.22a)$$

$$\underset{\sim}{\sigma}'(t,x_1) = \hat{\underset{\sim}{\sigma}}(t)e^{ikx_1} \qquad (4.22b)$$

For stretching with constant rate E, the periodicity of the disturbances change according to

$$\ell(t) = \ell(0)e^{Et} , \quad k(t) = \frac{2\pi}{\ell(t)} = k(0)e^{-Et} \qquad (4.23a,b)$$

where ℓ is the wavelength and k is the wave number. Then the continuity equation (Eq. (4.19)) relates the stretch rates as

$$\frac{\partial \bar{V}}{\partial x_1} = E , \quad \frac{\partial V'}{\partial x_1} = E' = -\frac{2}{R}\left[\frac{\partial \hat{\xi}}{\partial t} + \frac{E}{2}\hat{\xi}\right] e^{ikx_1} \qquad (4.24a,b)$$

Here the time derivative following the fluid (substantial derivative) has simplified to

$$\frac{D\xi}{Dt} = \frac{\partial \xi}{\partial t} + \bar{V}\frac{\partial \xi}{\partial z}$$

$$= \frac{\partial \hat{\xi}}{\partial t} e^{ikx_1} + \hat{\xi} i x_1 (-E) k e^{ikx_1} + E x_1 ik\xi$$

$$= \frac{\partial \hat{\xi}}{\partial t} e^{ikx_1} \qquad (4.25)$$

In this derivative we are looking at a particular point of an extending filament such as a necked position.

Now the fundamental equations for the stability analysis are both the basic relations and perturbed relations of equation of motion (Eq. (4.6) and Eq. (4.15)) and continuity equation (Eq. (4.9) and Eq. (4.19)). In order to relate the stress tensor of the equation of motion and kinematics of the continuity equation, we need to specify constitutive equation. First we consider the Newtonian fluid as the simplest case, and we go on to treat the viscoelastic fluid.

Newtonian Fluid Filaments

In extending Newtonian fluid filaments, breakup generally results from the interaction of capillary and ductile instability. For low viscosity fluids, we may neglect extension since filaments break rapidly only by capillarity, while for high viscosity fluids we may neglect inertia. Let us look at each of these cases in turn.

Capillary instability. For low viscosity fluids, the capillarity instability dominates the failure. This is the classical asymptote worked out by Rayleigh [112] and Weber [146] for an originally stationary filament. We can readily reproduce their asymptotic result of small kR starting with equations developed in the previous section.

The perturbed force balance (Eq. (4.15)) becomes

$$\rho R^2 \frac{\partial V'}{\partial t} = \frac{\partial}{\partial x_1} [R^2(\tau'_{11} - \tau'_{22} - P_\gamma')] \tag{4.26}$$

since the filament is originally stationary ($\bar{V} = 0$, $\bar{\tau}_{11} = \bar{\tau}_{22} = 0$). If we differentiate the above relation with respect to x_1 and introduce the following relations

$$\frac{\partial V'}{\partial x_1} = - \frac{2}{R} \frac{\partial \hat{\xi}}{\partial t} e^{ikx_1} \tag{4.27}$$

$$\tau'_{11} - \tau'_{22} = 3\eta \frac{\partial V'}{\partial x_1} \tag{4.28}$$

$$P'_\gamma = - \frac{\gamma}{R^2} (1-k^2R^2)\xi \tag{4.29}$$

we obtain

$$\frac{d^2\hat{\xi}}{dt^2} + \frac{3\eta k^2}{\rho} \frac{d\hat{\xi}}{dt} - \frac{\gamma k^2}{2\rho R} (1-k^2R^2)\hat{\xi} = 0 \tag{4.30}$$

This is a constant coefficient ordinary differential equation, so that the solution is of the form

$$\hat{\xi}(t) = \hat{\xi}(0)e^{\alpha t} \tag{4.31a}$$

where α is found by the characteristic equation

$$\alpha^2 + \frac{3\eta k^2}{\rho}\alpha - \frac{\gamma k^2}{2\rho R}(1-k^2R^2) = 0 \tag{4.31b}$$

This may readily be seen to be Weber's [146] asymptotic solution of Rayleigh's analysis [112] described earlier (see Eq. (2.52, page 36). The application of this equation is discussed there.

Interaction of capillary and ductile instability. Let us now turn to the stability problem of a relatively high viscosity Newtonian fluid. Here we consider the interaction of surface tension and ductility in the absence of inertial effects. The equation of motion Eq. (4.16) becomes

$$\frac{\partial}{\partial x_1}\left[R^2\left\{3\eta\frac{\partial V'}{\partial x_1} + \frac{\gamma}{R^2}(1-k^2R^2)\xi\right\} + \frac{2\xi}{R}3\eta\frac{\partial \bar{V}}{\partial x_1}\right] = 0 \tag{4.32}$$

If we substitute the following stretch rate relation (combined form of Eq. (4.19) and Eq. (4.20))

$$\frac{\partial \bar{V}}{\partial x_1} = -\frac{2}{R}\frac{\partial R}{\partial t}, \quad \frac{\partial V'}{\partial x_1} = -\frac{2}{R}\left[\frac{\partial \hat{\xi}}{\partial t} - \frac{1}{R}\frac{\partial R}{\partial t}\right]e^{ikx_1} \tag{4.33a,b}$$

Eq. (4.32) can be transformed to

$$\frac{1}{\xi}\frac{\partial \hat{\xi}}{\partial t} = -\frac{1}{R}\frac{\partial R}{\partial t} + \frac{\gamma}{6\eta R}(1-k^2R^2) \tag{4.34}$$

The maximum growth rate is for k equal to zero which means that the disturbance of very long wavelength is the most unstable mode. In this case $\hat{\xi}$ becomes equal to ξ (see Eq. (4.21)).

If we specify the kinematics to be stretching with a constant rate E, then

$$R = R(0)\, e^{-\frac{E}{2}t} \tag{4.35}$$

Eq. (4.34) can be integrated to give

$$\ln \frac{\xi(t)}{\xi(0)} = \frac{\gamma}{3\eta R(0)E}\left(e^{\frac{E}{2}t} - 1\right) + \frac{E}{2}t \tag{4.36}$$

This shows the additive effect of capillarity and ductility. Note that the capillarity progressively becomes important as time proceeds, since the filament radius becomes thinner with time. The first term of the above equation is equivalent to Eq. (32) of Tomotika [138] with $k = 0$. Thus it is seen that his analysis does not include the ductile instability (which is the second term of Eq. (4.36)).

For stretching with a constant speed V

$$L(t) = L(0) + Vt \tag{4.37}$$

then

$$\frac{1}{R(t)} = \frac{1}{R(0)}\sqrt{1+\frac{V}{L(0)}t}\,, \quad -\frac{1}{R}\frac{\partial R}{\partial t} = \frac{V}{2L} \tag{4.38a,b}$$

This gives the disturbance growth as

$$\ln \frac{\xi(t)}{\xi(0)} = \frac{\gamma L(0)}{9\eta R(0) V}\left\{\left(\frac{L(t)}{L(0)}\right)^{3/2} - 1\right\} + \frac{1}{2}\ln\frac{L(t)}{L(0)} \qquad (4.39)$$

We note that in the absence of surface tension γ, the above equation becomes equivalent to Eq. (4.36) since $Et = \ln[L(t)/L(0)]$. This means that the ductile instability of the Newtonian fluid is independent of kinematics and only depends on stretch ratio. In fact, if we neglect surface tension, Eq. (4.34) is rearranged to give

$$\frac{d}{dt}(R\xi) = 0 \qquad (4.40)$$

This is a linearized form of Orowan's ductile failure analysis [107] which is based on the model shown in Fig. 4.2 and does not require specifying the kinematics. Orowan showed that the cross-sectional area of a defect A' remained constant with time, that is

$$\frac{dA'}{dt} = \frac{d}{dt}\left[\pi R^2 - \pi(R-\xi)^2\right] = \pi\frac{d}{dt}(2R\xi - \xi^2) = 0 \qquad (4.41)$$

where linearization gives the same result as Eq. (4.40).

The error due to linearization is investigated here. If we did not linearize, Eq. (4.41) gives

$$\ln \frac{\xi(t)}{\xi(0)} = \frac{Et}{2} + \frac{1}{R}\{\xi(t) - \xi(0)\} \qquad (4.42)$$

When $\xi(t) \ll R$, the distance grows exponentially with a

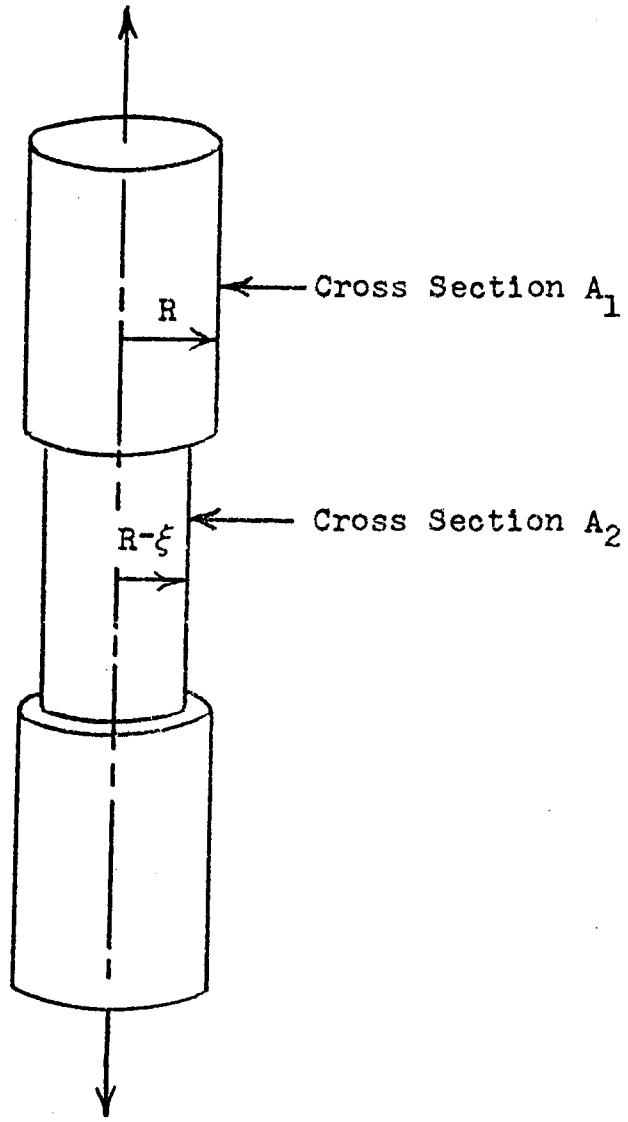


FIGURE 4.2 Orowan-Chang-Lodge model of disturbance in a filament being stretched.

rate $Et/2$, but when the disturbance $\xi(t)$ grows to the size of the cylinder radius R , the growth rate is further accelerated. However, as long as $\xi(t) \ll R$, this linearization error is negligible.

Viscoelastic Fluid Filaments

In this section, we turn to viscoelastic fluids and consider in particular the White and Metzner equation. In Cartesian coordinates, this constitutive equation is written as:

$$\tau_{ij} + \lambda_e \frac{\delta \tau_{ij}}{\delta t} = 2G\lambda_e d_{ij} \tag{4.42}$$

$$\frac{\delta \tau_{ij}}{\delta t} = \frac{\partial \tau_{ij}}{\partial t} + V_m \frac{\partial \tau_{ij}}{\partial x_m} - \frac{\partial V_i}{\partial x_l} \tau_{mj} - \frac{\partial V_j}{\partial x_m} \tau_{im} \tag{4.43}$$

We shall consider that the relaxation time is dependent on deformation rate. It was considered that the most useful form was to take the effective relaxation time used in the Bogue and White model, i.e.,

$$\lambda_e = \frac{\lambda}{1 + a\lambda\sqrt{2II_d}} \tag{4.44}$$

For the constant rate stretching, this takes the form

$$\lambda_e = \frac{\lambda}{1 + \sqrt{3}a\lambda E} \tag{4.45}$$

Perturbed equation of state. Although it is natural to proceed from the simplest case to more complicated

case, the perturbed relations of this constitutive equation will be derived in the most general case in this section, in order to avoid repetition. The most general case to be considered is that the viscoelastic fluid (whose relaxation time is dependent on deformation rate) is stretched at a constant rate E.

The procedure for obtaining the perturbed constitutive equation will be shown for axial component (1). The radial component (2) can be derived in the same way. The stretch rate relation was obtained in a previous section as

$$E = \frac{\partial \bar{V}_1}{\partial x_1}, \quad E' = \frac{\partial V'_1}{\partial x_1} = -\frac{2}{\bar{h}}\left[\frac{\partial \hat{\xi}}{\partial t} + \frac{E}{2}\hat{\xi}\right] e^{ikx_1} \qquad (4.46a,b)$$

The Oldroyd derivative is perturbed as

$$\frac{\delta \bar{\tau}_{11}}{\delta t} + \frac{\delta \tau'_{11}}{\delta t} = \frac{\partial \bar{\tau}_{11}}{\partial t} + \frac{\partial \tau'_{11}}{\partial t} + \bar{V}_1 \frac{\partial \tau'_{11}}{\partial x_1}$$

$$- 2(\bar{\tau}_{11} + \tau'_{11})\left(\frac{\partial \bar{V}_1}{\partial x_1} + \frac{\partial V'_1}{\partial x_1}\right) \qquad (4.47)$$

Then the basic relation and the perturbed relation are

$$\frac{\delta \bar{\tau}_{11}}{\delta t} = \frac{\partial \bar{\tau}_{11}}{\partial t} - 2E\bar{\tau}_{11} \qquad (4.48)$$

and

$$\frac{\delta \tau'_{11}}{\delta t} = \frac{\partial \tau'_{11}}{\partial t} + \bar{V}_1 \frac{\partial \tau'_{11}}{\partial x_1} - 2\left(\bar{\tau}_{11} \frac{\partial V'_1}{\partial x_1} + \tau'_{11} \frac{\partial \bar{V}_1}{\partial x_1}\right)$$

$$= \frac{\partial \hat{\tau}_{11}}{\partial t} e^{ikx_1} - 2\left(\bar{\tau}_{11} E' + \tau'_{11} E\right) \qquad (4.49)$$

The relaxation time is also perturbed as

$$\lambda_e + \lambda'_e = \frac{\lambda}{1+\sqrt{3}a\lambda(E+E')} \qquad (4.50)$$

Linearization gives

$$\lambda'_e = -\sqrt{3}a\lambda_e^2 E' \quad , \quad \lambda_e = \frac{\lambda}{1+\sqrt{3}a\lambda E} \qquad (4.51a,b)$$

Then the perturbed constitutive equation is

$$(\bar{\tau}_{11} + \tau'_{11}) + (\lambda_e + \lambda'_e)\left(\frac{\delta \bar{\tau}_{11}}{\delta t} + \frac{\delta \tau'_{11}}{\delta t}\right)$$

$$= 2G(\lambda_e + \lambda'_e)(E + E') \qquad (4.52)$$

This gives

$$\bar{\tau}_{11} + \lambda_e \frac{\delta \bar{\tau}_{11}}{\delta t} = 2G\lambda_e E \qquad (4.53)$$

$$\tau'_{11} + \lambda_e \frac{\delta \tau'_{11}}{\delta t} + \lambda'_e \frac{\delta \bar{\tau}_{11}}{\delta t} = 2G(\lambda_e E' + \lambda'_e E) \qquad (4.54)$$

With the aid of Eq. (4.49) and Eq. (4.51), Eq. (4.54) simplifies to

$$\frac{\partial \hat{\tau}_{11}}{\partial t} e^{ikx_1} + \left(\frac{1}{\lambda_e} - 2E \right) \tau'_{11} = 2\{G + (1-\sqrt{\beta}a)\bar{\tau}_{11}\}E' \qquad (4.55)$$

Dividing by e^{ikx_1} gives the time as the only independent variable. This is also true if $k = 0$. With the same method, constitutive equation for radial component (2) is easily obtained.

Finally, the constitutive equation for the basic state is

$$\frac{\partial \bar{\tau}_{11}}{\partial t} + \left(\frac{1}{\lambda_e} - 2E \right) \bar{\tau}_{11} = 2GE \qquad (4.56)$$

$$\frac{\partial \bar{\tau}_{22}}{\partial t} + \left(\frac{1}{\lambda_e} + E \right) \bar{\tau}_{22} = -GE \qquad (4.57)$$

and the perturbed constitutive equation is described by

$$\frac{\partial \hat{\tau}_{11}}{\partial t} + \left(\frac{1}{\lambda_e} - 2E \right) \hat{\tau}_{11} = 2\{(1-\sqrt{\beta}a)\bar{\tau}_{11} + G\}E' \qquad (4.58)$$

$$\frac{\partial \hat{\tau}_{22}}{\partial t} + \left(\frac{1}{\lambda_e} + E \right) \hat{\tau}_{22} = -\{(1-\sqrt{\beta}a)\bar{\tau}_{22} + G\}E' \qquad (4.59)$$

where

$$E' = -\frac{2}{R}\left[\frac{\partial \hat{\xi}}{\partial t} + \frac{E}{2}\hat{\xi}\right] \qquad (4.60)$$

Eq. (4.56) and Eq. (4.57) are the differential equations solved to obtain tensile stress (Eq. (3.24), page 94) in Chapter III.

Capillary instability. Viscoelastic fluids generally have high viscosity, however capillary failure can be important if we treat very thin filaments. The simplest case is where the filament is initially in a quiescent state. This is, of course, equivalent to the problem originally considered by Middleman [86] and by Yerushalmi and Shinnar [48,50].

The equation of state reduces to

$$\frac{\partial \hat{\tau}_{11}}{\partial t} + \frac{1}{\lambda}\hat{\tau}_{11} = -\frac{4G}{R}\frac{\partial \hat{\xi}}{\partial t} \tag{4.61}$$

$$\frac{\partial \hat{\tau}_{22}}{\partial t} + \frac{1}{\lambda}\hat{\tau}_{22} = \frac{2G}{R}\frac{\partial \hat{\xi}}{\partial t} \tag{4.62}$$

since $E = 0$, $\bar{\tau}_{11} = \bar{\tau}_{22} = 0$. This is equivalent to the linear viscoelastic fluids. The above equations are combined with the equation of motion (Eq. (4.26)) in the same manner as for Newtonian capillary instability described earlier. The solution is found to be of the form

$$\hat{\xi}(t) = \hat{\xi}(0)\, e^{\alpha t} \tag{4.63a}$$

where the exponent α is found by the following characteristic equation

$$\frac{2\rho}{k^2R}\left(\alpha^3 + \frac{\alpha^2}{\lambda}\right) + \left\{\frac{6\eta}{\lambda R} - \frac{\gamma}{R^2}\left(1-k^2R^2\right)\right\}\alpha - \frac{\gamma}{\lambda R^2}\left(1-k^2R^2\right) = 0 \tag{4.63b}$$

The eigenvalues α are generally complex numbers and an

unstable mode is given by the positive α .

When the inertia term can be neglected, we obtain

$$\alpha = \frac{\gamma (1-k^2R^2)}{6\eta R - \lambda\gamma(1-k^2R^2)} \tag{4.64}$$

where $k = 0$ gives maximum growth rate. When the relaxation time λ increases so will growth rate α . Thus the prediction of elasticity destabilizing a stationary filament is in agreement with the predictions of the above authors.

Interaction of capillarity and ductility. We now turn to the interaction of surface tension and ductility. For the slightly viscoelastic case, we generally are able to neglect the nonlinear effects of relaxation time and also inertial effects. We know that τ_{22} (which is numerically equal to isotropic pressure) is always less than τ_{11} . If we neglect τ_{22} , the mathematical problem is greatly simplified and the differential equation reduces from second order to first order.

In this case Eq. (4.56) and Eq. (4.58) with Eq. (4.60) are combined with the equation of motion (Eq. (4.16)). This gives the instantaneous growth rate as

$$\frac{1}{\hat{\xi}}\frac{d\hat{\xi}}{dt} = \frac{E(-\bar{\tau}_{11} + 2G) + \frac{\gamma}{R}\left\{3k^2R^2E + \left(\frac{1}{\lambda} - E\right)(1-k^2R^2)\right\}}{2\bar{\tau}_{11} + 4G - \frac{\gamma}{R}(1-k^2R^2)} \tag{4.65}$$

Here we do not have a simple additive effect of capillarity

and ductility as we had for Newtonian fluids. Again setting k equal to zero gives the maximum growth rate. For the case of stationary filaments ($E = 0$, $\bar{\tau}_{11} = 0$) the above equation reduces to the same form as Eq. (4.64) but the coefficient of the viscosity becomes 4 instead of 6 because we have neglected τ_{22}. This implies the effect of neglecting τ_{22} is not serious and it seems to give qualitatively correct results.

In order to study the influence of surface tension, we take the derivative of the maximum growth rate with respect to γ.

$$\frac{\partial}{\partial \gamma}\left(\frac{1}{\hat{\xi}}\frac{\partial \hat{\xi}}{\partial t}\right) = \frac{\bar{\tau}_{11}(2-3\lambda E)+2G(2-\lambda E)}{\lambda R(2\bar{\tau}_{11}+4G-\frac{\gamma}{R})^2} \qquad (4.66)$$

First, note that if λE is small, the above equation is positive; indicating that surface tension is destabilizing. However, if $\lambda E > 2$, the above derivative is always negative; that is, the influence of surface tension is stabilizing the filaments rather than propagating the disturbances as we had for Newtonian and linear viscoelastic fluids.

When the elongation rate E goes to zero, it is found that viscoelasticity destabilizes a filament. For finite E, however, viscoelasticity acts to stabilize the filament. When disturbances are introduced into stationary fluids, viscoelastic constitutive equations reduce to

linear viscoelasticity which is always "softening" and the stress level of the filament can not exceed the Newtonian level. It is possible that linear viscoelastic stability analyses may generally mispredict the growth characteristics of disturbances, when these reach finite amplitudes. This would be especially the case in a problem like the capillary instability of viscoelastic fluids which involves large deformation rates when the amplitude becomes large. Similar views are expressed by Gordon, Yershalmi, and Shinnar [50]. When steady flows exist, the convected terms of nonlinear viscoelasticity directly appear in the linearized analysis and this problem does not arise.

Ductile instability of constant relaxation time viscoelastic fluids. We now turn to the purely ductile asymptote where we need not be concerned with either surface tension or inertia. We consider the case where the relaxation time is not affected by deformation rate ($a = 0$). First we neglect τ_{22} for mathematical simplicity. The error does not occur for the Newtonian fluid asymptote ($\lambda E = 0$), because in the force balance equation (Eq. (4.16) with $P_1' = 0$) the viscosity factor (whether 2η or 3η) cancels out. The error is also negligible for highly viscoelastic fluids because τ_{22} is negligibly small compared to τ_{11} ($\tau_{11} \gg \tau_{22}$). In the intermediate viscoelasticity range ($0 < \lambda E < \frac{1}{2}$) a

quantitative error due to neglect of τ_{22} may occur. This point will be investigated later.

Neglecting τ_{22}, equations of state Eq. (4.56) and Eq. (4.58) with $a=0$, continuity equation Eq. (4.60), and force balance equation Eq. (4.16) are solved simultaneously in terms of the disturbance $\xi(t)$. The result is

$$\frac{1}{\xi}\frac{d\xi}{dt} = \frac{E}{2}\frac{-\bar{\tau}_{11}+2G}{\bar{\tau}_{11}+2G} \tag{4.67}$$

Here $\bar{\tau}_{11}$ is given as the solution of Eq. (4.56) as

$$\bar{\tau}_{11} = \frac{2G\lambda E}{A}\left[1-e^{-At/\lambda}\right], \quad A = 1-2\lambda E \tag{4.68a,b}$$

If we substitute Eq. (4.68) into Eq. (4.67) and carry out the integration, we obtain

$$\ln\frac{\xi(t)}{\xi(0)} = -\left(\frac{1}{2}+\frac{\lambda E}{1-\lambda E}\right)Et + \frac{\lambda E}{A}\ln\frac{(1-\lambda E)e^{AEt/\lambda E}-\lambda E}{A}$$

$$-\frac{(\lambda E)^2}{A(1-\lambda E)}\ln\frac{(1-\lambda E)-\lambda E e^{-AEt/\lambda E}}{A} \tag{4.69}$$

It is seen that the disturbance growth is a function of Et (which is equal to the Hencky strain $\ln L(t)/L(0)$), and the growth rate is completely characterized by a Weissenberg number λE.

The predictions of Eq. (4.69) are shown in Fig. 4.3 for varying viscoelasticity levels λE. Note that when strain Et is small, disturbances grow at a rate $Et/2$

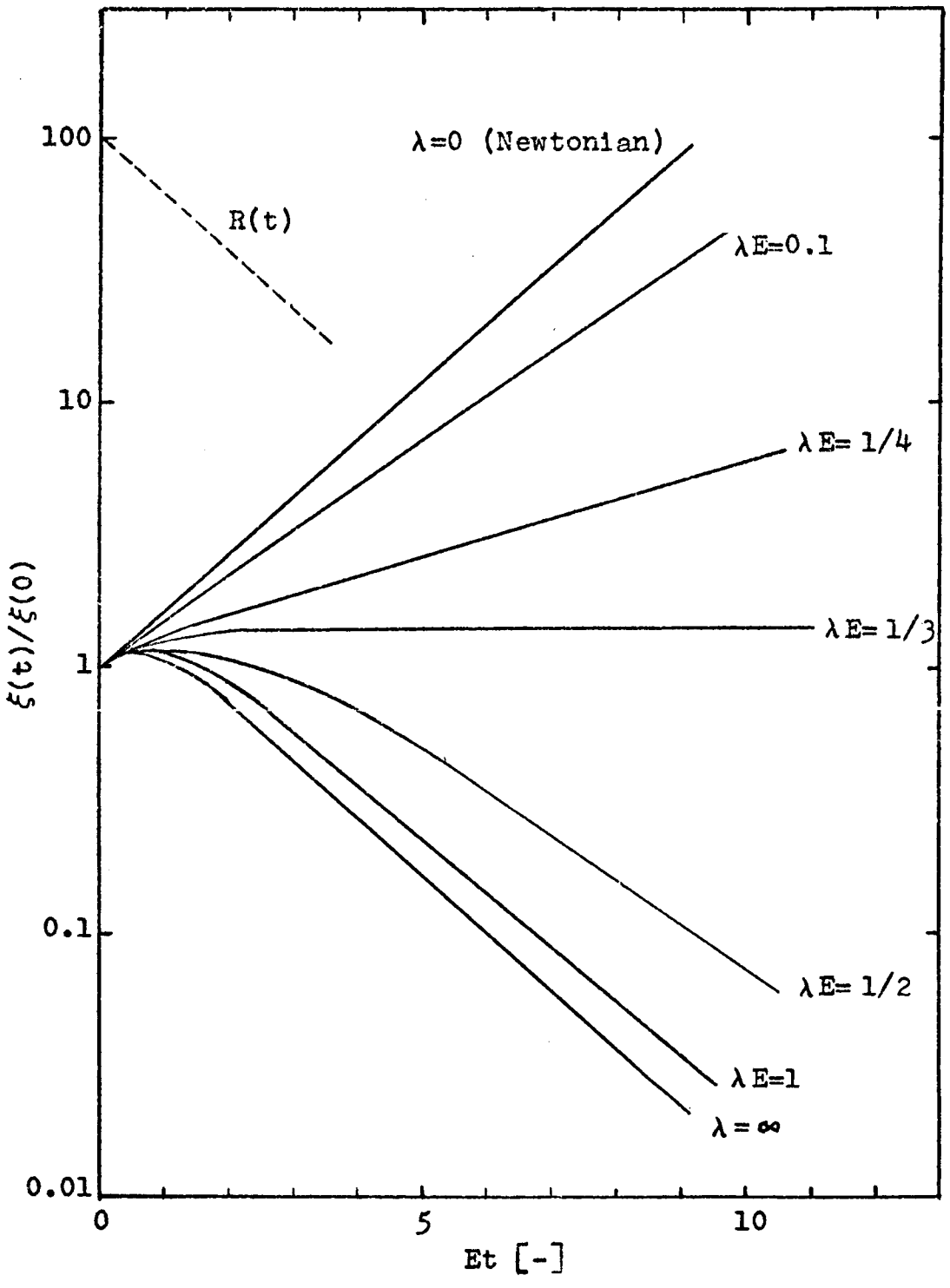


FIGURE 4.3 Disturbance growth plotted against strain Et for varying viscoelasticity levels λE for a=0 .

regardless of the viscoelasticity level. This is obvious when we examine Eq. (4.67) in which at early time $\bar{\tau}_{11} \equiv 0$. At large Et the disturbance generally grows linearly with Et and the slope is determined by the level of viscoelasticity. In this regime, the logarithmic terms of Eq. (4.69) may be simplified to yield:

$$\ln \frac{\xi(t)}{\xi(0)} = \frac{Et}{2} \frac{1-3\lambda E}{1-\lambda E} + \frac{\lambda E}{1-\lambda E} \ln \frac{1-\lambda E}{1-2\lambda E} \qquad (\lambda E < \tfrac{1}{2}) \qquad (4.70a)$$

$$\ln \frac{\xi(t)}{\xi(0)} = -\frac{Et}{2} + \ln (Et+1) \qquad (\lambda E = \tfrac{1}{2}) \qquad (4.70b)$$

$$\ln \frac{\xi(t)}{\xi(0)} = -\frac{Et}{2} + \frac{\lambda E}{1-\lambda E} \ln \frac{\lambda E}{2\lambda E-1} \qquad (\lambda E > \tfrac{1}{2}) \qquad (4.70c)$$

For small values of λE, the disturbance grows with time and when $\lambda \to 0$, this reduces to the Newtonian result Eq. (4.36) with $\gamma = 0$. When λE increases to a value of $1/3$, disturbances cease to grow and when λE is greater than $1/3$, the size of disturbances decrease during stretching.

This enhanced stability of viscoelastic fluid filaments during stretch is a direct consequence of increased elongational viscosity at high λE. Because of this effect, the deformation response to the higher stresses in regions of minimal cross-section is small and disturbances do not grow.

The neutral stability of disturbance growth of λE being equal to $1/3$ does not correspond to filament

stability for ductile failure. This is because the overall size of filament decreases according to $R(t) = R(0) \exp(-Et/2)$ (see Fig. 4.3, where initial defect size $\xi(0)/R(0) = 0.01$ is chosen) and reduces to the size of $\xi(t)$. Graphically the points of ductile failure are determined by the intersections of $R(t)$ curves and $\xi(t)$ curves, thus in order to aviod ductile failure the defects have to heal during stretch. Therefore, the critical value of ductile failure is $\lambda E = \frac{1}{2}$ just as for the stress growth criterion.

The present analytical solution is equivalent to the numerical solution by Chang and Lodge [22] for their integral equation, just as the Newtonian ductile instability analysis was equivalent to that of Orowan (who used a model shown in Fig. 4.2). It is easiest to compare at the asymptote of $\lambda \to \infty$. In this case, the stress can be expressed as the rubber elasticity equation:

$$\sigma_{11}(t) = \tau_{11} - \tau_{22} = G\left[\left(\frac{A(0)}{A(t)}\right)^2 - \frac{A(t)}{A(0)}\right] \qquad (4.71)$$

A simple force balance of two eylinders of different cross sectional area A_1 and A_2, as shown in Fig. 4.2, gives (after neglecting τ_{22})

$$\frac{A_2(t)}{A_1(t)} = \left(\frac{A_2(0)}{A_1(0)}\right)^2 \qquad (4.72)$$

The above expression seems to be able to approximate their results for the material parameters and conditions they employed. In terms of radius, the above equation becomes

$$\frac{\xi(t)}{\xi(0)} = 2\,\frac{R(t)}{R(0)} = 2e^{-\frac{E}{2}t} \tag{4.73}$$

which is the asymptotic value of Eq. (4.70c) for $\lambda \to \infty$. We can also obtain an analytical result without neglecting τ_{22} for this asymptotic case as

$$\frac{\xi(t)}{\xi(0)} = \frac{R(t)\left[R(t)^6+2R(0)^6\right]}{R(0)\left[R(0)^6+2R(t)^6\right]}$$

$$= \frac{2e^{2Et}+e^{-Et}}{e^{2Et}+2e^{-Et}}\, e^{-\frac{E}{2}t} \longrightarrow 2e^{-\frac{E}{2}t} \tag{4.74}$$

We note that neglecting τ_{22} does not affect our result if we are concerned with long time asymptote of a highly viscoelastic fluid.

As discussed before, the error associated with neglecting $\bar{\tau}_{22}$ may occur at intermediate viscoelasticity range $(0 < \lambda E < \frac{1}{2})$. This point will be investigated here. In this case we have to solve six differential equations (Eq. (4.16) with $P_{\gamma}' = 0$ and Eq. (4.56) through Eq. (4.60) with $a = 0$) simultaneously. The procedure is rather straight forward but manipulation is very tedious and intermediate steps will not be described here.

The differential equation describing the disturbance

growth $\xi(t)$ becomes (after considerable manipulation).

$$(\bar{\tau}_{11}+2\bar{\tau}_{22}+3G)\frac{1}{E^2}\frac{d^2\xi}{dt^2} + (4\bar{\tau}_{11}-4\bar{\tau}_{22}+\frac{3G}{\lambda E})\frac{1}{E}\frac{d\xi}{dt}$$

$$+ \frac{1}{4}(7\bar{\tau}_{11}-10\bar{\tau}_{22}-3G-\frac{6G}{\lambda E})\xi = 0 \qquad (4.75)$$

where $\bar{\tau}_{11}$ and $\bar{\tau}_{22}$ are the solutions of Eq. (4.56) and Eq. (4.57) and are given by

$$\bar{\tau}_{11} = \frac{2G\lambda E}{1-2\lambda E}\left[1-e^{-(1-2\lambda E)t/\lambda}\right] \qquad (4.76a)$$

$$\bar{\tau}_{22} = \frac{-G\lambda E}{1+\lambda E}\left[1-e^{-(1+\lambda E)t/\lambda}\right] \qquad (4.76b)$$

When $\lambda E < \frac{1}{2}$, steady state on $\bar{\tau}_{11}$ and $\bar{\tau}_{22}$ can be achieved. In this case Eq. (4.75) becomes a constant coefficient ordinary differential equation of the form

$$a'\frac{1}{E^2}\frac{d^2\xi}{dt^2} + b'\frac{1}{E}\frac{d\xi}{dt} + c'\xi = 0 \qquad (4.77)$$

where

$$a' = \lambda E(1-\lambda E), \quad b' = 2(\lambda E)^2-\lambda E+1 \qquad (4.78a,b)$$

$$c' = \frac{1}{4}\{13(\lambda E)^2+\lambda E-2\} \qquad (4.78c)$$

Eq. (4.77) has the solution of the form

$$\xi(t) = \xi(0)\, e^{\alpha E t} \qquad (4.79a)$$

where α is given by the positive root of the

characteristic equation as

$$\alpha = \frac{-(2P^2-P+1)+\sqrt{17P^4-16P^3+2P^2+1}}{2P(1-P)} \qquad (0 < P < \tfrac{1}{2}) \qquad (4.79b)$$

where $P = \lambda E$ is the Weissenberg number. The marginal stability ($\alpha = 0$) is calculated to be at

$$\lambda E = \frac{\sqrt{105}-1}{26} = 0.356 \qquad (4.80)$$

which is slightly higher value than $\lambda E = 1/3$ obtained by neglecting τ_{22}.

Eq. (4.79) is plotted in Fig. 4.4 together with Eq. (4.69) in order to clarify the error involved by neglecting τ_{22}. As clearly seen in the derivation, the Eq. (4.79) is not valid at small Et since stress is still in a transient state. It is seen that if we include τ_{22} the disturbance grows slightly faster. Note that the range to be affected is such a narrow one of Weissenberg numbers (approximately $0.1 < \lambda E < 0.5$), and that the strain obtained as an intersection of $R(t)$ curve and $\xi(t)$ curve will not be affected considerably. Thus it may be concluded that the error involved by neglecting τ_{22} is not serious.

Ductile instability of nonlinear relaxation time viscoelastic fluids. Again neglecting τ_{22}, Eq. (4.16), Eq. (4.56), Eq. (4.58), and Eq. (4.60) are combined to obtain the differential equation describing $\xi(t)$. The

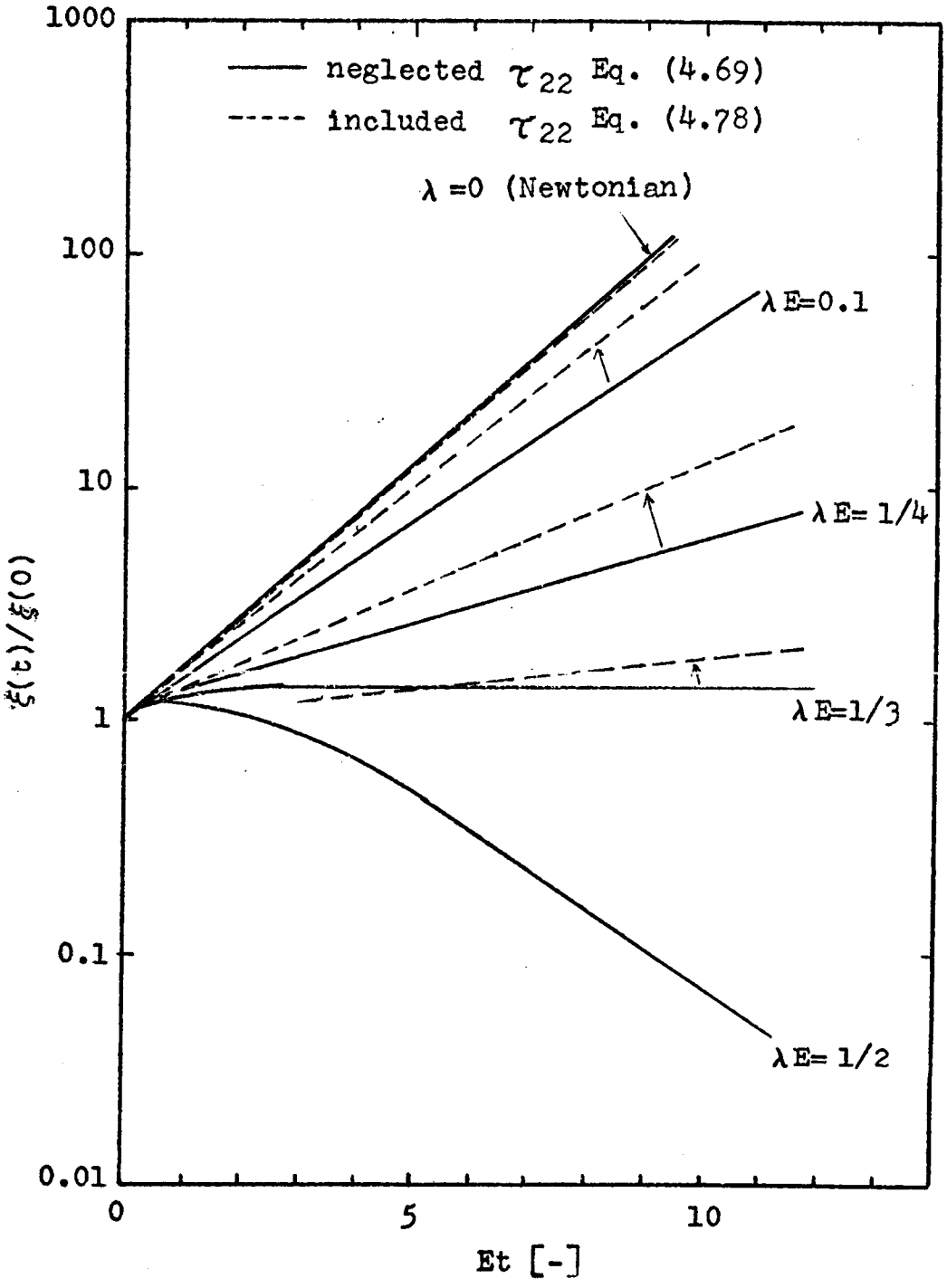


FIGURE 4.4 Comparison of disturbance growth analyses for neglected τ_{22} (Eq. (4.69)) and included τ_{22} (Eq. (4.78)).

result is

$$\frac{1}{\xi}\frac{d\xi}{dt} = \frac{E}{2}\frac{-(1-\sqrt{\beta}a)\bar{\tau}_{11}+2G}{(1-\sqrt{\beta}a)\bar{\tau}_{11}+2G} \tag{4.81}$$

Here $\bar{\tau}_{11}$ is given as the solution of Eq. (4.56) as

$$\bar{\tau}_{11} = \frac{2G\lambda_e E}{1-2\lambda_e E}\left[1-e^{-(1-2\lambda_e E)t/\lambda_e}\right]$$

$$= \frac{2G\lambda E}{A}(1-e^{-At/\lambda}) \tag{4.82a}$$

where

$$A = 1-(2-\sqrt{\beta}a)\lambda E \tag{4.82b}$$

The integrated form of Eq. (4.81) after substituting Eq. (4.82) is

$$\ln\frac{\xi(t)}{\xi(0)} = -Et\left(\frac{1}{2}+\frac{B}{C}\right) + \frac{P}{A}\ln\left\{\frac{C\exp(AEt/P)-B}{A}\right\}$$

$$-\frac{BP}{AC}\ln\left\{\frac{C-B\exp(-AEt/P)}{A}\right\} \tag{4.83a}$$

where

$$B = \lambda E(1-\sqrt{\beta}a),\quad C = 1-\lambda E\ ,\quad P = \lambda E \tag{4.83b,c,d}$$

It is seen that the disturbance growth is a function of Et and the growth rate is characterized by λE combined with the parameter a.

The predictions of Eq. (4.83) for $\lambda E = \frac{1}{2}$ and

$\lambda E = 10$ at various levels of parameter a are shown in Fig. 4.5. At $a = 0$ the disturbances damp out and the filaments are stable for the ductile instability. However as a becomes large the ductile failure may occur since the disturbances start to grow. At $a = 1/\sqrt{3} = 0.58$, the disturbance growth rate is the same as Newtonian fluids, which is also obvious by Eq. (4.81). When λ strongly depends upon E, such that $a > 1/\sqrt{3}$, the ductile instability is more severe than Newtonian fluids. This is more pronounced for higher values of λE.

For low levels of viscoelasticity, such as $\lambda_e E < \frac{1}{2}$ or $\lambda E < 1/(2-\sqrt{3}a)$, Eq. (4.83) can be simplified at long time asymptote as

$$\ln \frac{\xi(t)}{\xi(0)} = \frac{Et}{2}\left\{\frac{1-\lambda E(3-2\sqrt{3}a)}{1-\lambda E}\right\} + \frac{\lambda E}{1-\lambda E} \ln \frac{1-\lambda E}{1-(2-\sqrt{3}a)\lambda E} \quad (\lambda E < \frac{1}{2-\sqrt{3}a}) \tag{4.84}$$

When $a > 1/\sqrt{3}$, the denominator of Eq. (4.81) continuously decreases to zero as stress τ_{11} develops, so that the growth rate eventually becomes infinite (like the $a = 0.7$ curve for $\lambda E = 10$ in Fig.(4.5)). In this case, the total elongation Et is limited regardless of the initial size of disturbance. This maximum elongation to break is obtained when the denominator of Eq. (4.81) goes to zero. The strain limit is obtained as

$$Et = \frac{\lambda E}{(2-\sqrt{3}a)\lambda E - 1} \ln \frac{\lambda E - 1}{(\sqrt{3}a - 1)\lambda E} \quad (a > \frac{1}{\sqrt{3}}, \lambda E > 1) \tag{4.85}$$

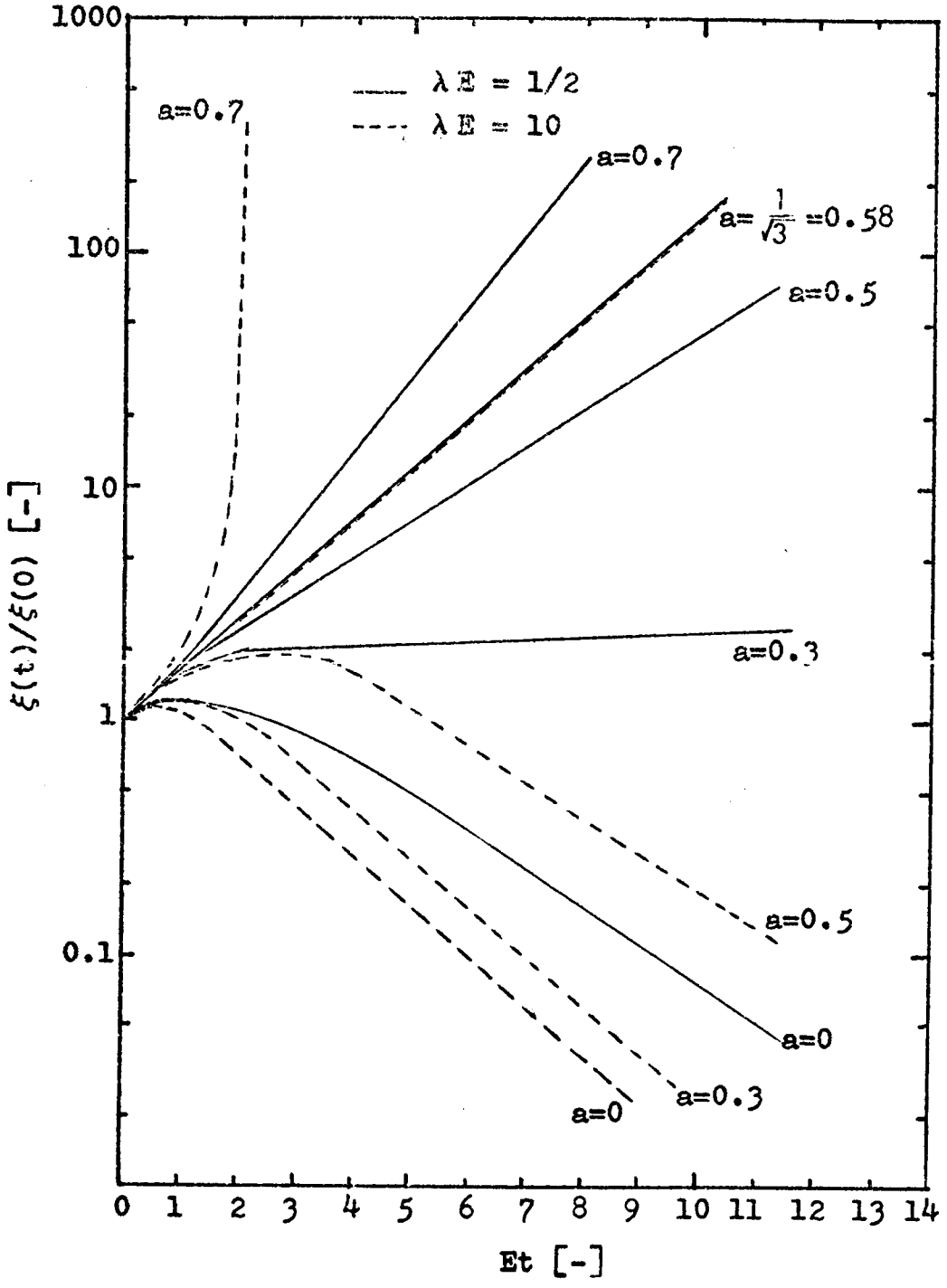


FIGURE 4.5 Disturbance growth of viscoelastic fluids at various values of a and λE .

This expression is valid for $\lambda E > 1$, and if $\lambda E < 1$, the disturbance grows at a finite rate according to Eq. (4.84) but at a faster rate than the Newtonian fluids as long as $a > 1/\sqrt{3}$.

C. Prediction of Elongation to Break

Interpretation from Stability Theory

It is possible to apply the stability analysis to predict the length of a thread which may be formed by extending a liquid cylinder. This is done by determining the time t_B (breaking time) required for the disturbance to grow to the size of the cylinder radius, i.e.,

$$\xi(t_B) = R(t_B) = R(0)\, e^{-Et_B/2} \tag{4.86}$$

The elongation to break is calculated by the Hencky strain

$$Et_B = \ln \frac{L(t_B)}{L(0)} \tag{4.87}$$

For the Newtonian capillary and ductile instability, Eq. (4.36) is introduced to Eq. (4.86) to give

$$\ln \frac{L(t_B)}{L(0)} = \ln \frac{R(0)}{\xi(0)} - \frac{\gamma}{3\eta R(0)} \left(\sqrt{\frac{L(t_B)}{L(0)}} - 1 \right) \tag{4.88}$$

We note that the elongation to break $L(t_B)/L(0)$ becomes equal to $R(0)/\xi(0)$ in the absence of surface tension for this linearized case. If we did not linearize, the elongation to break will be reduced (at most) to

$$\ln \frac{L(t_B)}{L(0)} = \ln \frac{R(0)}{\xi(0)} - 1 \qquad (4.89)$$

as will be obtained by introducing Eq. (4.42) into Eq. (4.86).

The predictions of Eq. (4.88) were determined as functions of $3\eta ER(0)/\gamma$ taking $\xi(0)/R(0)$ as a parameter and are plotted in Fig. 4.6. The dimensionless number $\gamma/3\eta ER(0)$ is the ratio of surface tension to viscous stress (capillarity number). This number determines the relative importance of capillary failure against ductile failure. It is seen that as the capillarity number is large or viscosity is low, the filament is dominated by capillary instability and the elongation to break is very low. When capillarity number is small or viscosity is large, the elongation to break levels off to $R(0)/\xi(0)$. The figure explains Ziabicki's correlation [165] of thread length in terms of the product of viscosity and extension velocity.

For viscoelastic fluids, Eq. (4.84) can be used to give elongation to break:

$$\ln \frac{L(t_B)}{L(0)} = \frac{1}{1-\lambda E(2-\sqrt{3}a)}\left\{(1-\lambda E)\ln \frac{R(0)}{\xi(0)} - \lambda E \ln \frac{1-\lambda E}{1-(2-\sqrt{3}a)\lambda E}\right\},$$

$$\left(\lambda E < \frac{1}{2-\sqrt{3}a}\right) \qquad (4.90)$$

This is for purely ductile failure and valid for low

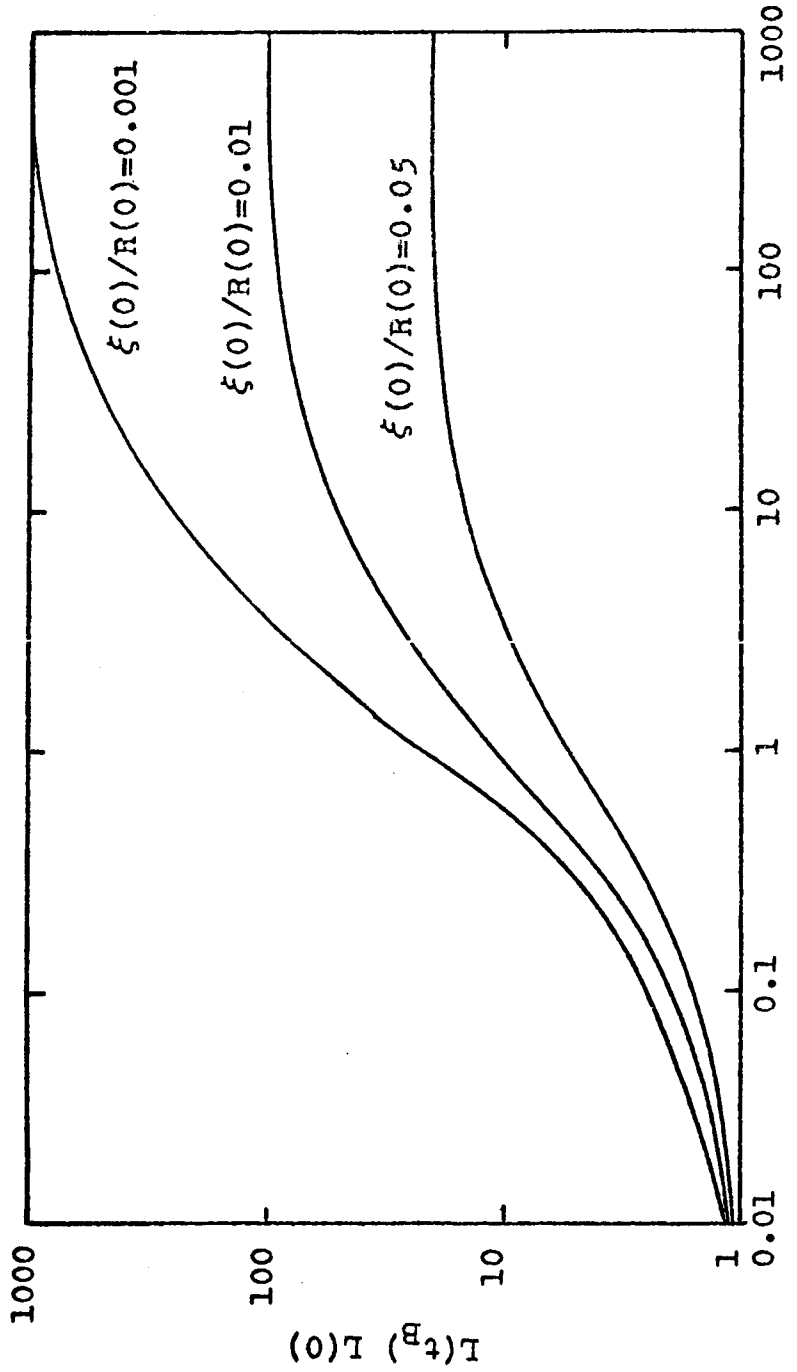


FIGURE 4.6 Elongation to break as a function of inverse of capillarity number for varying defect sizes.

levels of viscoelasticity, $\lambda E < 1/(2-\sqrt{3}a)$. At $\lambda E = 1$, it takes the following form:

$$\ln \frac{L(t_B)}{L(0)} = \frac{1}{\sqrt{3}a-1} \ln\left\{1+(\sqrt{3}a-1)\ln\frac{R(0)}{\xi(0)}\right\}, \quad (\lambda E = 1) \qquad (4.91)$$

When $a > 1/\sqrt{3}$, the ductile instability is always more severe than for Newtonian fluid and the maximum elongation is limited for infinitesimal disturbances to

$$\ln \frac{L(t_B)}{L(0)} = \frac{\lambda E}{(2-\sqrt{3}a)\lambda E-1} \ln \frac{\lambda E-1}{(\sqrt{3}a-1)\lambda E}, \quad (a>\frac{1}{\sqrt{3}}, \lambda E > 1) \qquad (4.92)$$

as derived earlier (Eq. (4.85), page 145).

Predictions of Eq. (4.90) through Eq. (4.92) are plotted against Weissenberg number λE in Fig. 4.7 for various levels of a parameter. The initial defect size is chosen as 1% ($\xi(0)/R(0) = 0.01$) in Eq. (4.90) and Eq. (4.91). When $a < 1/\sqrt{3} = 0.58$, as λE increases, so will elongation to break which eventually goes to infinity at finite value of λE , specifically at

$$\lambda E = \frac{1}{2-\sqrt{3}a} \qquad (4.93)$$

This means that the filament is stable with respect to the ductile instability of the Weissenberg number higher than the value specified by Eq. (4.93). However, when the dependence of λ upon E is large (such that $a > 1/\sqrt{3}$), the elongation to break decreases as λE increases and

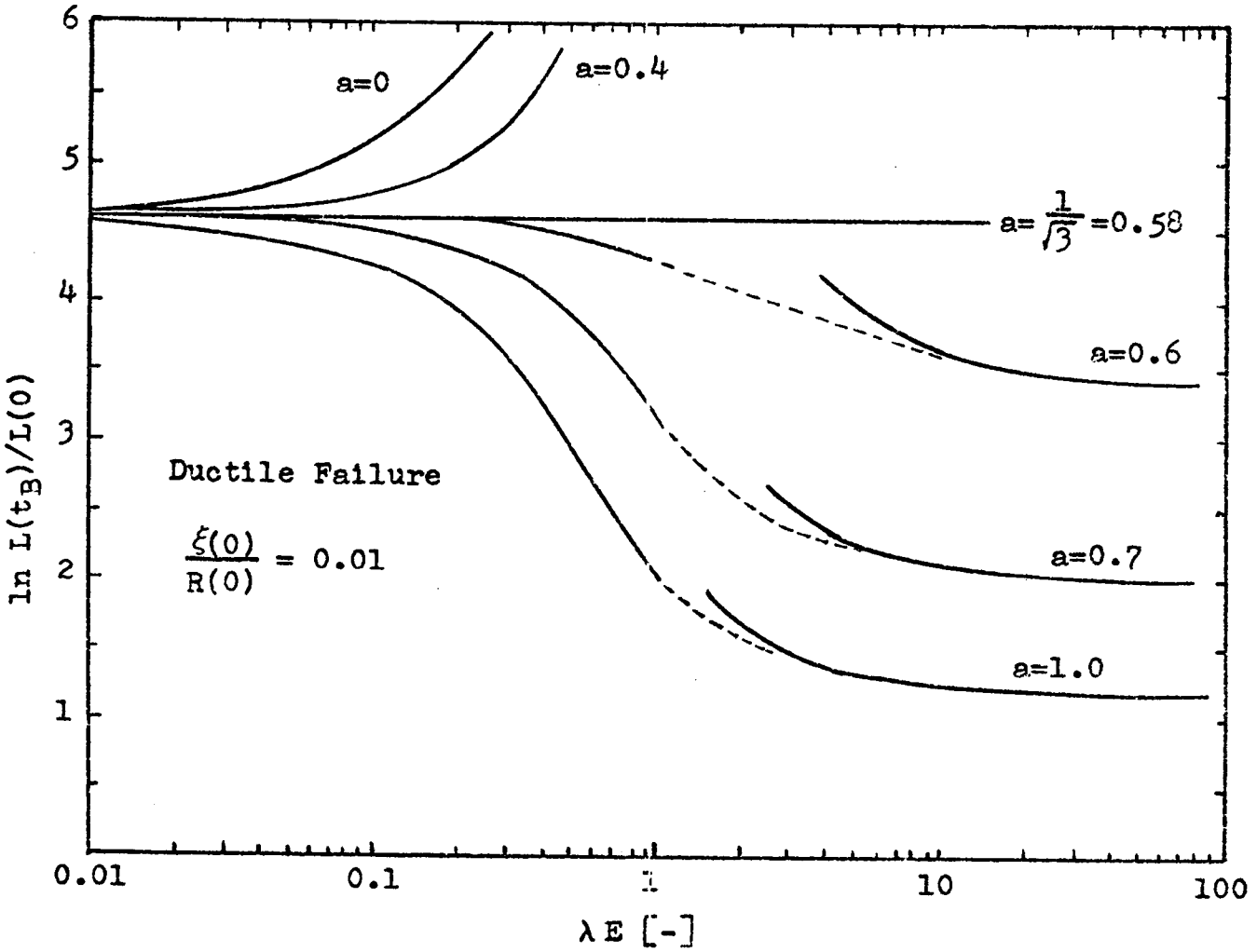


FIGURE 4.7 Visccelastic ductile failure at various levels of relaxation time dependence upon stretch rate.

levels off at a certain level depending upon a. Eq. (4.92) which is for infinitesimal disturbances and Eq. (4.90) and Eq. (4.91) which are for finite disturbances (1%) are naturally discontinuous but connected by a smooth curve (dotted line). This is acceptable because at high λE, the effect of defect size becomes negligible in Eq. (4.90). At $a = 1/\sqrt{3}$, the problem reduces to Newtonian ductile failure and $L(t_B)/L(0)$ is always equal to $R(0)/\xi(0)$.

Even when the filament is stable with respect to the ductile instability, the filament cannot necessarily be stretched out indefinitely. For a real material, we need also consider the cohesive fracture resulting from high tensile stresses or strain energies. There may be no true ductile failure because as the neck thins down a critical stress may always be exceeded. We shall presume that cohesive failure will always follow if the applied stress exceeds some critical stress. We see that when $\lambda E > 1/(2-\sqrt{3}a)$ the stress grows indefinitely so that in practice the stress always reaches the critical value which leads the material to fracture. In this case, τ_{22} is negligible and the total elongation is expressed as

$$\ln \frac{L(t_B)}{L(0)} = \frac{\lambda E}{(2-\sqrt{3}a)\lambda E-1} \ln \left[1 + \frac{\sigma_{cr}}{2G\lambda E}\{(2-\sqrt{3}a)\lambda E-1\}\right], \quad \left(\lambda E > \frac{1}{2-\sqrt{3}a}\right) \tag{4.94}$$

The predictions of the previous equation are shown in Fig. 4.8 for various values of a. The ratio of critical stress and the modulus is taken as $\sigma_{cr}/G = 10$. It is seen that the cohesive fracture occurs only when the Weissenberg number (λE) exceeds the value specified by Eq. (4.93). The critical value shifts to higher λE for higher values of a. When $a > 2/\sqrt{3} = 1.16$, the stress does not grow indefinitely so that the fracture may not occur for any λE, but this of course depends upon the critical stress and the elongation rate.

Extensibility as a Function of Weissenberg Number

When a viscoelastic fluid is stretched, both ductile failure and cohesive fracture can occur. Thus the failure is determined by the mechanism which occurs earlier, whichever it is. This means the ductile failure curves in Fig. 4.7 and cohesive fracture curves in Fig. 4.8 should be superposed and the curves which give shorter elongation to break determine the total elongation of the material. Fig. 4.9 shows the total elongation to break as a function of λE for various values of a. The parameters describing defects and critical stress are the same as before. At $a = 0$, the failure curve is spearated at $\lambda E = \frac{1}{2}$ and the failure mechanism is ductile failure at lower λE side and cohesive fracture at higher λE side. The case of $a = 0.4$ is the same except the critical λE shifts to higher values. For $a = 0.6$, the abrupt separation

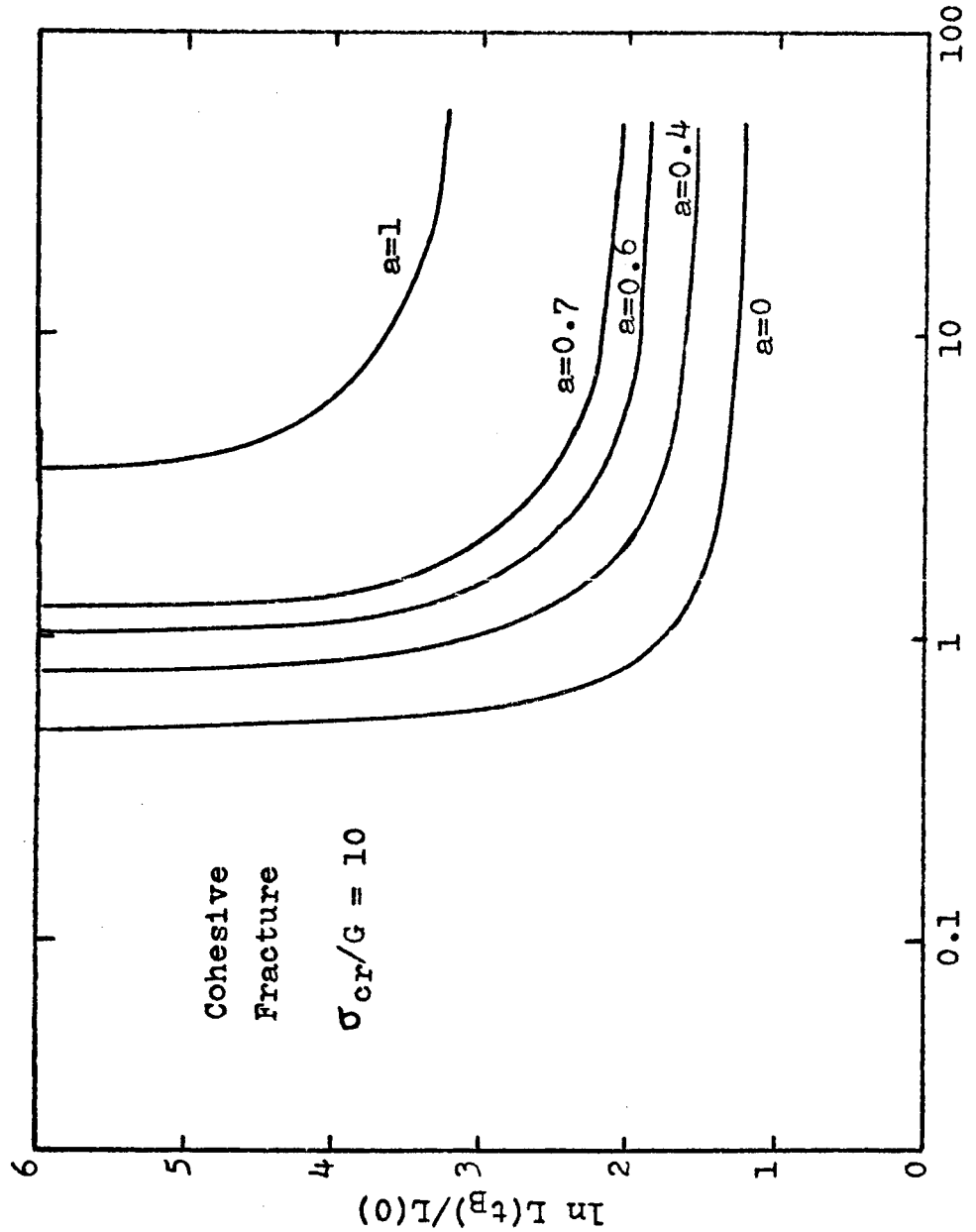


FIGURE 4.8 Cohesive fracture of viscoelastic fluids for various values of a .

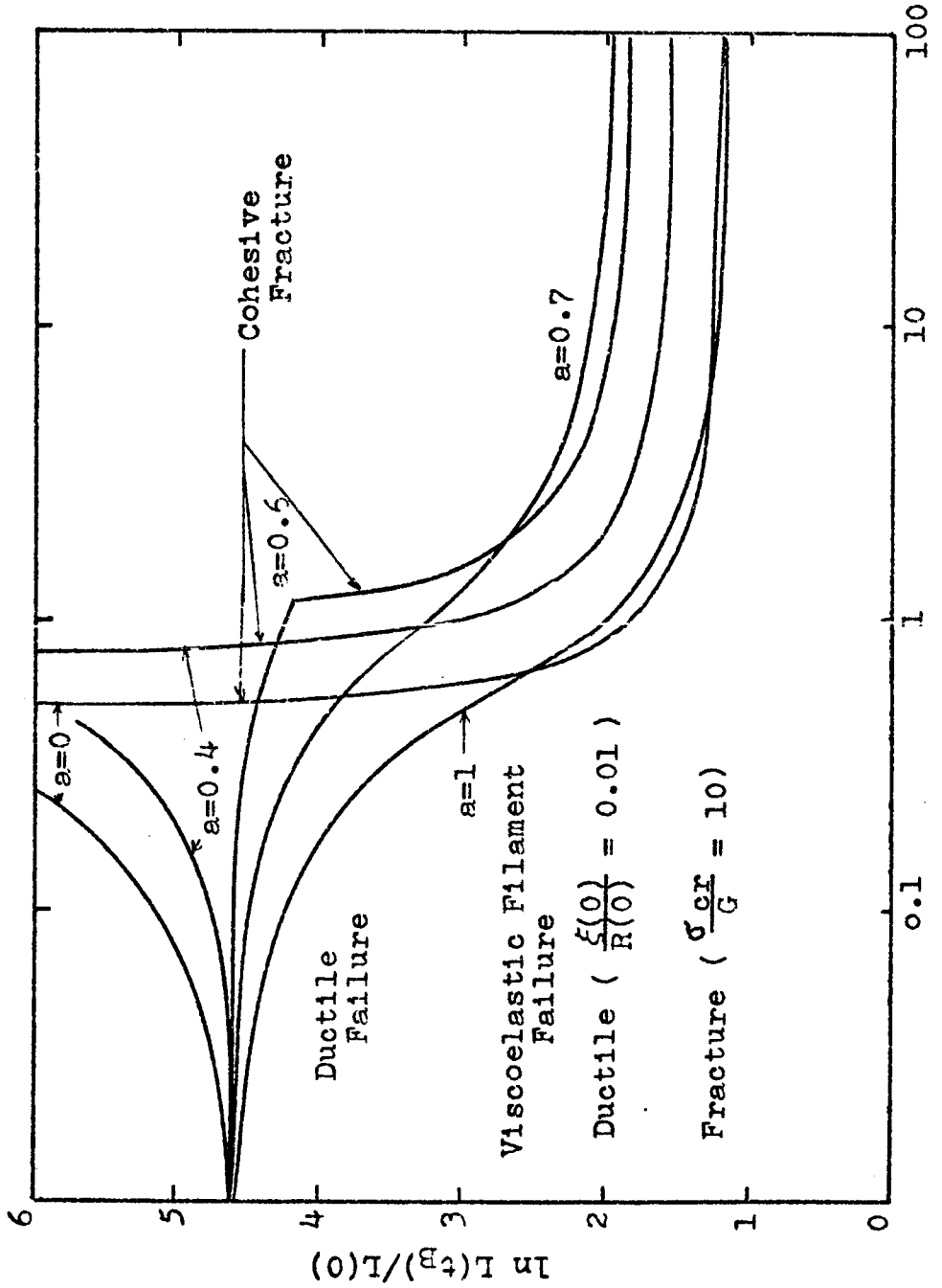


FIGURE 4.9 Predicted viscoelastic filament failure: elongation to break and failure mechanisms.

does not exist but ductile failure and cohesive fracture dominate each side. However, in this regime, both ductile instability and cohesive fracture are serious and they are thus combined. At high values of a ($a = 0.7$ and $a = 1.0$) the failure mechanism is dominated by ductile failure at any values of λE for the condition employed.

The transition from ductile failure to cohesive fracture is abrupt, especially for small values of a. This may be caused by employing a single relaxation time. It is shown that the transition occurs at a critical value of λE described by Eq. (4.93). Therefore if we include more than one relaxation time, the transition is expected to become smooth.

The level of ductile failure curve at small λE asymptote is dependent on the defect parameter $\xi(0)/R(0)$ but not on the a. At the asymptote of the large λE, on the other hand, the level is dependent on a but not on $\xi(0)/R(0)$. The level of cohesive fracture depends upon the critical stress parameter σ_{cr}/G and a.

The predictions of elongation to break shown in Fig. 4.9 are qualitatively in agreement with the experimental results described in Chapter III (page 101). For example, the results of low density polyethylenes (which includes the data of different melt indices and different temperatures) show that the total elongation to break decreases wiht increasing λE and the fracture occurs at

high λE . The relaxation time nonlinear parameter of this material is around $a = 0.4$ (see Fig 3.22, page 96) and agrees with the predictions of Fig. 4.9. The elongation to break data by Kamei and Onogi [62] for narrow molecular weight polystyrene resembles the curve for $a = 0.4$, including the maximum at the transition. High density polyethylenes, on the other hand, are described by relatively high values of a such as $a = 0.9$ (see Fig. 3.22, page 96). This material is found to fail in a ductile manner at any λE and the elongation to break is very small. It was also found that the ductile failure is severe for the higher molecular weight high density polyethylene and polypropylene. The predicted curves for large balues of a in Fig. 4.9 show that the failure mode is always ductile and the elongation to break decreases with λE .

Fig. 4.9 also explains the experimental findings by Chen, Hagler, Abbott, Bogue, and White [25] in their weight dropping apparatus. They found that low density polyethylene (which has a small a value) could be extended to long thin filaments, but high density polyethylene (which has a large a value) exhibited severe ductile failure.

Quantitative comparison is also possible for LDPE (MI = 1.7) and HDPE (MI = 2.6) since necessary material parameters to apply theoretical equations were determined

in a previous chapter (page 96). Fig. 4.10 shows the data of elongation to break plotted against Weissenberg number λE . The LDPE (MI = 1.7), which failed by cohesive fracture is compared with Eq. (4.94). The material parameters of this material have been determined as $\bar{\lambda}$ = 13.4 [sec] , G = 1.94×10^5 [dyn/cm] , a = 0.4 . The predictions of Eq. (4.94) are shown for two critical stress parameters: $\sigma_{cr} = 4 \times 10^6$ [dyn/cm^2] and $\sigma_{cr} = 10^7$ [dyn/cm^2] . It is seen that the prediction by theoretical equation gives the right order of elongation to break. The HDPE (MI = 2.6), which failed in a ductile manner, is compared with Eq. (4.90) which is valid at small λE and with Eq. (4.92) at large λE . The initial defect size of 3% ($\xi(0)/R(0) = 0.03$) in Eq. (4.90) seems to fit the data. At high λE , data can be described by Eq. (4.92) if we choose a = 0.7.

Extensibility as a Function of Molecular Weight

With knowledge of the relations between rheological properties and molecular weight, we can compute the dependence of spinnability upon molecular weight. In Fig. 4.11 the dependence of the elongation to break upon molecular weight for polystyrene is shown, using the theoretical equations developed in the previous section. Considerations were given to capillarity and ductile failure Eq. (4.90), and cohesive fracture of viscoelastic fluid Eq. (4.94). The rheological properties λ and

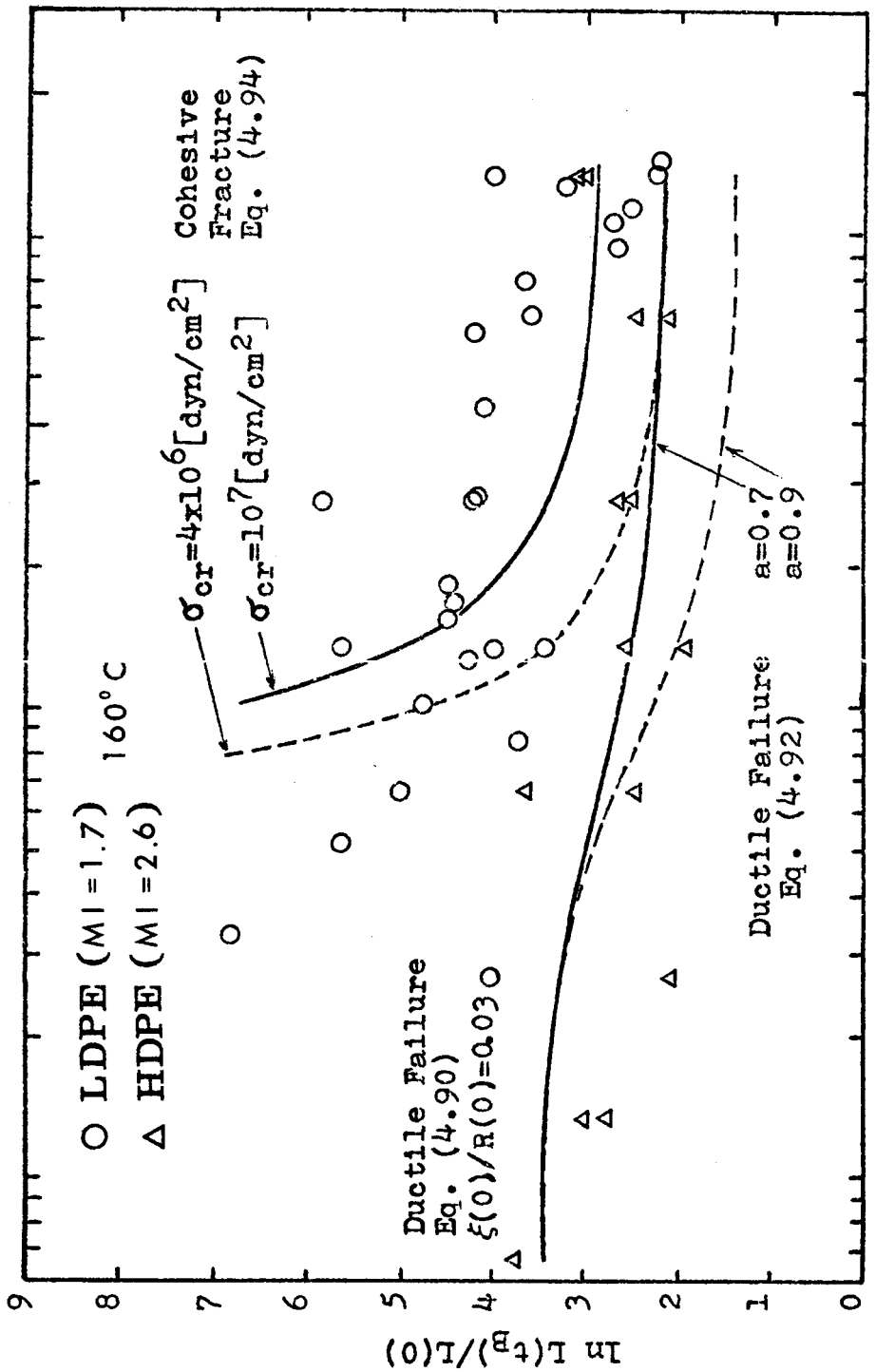


FIGURE 4.10 Comparison of elongation to break data with theoretical predictions.

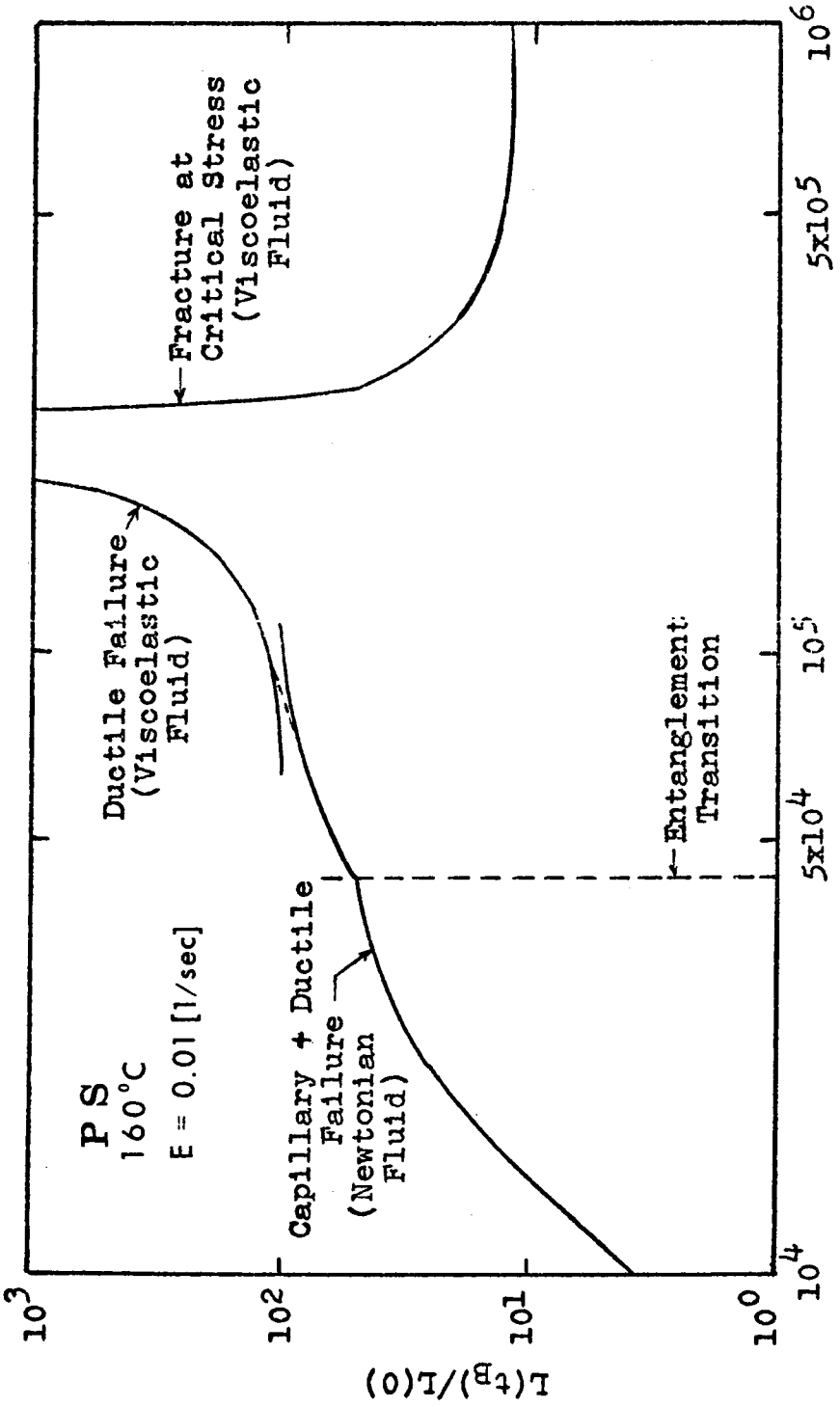


FIGURE 4.11 Predicted spinnability as a function of molecular weight.

G are taken from the data of narrow molecular weight polystyrene at 160°C by Onogi, Masuda, and Kitagawa [105]. Elongation rate $E = 0.01$ [1/sec] , initial defect size 1% ($\xi(0)/R(0) = 0.01$) , initial radius $R(0) = 0.1$ cm and surface tension $\gamma = 30$ dyns/cm , critical stress $\sigma_{cr} = 10^8$ [dyns/cm^2] are used, but a was taken as zero.

At low molecular weights, the polymer melt is low viscosity Newtonian fluid, so that the capillarity dominates the failure in this region. As molecular weight increases, it reaches an entanglement transition where viscosity increases rapidly and the capillary failure becomes less important. At a molecular weight whose relaxation time satisfies the condition $\lambda E = 0.5$, the transition from ductile failure to cohesive fracture occurs. At higher molecular weights, the failure mode enters the cohesive fracture regime. As the relaxation time λ increases rapidly with molecular weight, $L(t_B)/L(0)$ rapidly approaches the asymptote $\sqrt{\sigma_{cr}/G}$. The abrupt transition from ductile failure to cohesive fracture is probably due to single relaxation time employed.

The influence of molecular weight is very similar to that of Weissenberg number. Thus the interpretations concerning the a parameter are very similar to those made for Fig. 4.9. At low molecular weights range, the influence of a is negligible and the curve similar to

the low molecular weight side of Fig. 4.11 is expected for any kind of polymer. At high molecular weight range, however, the fracture regime may not exist for those polymers whose a parameters are large and, instead, the ductile failure would dominate even at very high molecular weight range. This would be the case for high density polyethylenes and polypropylenes.

CHAPTER V

CONSIDERATIONS OF MELT SPINNING PROCESS

A. Background Literature

Stable Melt Spinning Process

Ziabicki and his co-workers published their extensive investigations of the melt spinning process (see Fig. 5.1) in the early 1960's. Their investigations range from a basic spinnability study [163,165] to modeling the entire process [161,162,163]. These works and review of much of the earlier literature is summarized in "Man Made Fibers" [161]. We are mainly concerned with rheological aspects of the process here. Extensive investigations of the non-isothermal melt spinning process have been carried out by Kase and Matsuo [64,65] for the Newtonian fluids. Further analytical considerations using viscoelastic models were made in isothermal conditions by Matovich and Pearson [77], Bogue and white [11], Acierno, Dalton, Rodriguez and White [2], and Denn, Petrie, and Avenas [35].

Isothermal melt spinning. Integration of the force balance equation for a spinline was carried out by Ziabicki and Kedzierska [162] and Matovich and Pearson [77]. Presuming that the velocity profile is flat across the cross-section, the area integrated form of the axial force balance is given by

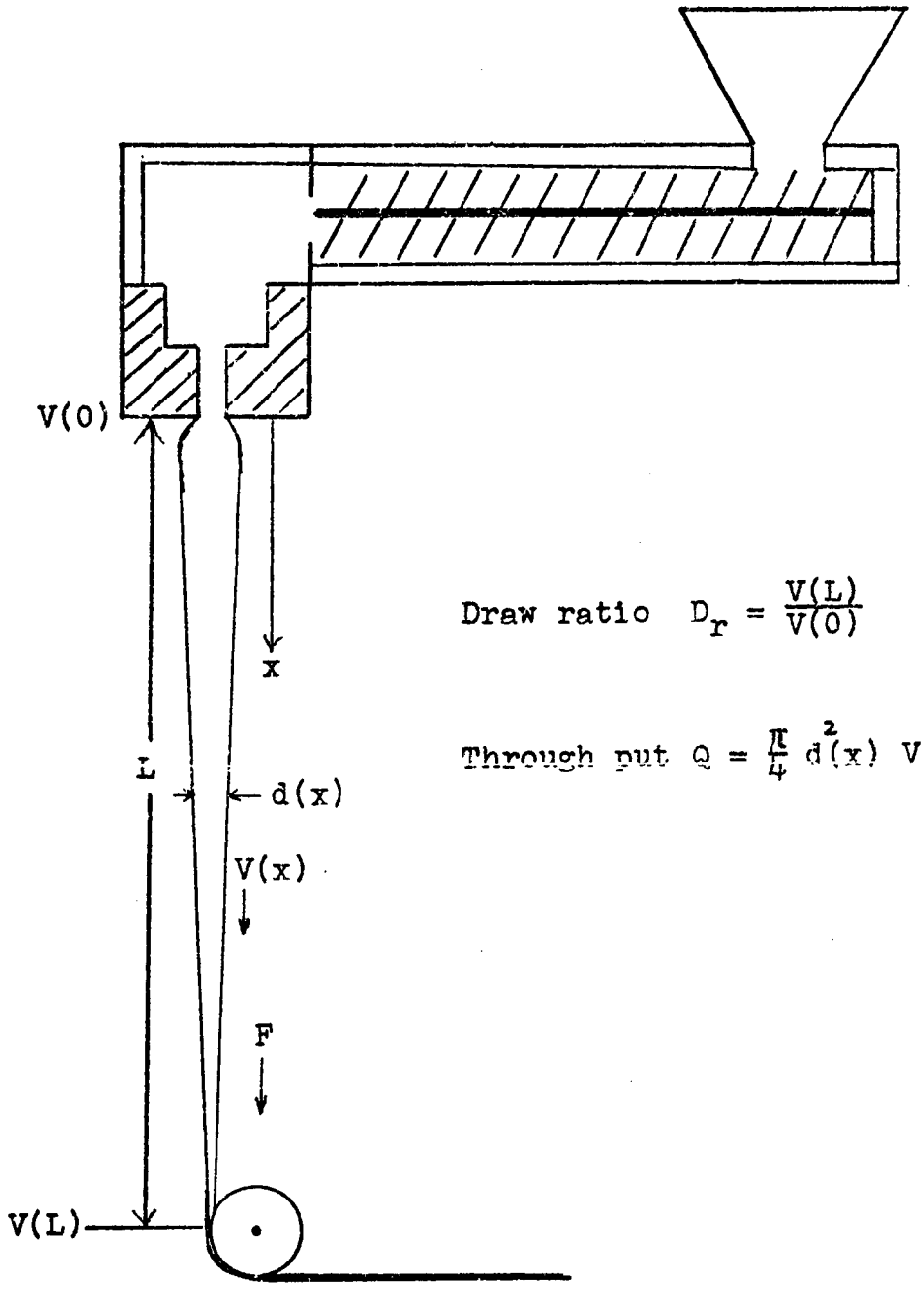


FIGURE 5.1 Continuous melt spinning process.

$$\pi R^2\rho\left[\frac{\partial V}{\partial t}+V\frac{\partial V}{\partial x}\right] = \frac{\partial}{\partial x}[\pi R^2\sigma] + \frac{\partial}{\partial x}[2\pi R\gamma] + \pi R^2\rho g \qquad (5.1)$$

If we integrate from the bobbin (x=L) along the length of the spinline x we obtain:

$$F_L = \pi R^2\sigma(x)+\rho Q(V_L-V)-\rho g\int_x^L \pi R^2 dx - 2\pi\int_x^L \gamma\frac{\partial R}{\partial x}dx \qquad (5.2)$$

Air drag term is neglected by the flat velocity profile assumption.

Over a wide range of take up velocities, take up force F_L is approximately balanced by rheological force (F_L=F(x)=F) so that

$$F = \frac{\pi}{4} d^2(x)\sigma(x) \qquad (5.3)$$

and the constant volumetric flow rate condition (continuity equation) relates diameter and velocity profiles as

$$Q = \frac{\pi}{4} d^2(x)V(x) \qquad (5.4)$$

Combining Eq. (5.3) and Eq. (5.4) gives

$$\sigma(x) = \frac{F}{Q} V(x) \qquad (5.5)$$

We note that the velocity distribution along the threadline should be the same as stress distribution.

For the Newtonian fluid, stress is simply related to instantaneous deformation rate as

$$\sigma(x) = \chi \frac{dV(x)}{dx} , \quad \chi = 3\eta \tag{5.6}$$

Substitution of the above relation into Eq. (5.5) and solving the simple differential equation yields

$$V(x) = V(0)\ e^{Fx/\chi Q} \tag{5.7}$$

Eq. (5.4) and Eq. (5.5) require that

$$d(x) = d(0)\ e^{-Fx/2\chi Q} \tag{5.8}$$

$$\sigma(x) = \sigma(0)\ e^{Fx/\chi Q} \tag{5.9}$$

For viscoelastic fluids, the situation becomes very complicated; since the stress depends not only upon instantaneous deformation rate but also on deformation history. There have been some attempts [56,58,75] to treat viscoelasticity using an elongational viscosity such as Eq. (2.45), page 24, with elongation rate $E = dV/dx$ dependant upon position or time. However, this procedure is not consistent with viscoelastic fluid theory as indicated by Acierno, et al. This is because a constant elongational viscosity such as Eq. (2.45) can be obtained only when the elongation rate is constant for long periods. Residence times in the spinline are often less than the maximum relaxation time, and during this period elongation rate varies significantly. This indicates that a full constitutive equation and not a long duration asymptote must be applied. In this sense, the analysis by Matovich

and Pearson [77] using the second order fluid [11,30,147] is not appropriate. This is because the application of the second order fluid is limited to long duration flows of sufficiently slow deformation rates compared to the material relaxation times.

In a series of publications, Bogue and White [11], Acierno, Dalton, Rodriguez, and White [2] and Chen, Hagler, Abbott, Bogue, and White [25] applied the Bogue and White model to the melt spinning dynamics with an analogous fashion to tensile stretching of a filament. The influence inside the spinneret was represented by an exponential stress decay term. Specifically, they wrote the spinline stress in terms of diameter profile.

$$\sigma(x) = \int_0^t m_1(z)\left[\left(\frac{d(0)}{d(z)}\right)^4 - \left(\frac{d(z)}{d(0)}\right)^2\right]dz + \sigma(0)\ e^{-t/\lambda_m} \qquad (5.10a)$$

with

$$z = \int_{x(t)}^{x(t-z)} \frac{dx}{V(x)} \qquad (5.10b)$$

They then numerically calculated the predicted stress from experimentally determined diameter profiles. Spearot and Metzner [125] approached this problem in a similar manner, but their experimental procedure was devised so that the elongation rate was apparently constant. The problem in these treatments seems to be prescribing the initial stress $\sigma(0)$. Polymer melt emerging from the spinnaret undergoes

complicated deformations, notably extrudate swell combined with transient flow from simple shear to simple elongation. The problem of extrudate swell under tension was investigated by White and Roman [151]. Rigorous analysis of the spinline stress considering the shear flow inside the spinnaret was recently nicely treated by Matsui [78].

Denn, Petrie and Avenas [35] have solved the velocity and stress profiles in the spinline using a modified convected maxwell model. In terms of the White-Metzner equation (Eq. (2.9), page 9), they in essence begin with the following equations of state:

$$\tau_{11} + \lambda \left[V \frac{d\tau_{11}}{dx} - 2\tau_{11} \frac{dV}{dx} \right] = 2\eta \frac{dV}{dx} \qquad (5.11a)$$

$$\tau_{22} + \lambda \left[V \frac{d\tau_{22}}{dx} + \tau_{22} \frac{dV}{dx} \right] = -\eta \frac{dV}{dx} \qquad (5.11b)$$

and the force balance

$$\tau_{11} - \tau_{22} = \frac{F}{Q} V(x) \qquad (5.12)$$

Eq. (5.11) and Eq. (5.12) are solved simultaneously for $V(x)$, $\tau_{11}(x)$ and $\tau_{22}(x)$. Analytically, only asymptotic solutions were possible and general solution was obtained numerically. The asymptote of large applied stress and of negligible internal pressure (τ_{22}) is of special interest. In this asymptote of infinite tension in the spinline, they showed that

$$\frac{V(x)}{V(0)} = 1 + \frac{1}{N_{We}} \frac{x}{L} \tag{5.13}$$

where $N_{We} = \lambda V_0/L$ is the Weissenberg number (or Deborah number) of the process. The linear variation in velocity is in striking contrast with the exponential variation predicted for the Newtonian fluid. We note that for a given Weissenberg number, Eq. (5.13) gives the maximum attainable draw ratio $V(L)/V(0)$.

Non-isothermal melt spinning. In a conventional melt spinning process, temperature variation in the spinline is the most significant factor for the spinline dynamics. Formulation of the process then requires simultaneous solution of both force and heat balances. The problem was analyzed by Kase and Matsuo [64,65] in terms of Newtonian elongational viscosity which depends upon temperature. In essence, Kase and Matsuo begin with the force balance (combined with continuity) and heat balance of the form:

$$\sigma(x) = \frac{F}{Q} V(x) = \chi(T) \frac{dV}{dx} \tag{5.14}$$

$$C_p \rho Q \frac{dT}{dx} = -\pi dh(T-T_a) \tag{5.15}$$

where C_p is the heat capacity and h is a heat transfer coefficient which contains the effects of convention and radiation, and T_a is the air temperature. If we specify the $\chi(T)$, and $h(x)$ functions, we can solve Eq. (5.14)

and Eq. (5.15) simultaneously to obtain various variables as a function of position; $\sigma(x)$, $V(x)$, $T(x)$, $d(x)$. This procedure was used by Kase and Matsuo to investigate a variety of spinline problems.

The works by Kase and Matsuo neglect viscoelastic characters of polymers being spun. Abbott and White [1] have indicated how non-isothermal effects might be handled in a spinline analysis using a nonlinear viscoelastic integral model. They suggested the application of thermorheological simplicity [96,97], i.e., hypothesizing the experimental facts of time-temperature superposition [154] being valid in dynamic experiments as first suggested by Morland and Lee [92]. Thus the relaxation functions are generalized to the form

$$m_1(t-s,T(s)) = m_1(\bar{z},T_0) \tag{5.16a}$$

$$\bar{z} = \int_s^t \frac{d}{a_T(T)} \tag{5.16b}$$

where a_T is the temperature dependent shift factor and T_0 is a reference temperature. Matsui [78] with Bogue has proceeded using this approach and found a "delay effect" of the stress in viscoelastic fluids when the temperature changed suddenly. This effect suggests that apparently elongational viscosities in the non-isothermal spinline are much lower than data obtained at corresponding static temperatures [55]. They have also given an analysis

showing the influences of the spinneret capillary on the stress in the cooling spinline of a viscoelastic fluid.

Unstable Melt Spinning Process

Spinnability in the continuous process. There are limitations to the conditions under which steady state melt spinning can be formed. Ziabicki and Takserman-Krozer [161,164,165] have made a basic contribution to the problem of spinnability in the continuous process. They demonstrated the existence of two regimes of breakage: capillary breakup and cohesive fracture. Ziabicki [161] correlated the breakup length of various investigators against the product of viscosity and pulling velocity, and he attributed the observed maximum to the two mechanisms. Capillary breakup is usually observed in very low viscosity liquids and cohesive fracture in very high viscosity liquids, and generally both mechanisms do not overlap. Ziabicki apparently ignored the ductility related instability.

Even after a spinline is formed, the spinline is not necessarily stable. One sometimes obtains kneeing just after the spinneret or fibers with periodic diameter fluctuation. The kneeing phenomena sometimes is associated with vibrations and can cause non-uniform fibers. This phenomena has been variously attributed, but the main cause seems to be non-uniform viscosity in the spinneret [124]. The periodic diameter fluctuations may be due to forced

oscillations of the system or due to inherent instabilities in the system. One sometimes observes severe fluctuations of the fiber diameter when spinning is performed under near isothermal conditions. This phenomena is called draw resonance and has been paid particular attention. The results obtained by many investigators will be discussed next.

Draw resonance phenomena. The periodic fluctuations in fiber diameter and tension were described by Miller [89] and Freeman and Coplan [43], Bergonzoni and Cresce [7] and Kase, Matsuo, and Yoshimoto [66] in the mid 1960's. Freeman and Coplan, based upon their experimental results for polypropylene, explained the phenomena by inhomogeneities in the melt.

Kase, Matsuo, and Yoshimoto investigated the draw resonance phenomena both theoretically and experimentally for film extrusion. In the isothermal case, they began with the unsteady state forms of the continuity equation and the force balance for Newtonian fluids.

$$\frac{\partial A}{\partial t} + \frac{\partial}{\partial x}(AV) = 0 \qquad (5.17)$$

$$\frac{F}{A} = \chi \frac{\partial V}{\partial x} \qquad (5.18)$$

After steady state solutions ($\partial A/\partial t = 0$) are obtained as Eq. (5.7) and Eq. (5.8), the infinitesimal disturbances are imposed to the steady state values:

$$A(x,t) = \bar{A}(x)[1+a(x,t)] \tag{5.19a}$$

$$V(x,t) = \bar{V}(x)[1+b(x,t)] \tag{5.19b}$$

These perturbed values are substituted into governing equations, Eq. (5.17) and Eq. (5.18), and linearization with respect to first order disturbance is carried out. The differential equation describing the area fluctuation becomes (see Pearson et al. [108] Eq. (20) or Kase et al. [66] Eq. (31))

$$\frac{\partial^2 a}{\partial t \partial z} + \bar{V} \frac{\partial^2 a}{\partial x^2} = 0 \tag{5.20}$$

where $\bar{V}(x)$ is given by Eq. (5.7). Kase and Matsuo and Yoshimoto [66] first solved this problem and found that the systems with draw ratio $V(L)/V(0)$ above 20 are unstable. Later Pearson and Matovich [108] solved this problem analytically. Numerical solution was given by Gelder [46].

Experimentally the fluctuation period (which is closely related to residence time in the spin path) is in good agreement, but the amplitude of the oscillation remains constant with time rather than increasing exponentially as suggested by the linear theory. Kase et al. [63,66] attributed this phenomena to a limit cycle of non-linear oscillation. Recent experiment for a Newtonian fluid (silicone oil) by Donnelly and Weinberger [36] supports the theory in terms of the critical draw ratio of about 20.

Ishihara and Kase [60,61] and Fisher and Denn [41,42] solved the draw resonance problem without linearization. The results are the same as linear theory in terms of the critical draw ratio but show a longer period of oscillation. The nonlinear theory also shows the sustained oscillation at a certain amplitude corresponding to the limit cycle regardless of the magnitudes of initial disturbances.

There have also been studies for non-Newtonian fluid models. Shah and Pearson [120] have studied this problem for a power law fluid (elongational viscosity χ varies with deformation rate E to a power) and found that the critical draw ratio increases when χ increases with E. Zeichner [160] with Metzner, Denn, and Anshus performed linearized stability analysis for a viscoelastic fluid using a convected Maxwell model of White-Metzner form. They showed that the stability increases with the Weissenberg number and found a second stable region at high draw ratios where the spinline tension is close to infinity. This analysis was recently improved by Fisher and Denn [41,42] employing nonlinear stability theory and a power law for the relaxation time of the viscoelastic model. They showed that the critical draw ratios are very sensitive to the power law exponent and decrease considerably with increasing deformation rate dependence.

Shah and Pearson [118,119] and Kase [63] studied the

draw resonance problem for the non-isothermal case neglecting the fluid elasticity. Shah and Pearson found that the effects of cooling greatly stabilize the spinline. Kase found that draw resonance never develops if the solidification takes place prior to take up. This great stabilization due to solidification prior to take up is also found by Pearson, Shah, and Mhaskar [109]. Several experimental studies have shown this. The experimental finding of Han, Lamonte, and Shah [57] that draw resonance is more severe in non-isothermal spinning conditions is highly contradictory. More detailed discussions on the spinline instabilities are found in a review paper by Petrie and Denn [110].

It was found that the feature of elongational viscosity increases in the neck (due to cooling or elasticity effects) make the system more stable. This suggests that the draw resonance phenomena becomes a serious problem only when one tries to spin fluids (whose χ does not increase with elongation rate) in isothermal or near isothermal conditions.

B. Theoretical Investigation

Stable Spinning of a Viscoelastic Fluid

The rheological problems of the isothermal spinning of a viscoelastic fluid were recently treated by Denn, Petrie, and Avenas [35] using a convected Maxwell model

with a slight deformation rate thinning character. They found a limited draw ratio for a finite Weissenberg number. Specifically, draw ratio is limited by

$$\frac{V(L)}{V(0)} = 1 + \frac{L}{\lambda V(0)} = 1 + \frac{1}{N_{We}} \qquad (5.21)$$

This limited draw ratio seems very low, since the Weissenberg number often becomes more than unity. An attempt was made to improve the analysis using the effective relaxation time as discussed before (page 129).

In terms of the White and Metzner model employing the effective relaxation time, the process may be described by

$$\tau_{11} + \lambda_{eff}\left(V \frac{d\tau_{11}}{dx} - 2\tau_{11} \frac{dV}{dx}\right) = 2G\lambda_{eff} \frac{dV}{dx} \qquad (5.22a)$$

$$\tau_{22} + \lambda_{eff}\left(V \frac{d\tau_{22}}{dx} + \tau_{22} \frac{dV}{dx}\right) = -G\lambda_{eff} \frac{dV}{dx} \qquad (5.22b)$$

where

$$\lambda_{eff} = \frac{\lambda}{1+\beta a \lambda \frac{dV}{dx}} \qquad (5.23)$$

The continuity and the force balance are combined to give

$$\sigma(x) = \tau_{11}(x) - \tau_{22}(x) = \frac{F}{Q} V(x) \qquad (5.24)$$

The case for a=0 was solved by Denn et. al. [35]. The complete analytical solution is not possible, but the asymptotic solutions were obtained. The asymptote of

large applied stress is of practical interest, however, the solution is implicit and very complicated. They found that the internal pressure τ_{22} is small compared to axial stress τ_{11} in practical cases. We will neglect τ_{22} for mathematical simplicity as Zeichner [160] did for his stability analysis of this process.

Then, Eq. (5.22a), Eq. (5.23), and Eq. (5.24) can be solved simultaneously without any difficulty. The result for velocity distribution along the thread line is

$$\frac{F}{Q}\left\{x+(\sqrt{3}a-1)\lambda(V(x)-V(0))\right\} = 2G\lambda \ln\frac{V(x)}{V(0)} \qquad (5.25)$$

At $a=0$, this is equivalent to Zeichner's solution [33, 160] and when $a=1/\sqrt{3}$, the distribution is exponential as in Newtonian fluids. If we introduce draw ratio $D_r = V(L)/V(0)$, Eq. (5.25) is rearranged to give

$$\frac{x}{L} = \alpha'\left\{\frac{V(x)}{V(0)}-1\right\}+\left\{1-\alpha'(D_r-1)\right\}\frac{\ln(V(x)/V(0))}{\ln D_r} \qquad (5.26a)$$

where

$$\alpha' = (1-\sqrt{3}a)\lambda\frac{V(0)}{L} \qquad (5.26b)$$

α' can be considered as an effective Weissenberg (or Deborah) number. Eq. (5.26) is plotted in Fig. 5.2 for various values of α'. It is seen that the velocity distribution along the threadline is almost identical with the numerical soultion by Denn et al. [35] except we can

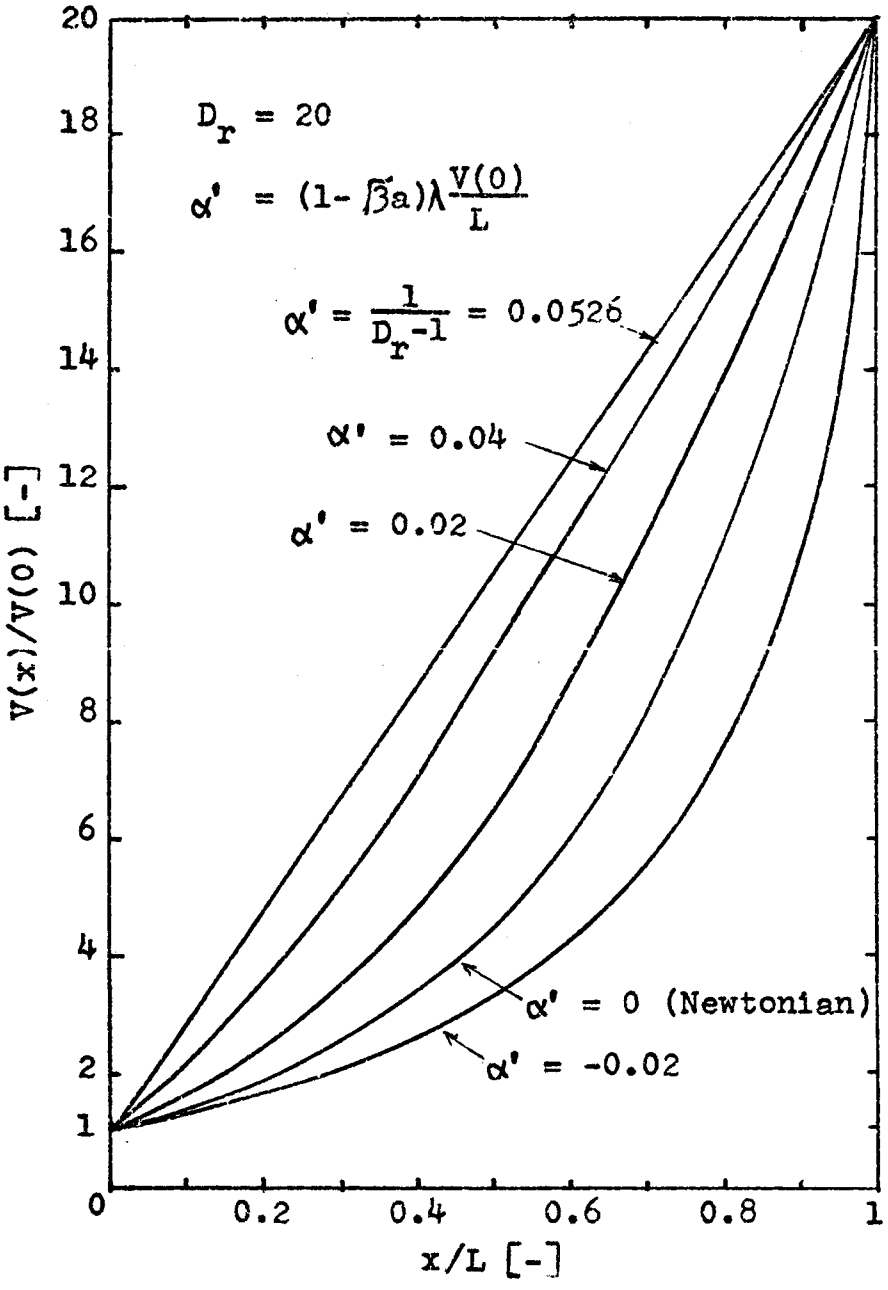


FIGURE 5.2 Velocity distribution along the threadline for various values of an effective Deborah number.

have negative α' if $a > 1/\sqrt{3}$.

The stress distribution along the threadline is identical with the velocity distribution as required by Eq. (5.24). The cross section distribution is the inverse of the velocity distribution to satisfy the continuity equation $Q = A(x)V(x)$.

The maximum stress which occurs at the take up is expressed as

$$\sigma(L) = \frac{2\eta V_0 D_r \ln D_r}{L-(1-\sqrt{3}a)\lambda V_0(D_r-1)} = \frac{2\eta V_0 D_r \ln D_r}{L(1-\alpha'(D_r-1))} \qquad (5.27)$$

When a is small such that $a < 1/\sqrt{3}=0.58$, as draw ratio increases the stress increases rapidly and becomes infinite at a finite draw ratio. In this case cohesive fracture occurs for any critical stress and the maximum draw ratio is limited by

$$D_{rm} = 1 + \frac{L}{(1-\sqrt{3}a)\lambda V(0)} \qquad (5.28)$$

When a is large enough $(a > 1/\sqrt{3})$, there are no limited draw ratios and very high draw ratios are possible.

It is interesting to note the critical value of the parameter a is $1/\sqrt{3}=0.58$ to reduce the problem to Newtonian fluid case, just as in the ductile instability problem. This value is half the critical value for the unbounded stress growth (which is $a=2/\sqrt{3}$, see page 79).

Analogy between Ductile Instability and Draw Resonance Analyses

We shall consider a general instability problem associated with uniaxial stretching. Inertia, surface tension, and the gravity effects will be ignored, so that force becomes constant along the length as stated by the equation of motion.

$$\frac{\partial}{\partial z}(\pi R^2 \sigma_{11}) = 0 \qquad (5.29)$$

The area integrated continuity equation is (see Eq's. (4.9) and (4.10), page 117)

$$\frac{\partial V}{\partial z} = -\frac{2}{R} U_R \qquad (5.30a)$$

where

$$U_R = \frac{DR}{Dt} = \frac{\partial R}{\partial t} + V \frac{\partial R}{\partial z} \qquad (5.30b)$$

Eq. (5.29) and Eq. (5.30) are general fundamental equations which can be applied either to tensile tests or melt spinning problems.

For the tensile tests, we have $\partial R/\partial z = 0$, so that Eq. (5.30) can be reduced to

$$\frac{d}{dt}(\pi R^2 L) = 0 \qquad (5.31)$$

as shown on pages 117 and 118. For the steady melt spinning process, we have $\partial R/\partial t = 0$, so that Eq. (5.30) is

reduced to

$$\frac{d}{dz}(\pi R^2 V) = 0 \tag{5.32}$$

This is the constant through put condition $(Q = \pi R^2 V)$. If it is not the steady state, Eq. (5.30) is simply re-arranged to give

$$\frac{\partial}{\partial t}(\pi R^2) + \frac{\partial}{\partial z}(\pi R^2 V) = 0 \tag{5.33}$$

which is the continuity equation in the melt spinning process as first derived by Kase and Matsuo [64].

We shall consider the stability problem of the system described by Eq. (5.29) and (5.30), which includes both tensile instability and melt spinning instability. It will be shown that the draw resonance in the melt spinning process is the analogue of the ductile instability in tensile tests. For simplicity, we prove the analogy using the Newtonian fluid model. The method is the straight forward linear stability analysis employing a perturbation technique. When the radius is perturbed by an amount

$$R = \bar{R} + \xi \tag{5.34}$$

the velocity fields are perturbed according to

$$V = \bar{V} + V' \tag{5.35a}$$

$$U_R = \bar{U}_R + U'_R \tag{5.35b}$$

The continuity equation Eq. (5.30) is perturbed as

$$\frac{\partial \bar{V}}{\partial z} + \frac{\partial V'}{\partial z} = - \frac{2}{R+\xi} (\bar{U}_R + U'_R) \tag{5.36}$$

The radial velocity at the cylinder surface is also perturbed as

$$\bar{U}_R + U'_R = \frac{\partial (R+\xi)}{\partial t} + (\bar{V}+V')\left(\frac{\partial R}{\partial z} + \frac{\partial \xi}{\partial z} \right) \tag{5.37}$$

Linearization of Eq. (5.36) gives

$$\frac{\partial \bar{V}}{\partial z} = - \frac{2}{R} \bar{U}_R \ , \quad \frac{\partial V'}{\partial z} = - \frac{2}{R}(U'_R - \frac{\xi}{R} \bar{U}_R) \tag{5.38a,b}$$

The perturbed equation of motion for the newtonian fluid is

$$\frac{\partial}{\partial z} (\pi R^2 \sigma'_{zz} + 2\pi R \xi \bar{\sigma}_{zz}) = 3\eta\pi \frac{\partial}{\partial z} (R^2 \frac{\partial V'}{\partial z} + 2R\xi \frac{\partial \bar{V}}{\partial z}) = 0 \tag{5.39}$$

If we substitute Eq. (5.38) into Eq. (5.39), we obtain

$$\frac{\partial}{\partial z} (\xi \bar{U}_R + R U'_R) = 0 \tag{5.40a}$$

where $\bar{U}_R$ and U'_R are obtained form Eq. (5.37) as

$$\bar{U}_R = \frac{\partial R}{\partial t} + \bar{V} \frac{\partial R}{\partial z} \ , \quad U'_R = \frac{\partial \xi}{\partial t} + \bar{V} \frac{\partial \xi}{\partial z} + V' \frac{\partial R}{\partial z} \tag{5.40b,c}$$

This is the equation describine the instability caused by varying cross-section along the length.

It will be shown that the ductile instability and the draw resonance are special cases of Eq. (5.40). For the

tensile test, we have $\partial R/\partial z = 0$ so that Eq (5.40) simplifies to

$$\frac{\partial}{\partial t}(R\hat{\xi}) = 0 \tag{5.41}$$

This is the ductile instability equation derived earlier (Eq. (4.40), page 126).

For the melt spinning process, we have $\partial R/\partial t = 0$ then Eq. (5.40) becomes

$$\frac{\partial}{\partial z}\left\{R\frac{\partial \xi}{\partial t} + \bar{V}\frac{\partial}{\partial z}(R\xi) + RV'\frac{\partial R}{\partial z}\right\} = 0 \tag{5.42}$$

This is the equation describing the draw resonance phenomena. It will be proved that the above differential equation is the same as equations of previous investigators on draw resonance. The relations between their notations and our notation are

$$A = \bar{A}(1+a) = \pi R^2 + 2\pi R\xi \tag{5.43a}$$

$$V = \bar{V}(1+b) = \bar{V} + V' \tag{5.43b}$$

In terms of the previous investigator's notation, the continuity equation Eq (5.38) becomes

$$\bar{V}\frac{\partial \bar{A}}{\partial z} + \bar{A}\frac{\partial \bar{V}}{\partial z} = 0 \tag{5.44a}$$

$$\frac{\partial a}{\partial t} + \bar{V}\left(\frac{\partial a}{\partial z} + \frac{\partial b}{\partial z}\right) = 0 \tag{5.44b}$$

where

$$\bar{V}(z) = \bar{V}(0) \exp(Fz/\chi Q) \qquad (5.44c)$$

If we replace our notation by their notation using Eq. (5.43) and Eq. (5.44), then Eq. (5.42) is transformed to

$$\frac{\partial^2 a}{\partial z \partial t} + \bar{V} \frac{\partial^2 a}{\partial z^2} = 0 \qquad (5.45)$$

This is the differential equation describing the draw resonance phenomena and is the same as Pearson et al. [108] Eq. (20) or Kase et al. [66] Eq. (31).

It has been proved that the draw resonance in the melt spinning process (a continuous process) is an analogue of ductile instability in the tensile test (a batch process). Therefore the results obtained in the ductility analysis in Chapter IV have direct implications to the draw resonance phenomena. For instance, the viscoelasticity which stabilizes the ductile instability by enhanced elongational visocsity would stabilize draw resonance. This has been shown by Zeichner [160], Fisher and Denn [42], and to a similar extent by power law analyses of Pearson et al. [109,120], and Ishihara and Kase [61]. However strong dependence of relaxation time upon deformation rate would destabilize the draw resonance. This is also proved by Fisher and Denn [42]. In terms of the White and Metzner model, employing effective relaxation time (Eq. (5.22) and Eq. (5.23)), it might be

expected that the effective Deborah number (derived in the previous section)

$$\alpha' = (1-\sqrt{3}a)\,\lambda\,\frac{V(0)}{L} \qquad (5.46)$$

determines the critical draw rstio. If $\alpha' > 0$ the critical draw ratio would be more than 20 but if $\alpha' < 0$ it would be less than 20 . If $a > 1/\sqrt{3}$ the critical draw ratio would be always less than 20 and it would decrease with increasing $\lambda\, V(0)/L$.

C. Experimental Study on Limitations of Melt Spinning

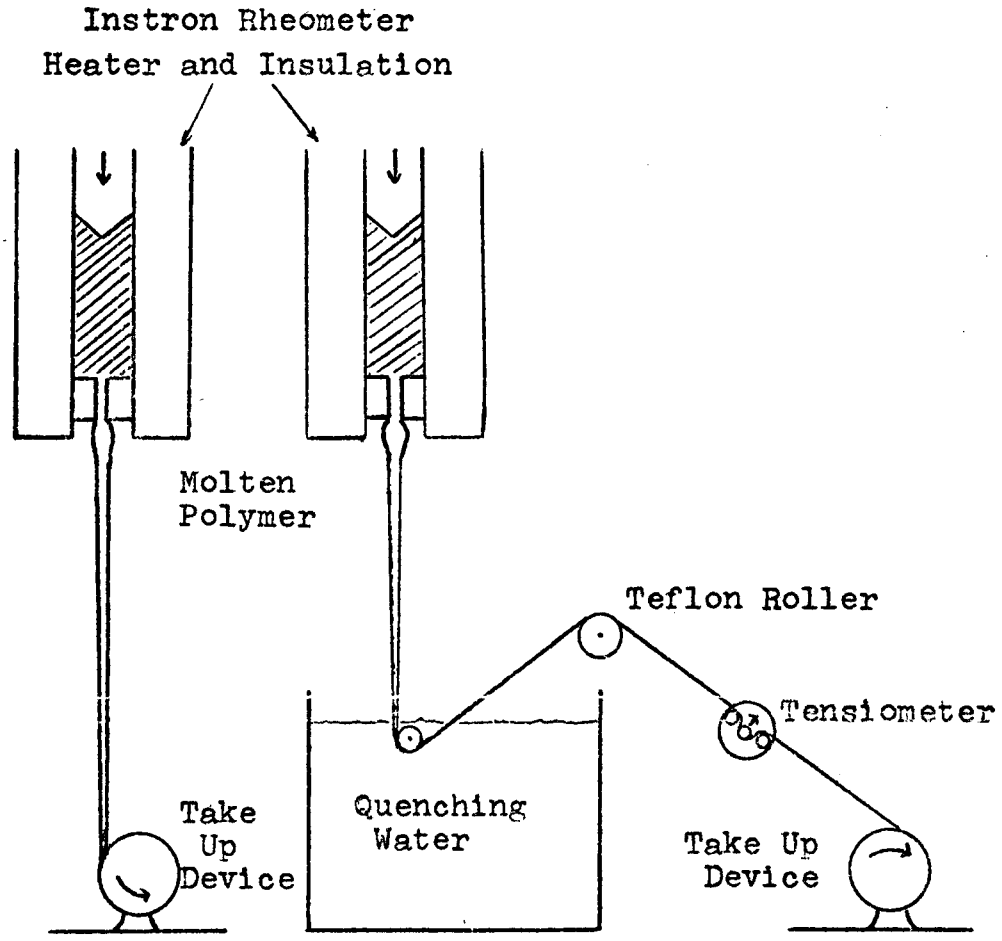
Materials

Limitations of the melt spinning were observed for most of the materials listed in Table II (page 42) plus Union Carbide DYLT LDPE (MI = 400). Some of the observations were made when preparations of cylindrical filaments for the tensile tests were attempted. For most of the polymers listed in the table, only qualitative observations proved possible. Quantitative studies were made for a low density polyethylene (LDPE, MI = 1.7), and a high desnity polyethylene (HDPE, MI = 2.6). Particular attention was paid to the failure characteristics of the stable spinline of LDPE and HDPE, because they failed in a very different manner in tensile tests. "Bouncing Putty" supplied by Cogswell was used for a close observation of draw resonance phenomena at room temperature. According

to Cogswell [29], this sample has stress independent material parameters of viscosity 8×10^6 [poise], and a modulus of 2.5×10^6 [dyn/cm^2] at room temperature. The temperatures (inside the die) were mainly kept the same as those of the tensile tests, that is, 160°C for LDPE, HDPE, and PS, 180°C for PP.

Melt Spinning Apparatus

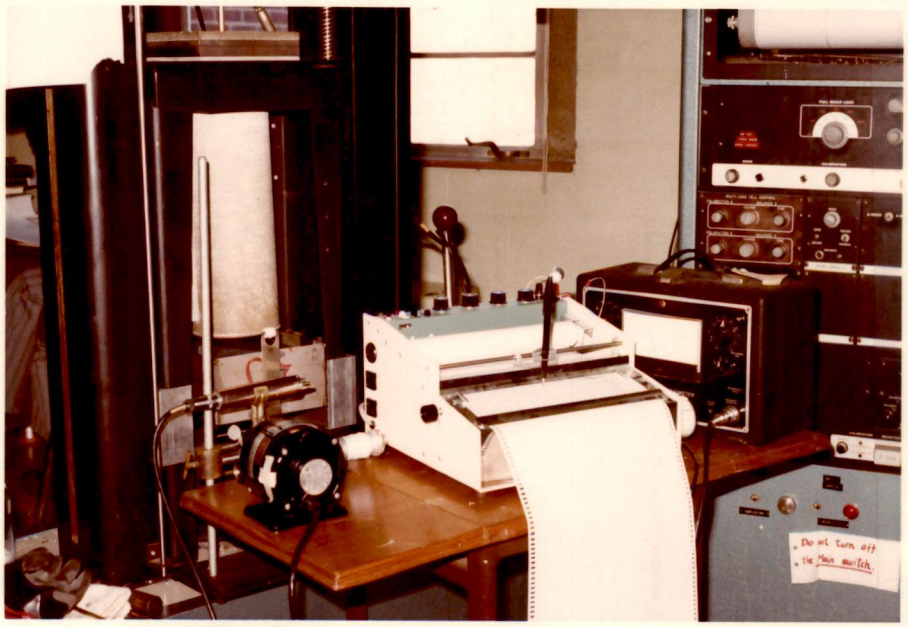
Melt spinning experiments were carried out using the Instron capillary rheometer and a take up device. Two types of experiments were performed using the set-ups shown in Fig. 5.3. Qualitative observations of spinnability for various kinds of polymer melts were made using the set-up shown in (a). The spinpath was 19.4 cm and the cooling of the filament took place in the air. Most of these observations were made when preparation of filaments for the tensile tests was attempted. The die diameter was 2.11 mm, as before. The set-up shown in (b) was used for draw resonance experiments. In order to take force readings, a Rothschild tensiometer (10 gram full scale) was placed after a water quenching bath. We should note that the tensiometer detects not only the tension in the spinline, but also the diameter and the stiffness of the thread as is clearly seen from the design. Photographs of the set-up for the draw resonance experiments are shown in Fig. 5.4 for a detailed view.



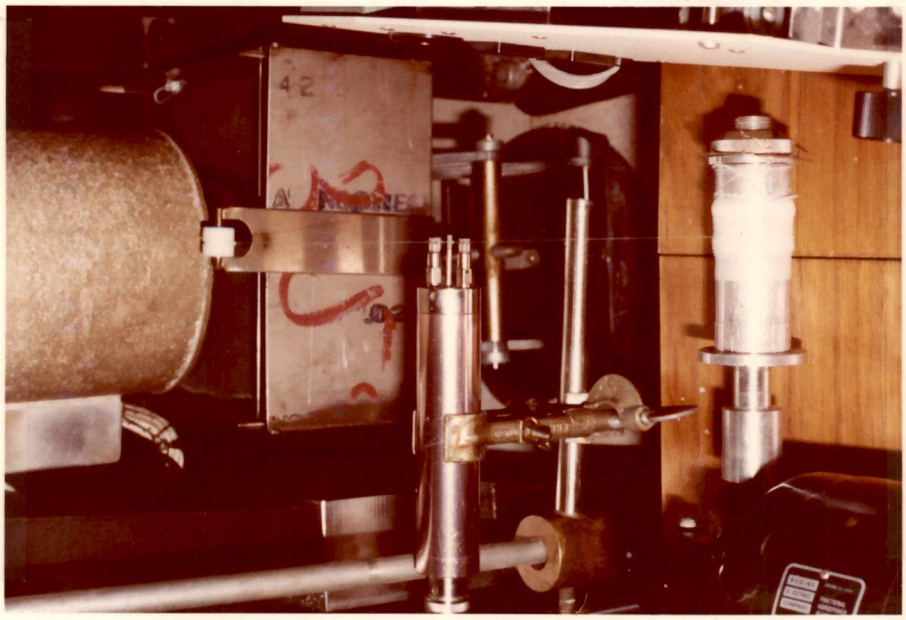
(a) Melt spinning into quiescent air.

(b) Draw resonance experiment.

FIGURE 5.3 Schematic diagram of the melt spinning apparatus.



a) Overall view of the apparatus.



b) Close up view of the spinline.

FIGURE 5.4 Experimental set up for the draw resonance experiments.

The diameter of the take up roll is 3.18 cm which is driven by a 1/20 horsepower Bodine Elcetric Company motor (173 r.p.m. maximum speed). For the draw resonance experiments using the set up (b), die of diameter 0.775 mm (L/D = 28.9) is mounted in the 9.53 mm diameter Instron barrel. Experimental conditions were limited to rather narrow ranges due to one decade ranges of the tensiometer and the take up speed, although extrusion speed could be varied over a wide range. The spinpath (from the die exit to water surface) was rather short (7.3 cm, most of the time) and the residence time was of the order of a few seconds. Thus the draw resonance experiments were carried out in nearly isothermal conditions, although cooling in the spinpath was not inevitable.

Melt Spinning into Quiescent Air

Qualitative observations. When preparations of filaments for the tensile test were attempted using the set up shown in Fig. 5.3 (a), it was found impossible to prepare the filaments of low viscosity liquids. At high temperatures polymer wax broke up due to the action of surface tension and gravity and never reached the take up roll. LDPE (MI = 400) was subject to gravity induced ductile instability, but often could reach the take up roll by gravity spinning. The filament, however, was thinned down too much and the taken-up filament stuck together so that the filament preparation was unsuccessful

at high temperatures. It was found that the barrel temperature has to be slightly above the melting point of the polymer and the filament should freeze before the take up roll.

At the start of melt spinning, descending extrudate is pulled to the take up roll. It was found that the materials such as HDPE and PP have to be pulled very carefully to avoid ductile failure, but such materials as LDPE, PS, and PMMA do not require this care. Based upon the discussions above, it may be seen that the failure mechanisms in the tensile test discussed in Chapter III and Chapter IV can be applied to a significant extent to the failure of filaments as long as steady spinline has not been established.

After a spinline was formed at a slow take up speed, the take up speed was increased. For the spinning of LDPE (MI = 60, 23, 5.0, 1.7), it was found that the lower the viscosity, the higher the take up velocity attained. The failure mode was obviously fracture, so this trend is expected. However, HDPE (MI = 0.1) which has higher viscosity than LDPE (MI = 1.7) could be taken up at higher speed than the LDPE (MI = 1.7).

Quantitative data. The maximum draw ratio attained for the LDPE (MI = 1.7) was compared with the theory developed in a previous section, specifically with Eq. (5.28), page 179. Maximum draw ratios exist because

cohesive failure follows if the spinline tension becomes infinite. The maximum draw ratio D_{rm} is written as

$$\log (D_{rm}-1) = - \log\left\{(1-\sqrt{3}a)\,\lambda\,\frac{V(0)}{L}\right\} \qquad (5.47)$$

For the LDPE (MI = 1.7), λ = 13.4 [sec] (at 160 °C) had been determined. The Deborah number was varried by changing extrusion speed V(0) and L was kept at 19.4 cm. At a fixed V(0), the take up speed was gradually increased and the maximum attained take up speed was determined (as an average of at least three trials).

Fig. 5.5 shows the comparison of Eq. (5.47) with the experimental data, taking a as a parameter. It may be seen that Eq. (5.47) gives a right order of draw ratio if we take a around 0.5. For a=0, however, the critical draw ratio is estimated about one decade lower. The trend of data points being lower at low Deborah numbers and not giving straight line of slope -1 is attributed to cooling in the air and the approximate character of the theory. At low extrusion speed V(0), material cools and relaxation time λ increases and, in effect, actual data points should shift to higher Deborah number side.

Draw Resonance Experiments

Qualitative observations. When near isothermal melt spinning was performed using the set up shown in Fig 5.3 (b),

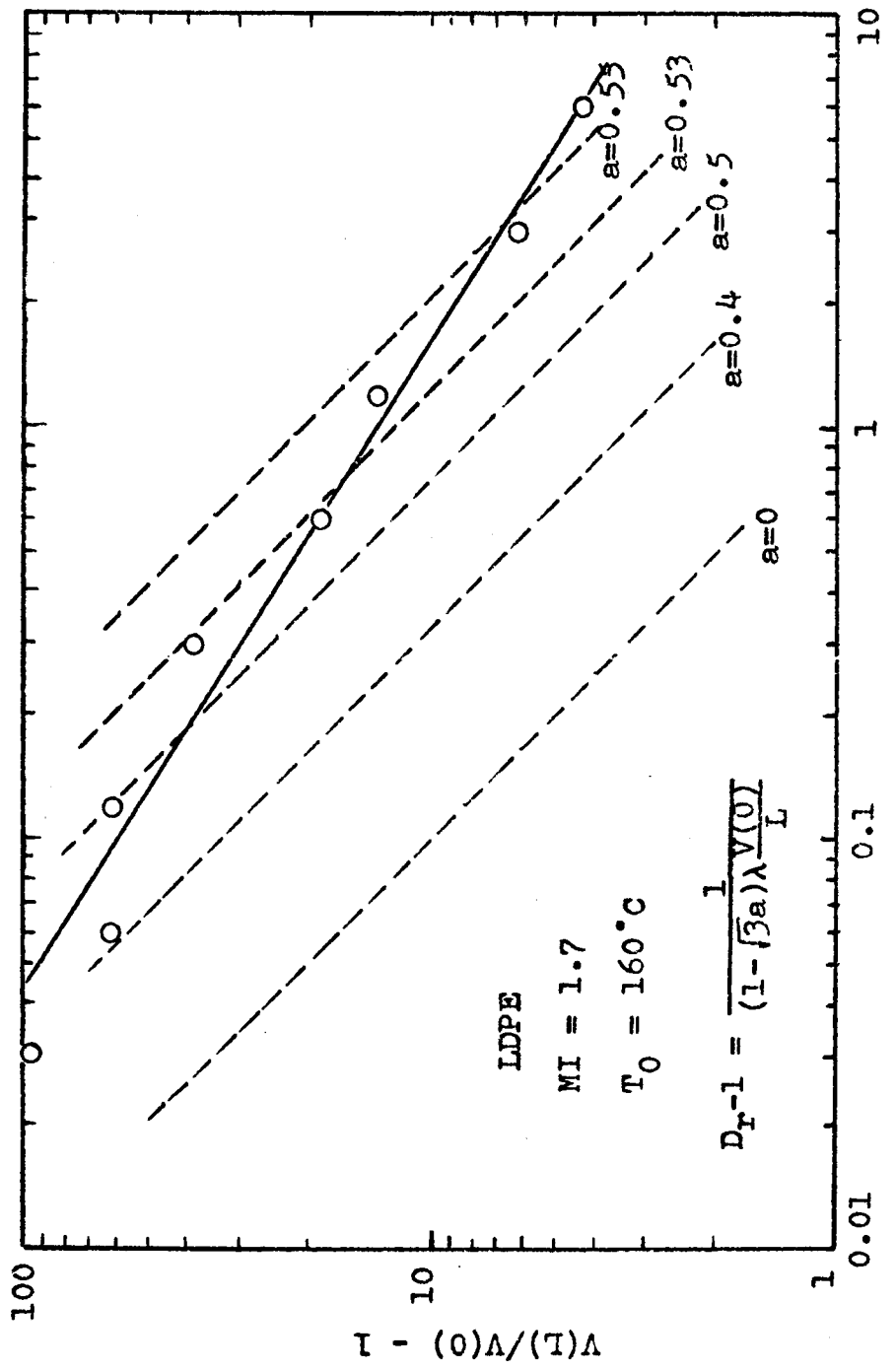
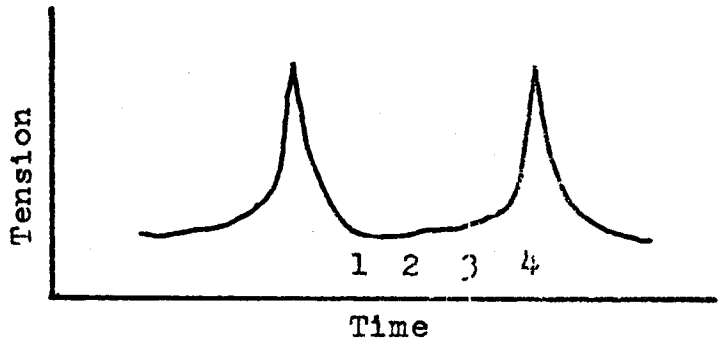


FIGURE 5.5 Maximum draw ratio attained plotted against Deborah number.

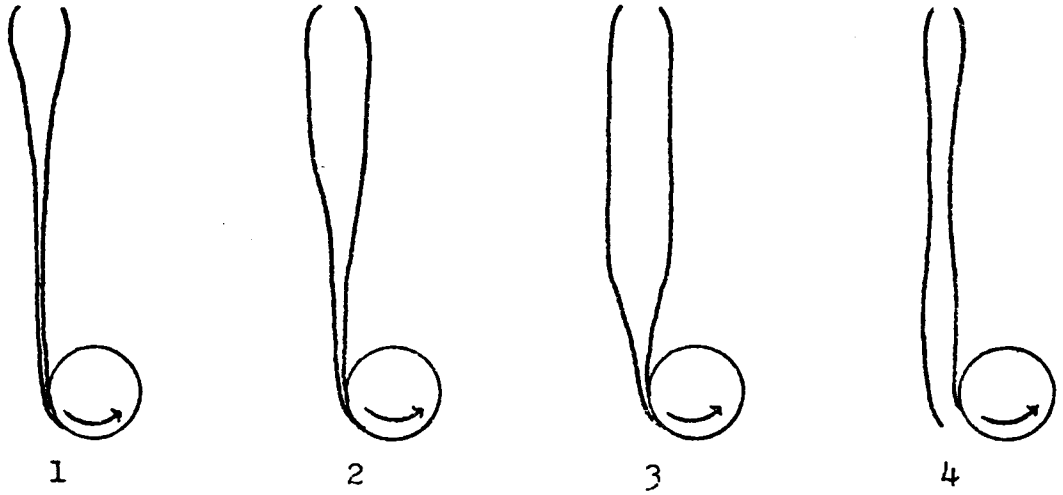
HDPE and PP showed severe diameter fluctuations above a specific draw ratio. However LDPE and PS did not show such fluctuations within the experimental ranges performed. For these materials, the spinline tension became too high to be recorded in the 10 gram weight tensiometer.

The polypropylenes (MI = 0.42, 6.6) were very hard to spin at 180°C because filaments often failed in a ductile manner before steady spinlines were established. At higher temperature (200°C), spinlines were easier to establish, but still showed fluctuations of short periods at low draw ratios. The polypropylenes seemed to be more stable at high temperatures. This observation agrees with that of Ishihara and Kase [61] who showed strong dependence of critical draw ratio upon temperature for polypropylenes.

Using "Bouncing Putty," draw resonance phenomena was closely observed. The observation was performed at room temperature using the set up (a), since this silicone based material was a viscoelastic fluid at room temperature. The resonance period was about 30 seconds, so that a close observation was possible. The observed spinline profile is sketched in Fig. 5.6. The force fluctuation based upon tensiometer recording of the HDPE (MI = 2.6) is also shown in the same figure to illustrate the in phase fluctuation. This sketch is very similar to that of Ishihara and Kase [61] who simulated and photographed the spinline profiles during a stable draw resonance.



(a) Force fluctuation.



(b) Spinline side profiles during one cycle.

FIGURE 5.6 Force and diameter fluctuations during draw resonance.

From the figure, it is clear that the draw resonance phenomena is not a resonance of small fluctuations entering the system. It is caused by an accumulation of the material in the spinpath. The thick portion is forced to come down because material is continuously extruded out and is eventually taken up. It is also seen that the large force reading corresponds to taking up the thick portion which causes the in phase fluctuations of force and diameter. This phenomena caused by the accumulations of the material occurs periodically due to continuous nature of the process.

Quantitative data. The strip chart recording of the transient draw resonance phenomena which occured for HDPE (MI = 2.6) is shown in Fig. 5.7. Careful observations during the resonance showed that the large peaks recorded are due to the passing of thick portion at the sensing position of the tensiometer, and the small peaks are actual threadline tension readings. It is seen that when the draw ratio is 3.50 the fluctuations damp out, but when it is changed to 5.25 the fluctuations start to magnify. The amplitudes do not grow indefinitely, but level off at a certain level as suggested by the nonlinear theory.

The spinline tensions during steady draw resonance are plotted as a function of draw ratio in Fig. 5.8. One can see that the critical draw ratio when the system becomes unstable is around 5 for the HDPE (MI = 2.6).

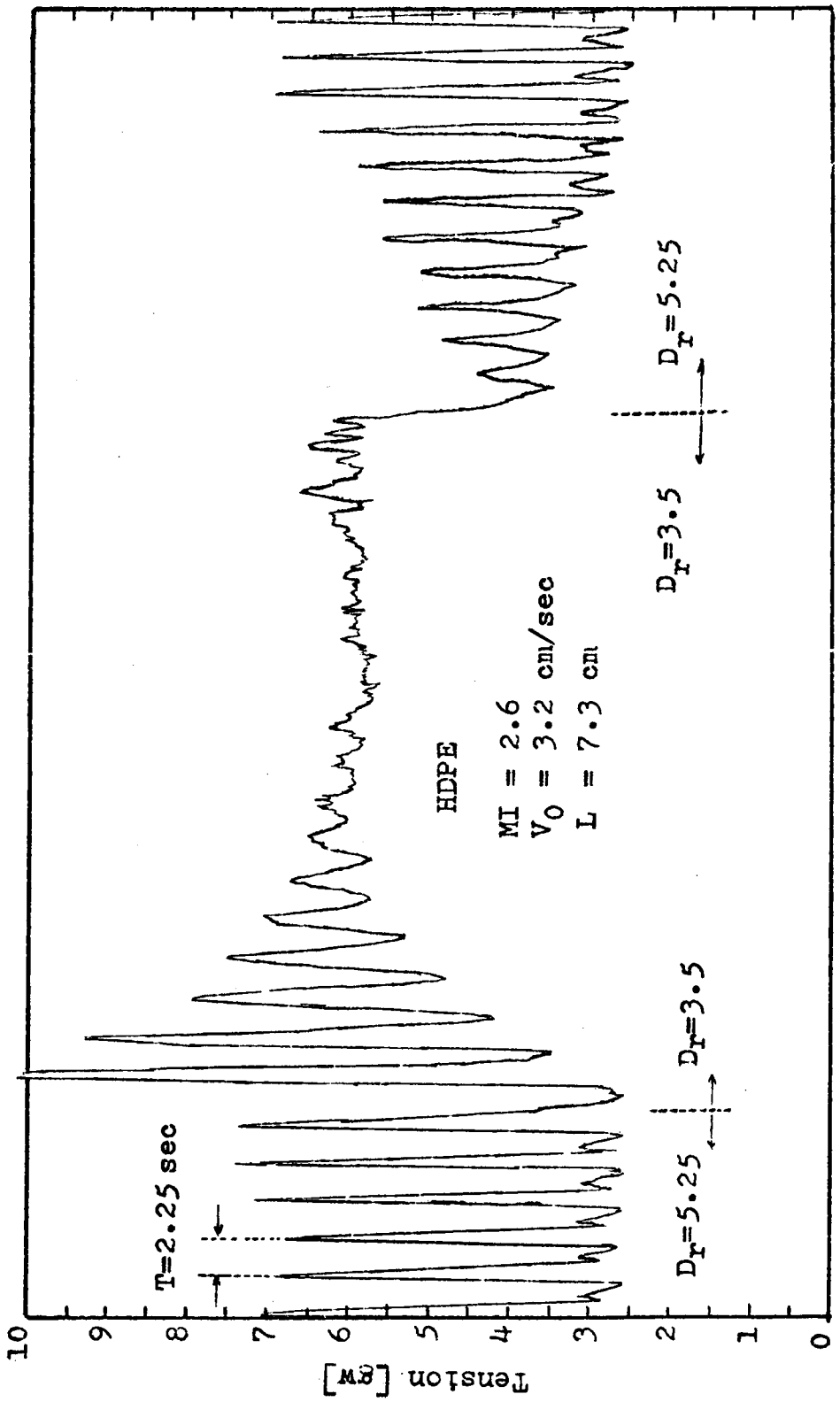


FIGURE 5.7 Transient states of the draw resonance phenomena.

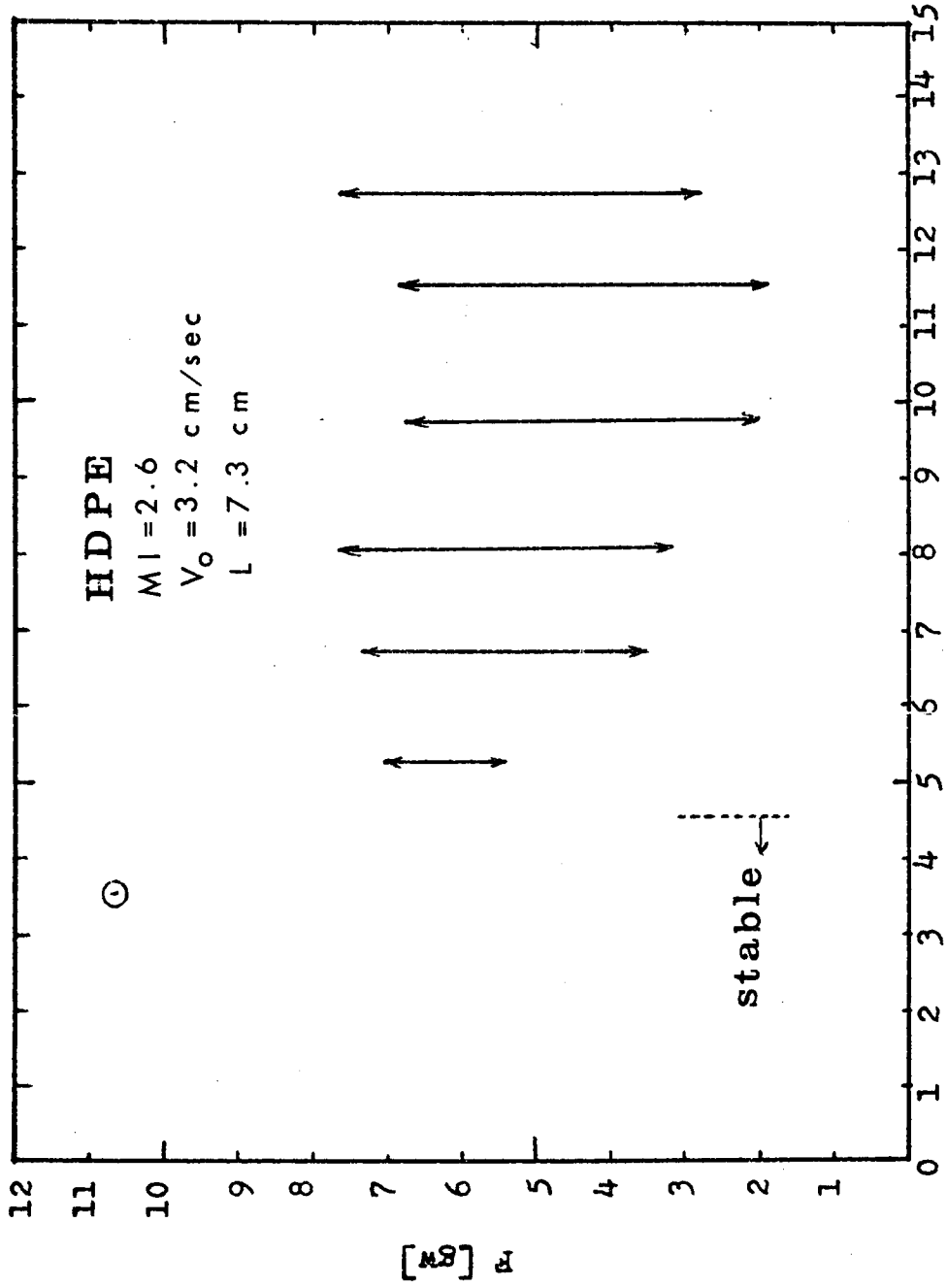


FIGURE 5.8 Spinline tension as a function of draw ratio.

As the draw ratio increases, the fluctuation of the tension becomes more severe.

The resonance period during the steady draw resonance is plotted against draw ratio in Fig. 5.9. Process variables of extrusion speed V and spinpath L were varied. It is seen that the stability criteria is completely determined by the draw ratio (and this value is around 5 for the HDPE (MI = 2.6)). One observes that the resonance period becomes long when the extrusion speed is lowered and the spinpath is increased. This is closely related to the residence time in the spinpath. The residence time based upon steady spinning of the Newtonian fluid for one condition is also shown in the figure for reference. The resonance periods are seen to be about twice the residence times.

Interpretations of the Failures of Stable Melt Spinning Process

In the non-isothermal condition, it was found that the spinline tensions of LDPE's and PS's became very high when take up speeds were increased and the failures of the process were caused by a fracture. However the spinline tensions of HDPE's did not increase strongly with the take up speed and a stable melt spinning was possible over a wide range of take up velocities. These observations agree with those of Abbott and White [1] for a LDPE and a HDPE.

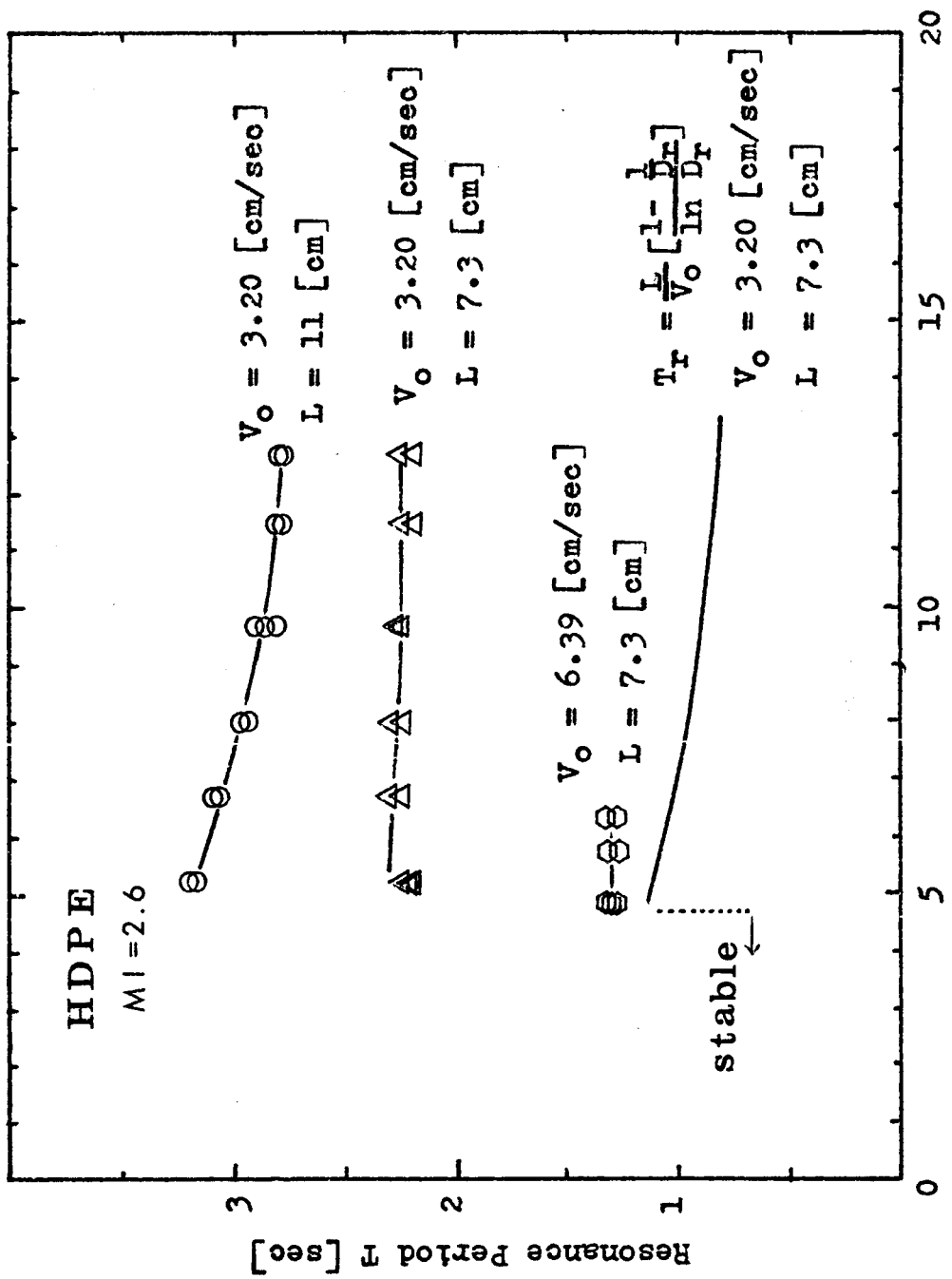


FIGURE 5.9 Resonance periods for various process variables.

In isothermal or near isothermal conditions, however, HDPE and PP showed the draw resonance phenomena and the draw ratios were limited to small values. This means the take up speeds are limited, since extrusion rates were restricted by the onset of melt fracture. For LDPE's and PS's, on the other hand, much higher draw ratios were possible. These observations can be explained by cohesive fracture and draw resonance instabilities. The different responces of various materials can be characterized by the dependences of relaxation times upon deformation rate (specifically a parameter). For LDPE and PS whose a parameter is small, the cohesive fracture limits the draw ratio. Such materials as HDPE and PP whose a parameter is large, the draw resonance limits the draw ratio, but this phenomena does not occur if material freezes before take up.

The draw resonance phenomena is the continuous melt spinning analogue of ductile instability in the tensile tests. Both phenomena are proved to be caused by a stress concentration due to perturbed cross-section when a constant force along the length is applied. The draw resonance phenomena may te interpreted to be initiated by a local deformation near the take up roll (where the stress is maximum). When a necking occurs, material starts to accumulate in the spinpath at the critical draw ratio because smaller amounts of material than extruded can be

taken out of the spinline. However the accumulation is limited to the amount of die swell cross-section times spinpath length as long as the extrusion rate and the take up speed are kept constant. This is why the amplitudes of the draw resonance level off to a certain level (the limit cycle) regardless of the initial perturbations, as predicted by the nonlinear analyses [41,60]. The stabilizing phenomena when the spinpath is decreased to the order of less than 1 cm [41,61] can also be easily explained. At such short spinpath, material accumulation is extremely limited because dead space becomes so small. In this region, the combined effects of die swell and the decaying normal stress might become important. Thus draw resonance is proved to be the continuous melt spinning analogue of ductile failure.

CHAPTER VI

CONCLUSIONS AND RECOMMENDATIONS

Elongational flow behaviors of various kinds of polymer melts were investigated. These include different molecular weight levels of low density polyethylenes (LDPE), high density polyethylenes (HDPE), polystyrenes (PS), and polymethyl methacrylate (PMMA).

The uniaxial elongational flow behaviors of these polymer melts were first studied under a controlled kinemetic of constant stretch rates. Simple equipment to provide a constant stretch condition was designed and constructed for this purpose. The stress responses can be described by the Bogue and White model or generalized convected Maxwell model, especially if we take relaxation times as deformation rate dependent such as Eq. (2.23) (page 15) or Eq. (3.20) (page 93). Parameter a of the effective relaxation times describes a dependence upon deformation rate. It was found that LDPE and PS can be described by samll a values (0.3 to 0.5), and for HDPE and PP, on the other hand, by large a values (0.5 to 0.9).

The elongational viscosities for the various polymers were obtained as maximum attained values. When they were plotted against elongation rate, they were approximately equal to three times the shear viscosity or Trouton viscosity at low elongation rates. But with increasing elongation

rate, values of LDPE increased very rapidly and those of PS also increased at a lesser rate. However elongational viscosities of HDPE and PP did not increase with elongation rate but rather showed a decrease, especially for high molecular weight ones. These elongational viscosities seem, however, mostly apparent ones due to the presence of instabilities in the elongation.

Failure characteristics of the filaments during the elongational flow were carefully observed. Based upon these observations, three mechanisms of filament instabilities; "capillarity," "ductility," and "cohesive fracture" are revealed. A mathematical theory integrating all the instability mechanisms has been developed using linear stability theory. Viscoelastic fluids were represented by the White and Metzner equation with the effective relaxation time. The stability theory suggests that viscosity stabilizes the capillary instability, and the Weissenberg number stabilizes the ductile instability, but this leads to cohesive fracture when stretched at constant rates. The transition from the ductile instability to cohesive fracture is found to occur at the Weissenberg number $\lambda E = 1/(2-\sqrt{3}a)$. The parameter a was found to give a very strong influence on the ductile instability and large values of a such as $(a > 1/\sqrt{3} = 0.58)$ make the ductile instability more severe than that of Newtonian fluids.

The stability theory has been applied to the spinnability

or extensibility problem. The extensibility is predicted to show a maximum in the molecular weight due to the three competing mechanisms. The different failure characteristics of LDPE and PS against HDPE and PP can be explained by different magnitudes of the a parameter. For large values of a, the failure mode is always ductile failure and the extensibility decreases with increasing molecular weight. The elongation to break was compared with the theory for a LDPE and a HDPE, and a good agreement was obtained for reasonable values of parameters.

The concepts developed for simple elongational flow were applied to a continuous melt spinning process. The theory developed for tensile tests can be applicable to the spinline to a significant extent as long as steady spinline has not been established. However, it is not applicable to the steady spinline because kinematics are different due to different forms of the continuity equation. Draw resonance was noted to be caused by accumulation of materials in the spinline but not by the resonance of small fluctuations of the system. It was shown (both mathematically and experimentally) that the draw resonance in continuous spinline was an analogue of ductile instability in tensile tests.

Important process variables in the spinline dynamics were found to be the effective Deborah number (or Weissenberg number) $\alpha' = (1-\beta a)\lambda V(0)/L$ and the draw ratio $V(L)/V(0)$. The α' determines the stress or diameter distributions in the stable thread line. The draw resonance

phenomena under nearly isothermal conditions are controlled by α' and the draw ratio. Cooling of the threadline is an important factor in the failure of the stable melt spinning process, because the dominant instability mechanism depends upon cooling rate. When the process is highly non-isothermal such that solidification takes place before take up, the failure is caused by cohesive fracture. Thus such materials as LDPE and PS which have small a parameter and high values of α' are less stable. However, when the process is nearly isothermal, then the draw resonance mainly limits the draw ratio. Therefore such materials as HDPE and PP, whose a are small and thus have small or negative α', are less stable.

The basic problems of uniaxial elongational flow which include both stable and unstable problems have now been solved for isothermal conditions. The significance and importance of the dependence of relaxation time upon deformation rate were pointed out. Further investigations of polymer melt processing operations involving elongational flow are recommended to take this dependence into consideration. It is also recommended that the effects of cooling, especially solidification be investigated, since most polymer processing operations are performed under highly non-isothermal conditions.

LIST OF REFERENCES

LIST OF REFERENCES

1. Abbott, L.E. and J.L. White, J. Appl. Poly. Symp., 20, 247 (1973).

2. Acierno, D., J.N. Dalton, J.M. Rodriguez, and J.L. White, J. Appl. Poly. Sci., 15, 2395 (1971).

3. Adam, N.K., "The Physics and Chemistry of Surfaces," 4th ed., Dover, N.Y., 1968.

4. Andrews, E.H., "Fracture in Polymers," American Elsevier, N.Y., 1968.

5. Bachelor, G.K., Q. J. Mech. Appl. Math., 7, 179 (1954).

6. Ballman, R.L., Rheol. Acta, 4, 137 (1965).

7. Bergonzoni, A., and A.J.D. Cresce, Poly. Eng. Sci., 6, 45, 55 (1966).

8. Bernstein, B., E.A. Kearsley, and L.J. Zapas, Trans. Soc. Rheol. 7, 391 (1963).

9. Bogue, D.C., Ind. Eng. Chem. Fund., 5, 253 (1966).

10. Bogue, D.C., T. Masuda, Y. Einaga, and S. Onogi, Poly. J., 1, 563 (1970).

11. Bogue, D.C. and J.L. White, "Engineering Analysis of Non-Newtonian Fluids," NATO Agardograph #114 1971, and also available in Japanese translated by N. Mitsuishi and A. Yamanaka, Kogyo Chosakai, Tokyo, 1972.

12. Bolton, E.K., Ind. Eng. Chem., 34, 53 (1942).

13. Boltzmann, L., Sitzungber, Akad. Wiss. Wien., 70, 275 (1874).

14. Boys, C.V., "Soap Bubbles," reprint of 1911 edition, Dover, N.Y., 1958.

15. Bridgman, D.W., Trans. Amer. Soc. Metals, 32, 554 (1944).

16. Brodnyan, J.G., F.H. Gaskins, and W. Philippoff, Trans. Soc. Rheol., 1, 109 (1957).

17. Carothers, W. and J.W. Hill, J. Amer. Chem. Soc., 54, 1579 (1932).

18. Carothers, W. and Van Natta, J. Amer. Chem. Soc., 55, 4714 (1933).

19. Carreau, P.J., Trans. Soc. Rheol., 16, 99 (1972).

20. Chandrasekhar, S., "Hydrodynamic and Hydromagnetic Stability," Clarendon Press, Oxford, 1961.

21. Chang, H. and A.S. Lodge, Rheol. Acta, 10, 448 (1971).

22. _____, Ibid., 11, 127 (1972).

23. Chen, I.J., Ph.D. Dissertation, Dept. of Chem. and Met. Engr. Univ. of Tennessee, 1971.

24. Chen, I.J. and D.C. Bogue, Trans. Soc. Rheol., 10, 59 (1972).

25. Chen, I.J., G.E. Hagler, L.E. Abbott, D.C. Bogue, and J.L. White, Trans. Soc. Rheol., 16, 473 (1973).

26. Cogswell, F.N., Plastics and Polymers, 36, 109 (1968).

27. _____, Trans. Soc. Rheol., 16, 383 (1972).

28. _____, Poly. Eng. Sci., 12, 64 (1972).

29. _____, J. Appl. Symp., 27, 1 (1975).

30. Coleman, B.D. and W. Noll, Arch. Rat. Mech. Anal., 6, 355 (1960).

31. De Witt, T.W., J. Appl. Phys., 26, 889 (1955).

32. Dealy, J.M., Poly. Eng. Sci., 11, 433 (1971).

33. Denn, M.M., "Stability of Reaction and Transport Process," Prentice-Hall, Englewood Cliffs, p. 160, 1975.

34. Denn, M.M. and G. Marrucci, A.I.Ch.E.J., 17, 101 (1971).

35. Denn, M.M., C.J.S. Petrie, and P.J. Avenas, A.I.Ch. E.J., 21, 791 (1975).

36. Donnelly, C.J. and C.B. Weinberger, Ind. Eng. Chem. Fund., 14, 334 (1975).

37. Eringen, A.C., "Nonlinear Theory of Continuous Media," McGraw Hill, 1962.

38. Everage, E.A. and R.L. Ballman, unpublished manuscript, May, 1975.

39. Fenn, R.W. and S. Middleman, A.I.Ch.E.J., 15, 379 (1969).

40. Ferry, J.D., "Viscoelastic Properties of Polymers," John Wiley, Second ed., N.Y., 1970.

41. Fisher, R.J. and M.M. Denn, J. Appl. Poly. Symp., 27, 103 (1975), also Chem. Eng. Sci., 20, 1129 (1975).

42. _____, A.I.Ch.E.J., 22, 236 (1976).

43. Freeman, H.I. and M.J. Coplan, J. Appl. Poly. Sci., 8, 2389 (1964).

44. Furuta, I, V.M. Lobe, and J.L. White, J. Non-Newtonian Fluid Mech., 1 (1976).

45. Gaines, G.L., Poly. Eng. Sci., 12, 1 (1972).

46. Gelder, D., Ind. Eng. Chem. Fund., 10, 534 (1971).

47. Goedda, E.F. and M.C. Yuen, J. Fluid Mech., 40, 495 (1970).

48. Goldin, M., J. Yerushalmi, R. Pfeffer, and R. Shinnar, J. Fluid. Mech., 38, 44 (1969).

49. Goldstein, S., "Modern Developments in Fluid Dynamics," Clarendon Press, Oxford, 1938.

50. Gordon, M., J. Yerushalmi, and R. Shinnar, Trans. Soc. Rheol., 17, 303 (1973).

51. Green, A.E. and R.S. Rivlin, Arch. Rat. Mech. Anal., 1, 1 (1957).

52. Green, M.S. and A.V. Tobolsky, J. Chem. Phys., 14, 80 (1946).

53. Greensmith, H.W., L. Mullins, and A.G. Thomas, Trans. Soc. Rheol., 4, 179 (1960).

54. Griffith, A.G., Phil. Trans. Roy. Soc., A221, 163 (1920).

55. Hamana, I., M. Matsui, and S. Kato, Meilland Textilberichte, 5, 499 (1968).

56. Han, C.D. and R.R. Lamonte, Trans. Soc. Rheol., 16, 447 (1972).

57. Han, C.D., R.R. Lamonte, and Y.T. Shah, J. Appl. Poly. Sci., 16, 3307 (1972).

58. Han, C.D. and L. Segal, J. Appl. Poly. Sci., 14, 2973 (1970).

59. Hencky, H., Ann. Phys., 2, 617 (1929).

60. Ishihara, H. and S. Kase, J. Appl. Poly. Sci., 19, 557 (1975).

61. _____, Ibid., 20, 169 (1976).

62. Kamei, E. and S. Onogi, Appl. Poly. Symp., 27, 19 (1975).

63. Kase, S., J. Appl. Poly. Sci., 18, 3279 (1974).

64. Kase, S. and T. Matsuo, J. Poly. Sci., A3, 2541 (1965).

65. _____, J. Appl. Poly. Sci., 11, 251 (1967).

66. Kase, S., T. Matsuo, and Y. Yoshimoto, Seni Kikai Gakkai Shi, 19, T63 (1966).

67. Kroesser, F.W. and S. Middleman, A.I.Ch.E.J., 15, No. 3, 383 (1969).

68. Landel, R.F. and R.F. Fedors, "Fracture Processes in Polymeric Solids," edited by B. Rosen, Interscience, N.Y., p. 361, 1964.

69. Lee, B.L. and J.L. White, Trans. Soc. Rheol., 18, 467 (1974).

70. Levich, V., "Physico-Chemical Hydrodynamics," translated from Russian by L.E. Scriven, Prentice-Hall, Englewood Cliffs, 1962.

71. Lodge, A.S., Proc. 2nd Int. Rheol. Cong. p. 229 (1954).

72. _____, Trans. Faraday Soc., 52, 120 (1956).

73. Lodge, A.S., in "Rheology of Elastomers," edited by Mason and Wookey, Pergamon, 1958.

74. _____, "Elastic Liquids," Academic Press, N.Y., 1964.

75. Lamonte, R.R. and C.D. Han, J. Appl. Poly. Sci., 16, 3285 (1972).

76. Masuda, T., Ph.D. Dissertation, Dept. of Poly. Chem., Kyoto University, 1973.

77. Matovich, M. and J.R.A. Pearson, Ind. Eng. Chem. Fund., 8, 512 (1969).

78. Matsui, M., M.S. Thesis, Dept. of Chem. and Met. Eng. Univ. of Tennessee, 1976.

79. Maxwell, J.C., Phil. Trans. Roy. Soc., 157, 249 (1866).

80. _____, "Capillarity," in Encyclopedia Britannica, 1878; also in Scientific Papers, 2, 541, Dover, N.Y., (1890).

81. _____, "Constitution of Bodies," in Encyclopedia Brittanica, 1878; also in Scientific Papers, 2, 616 (1890).

82. Meissner, J., Rheol. Acta, 8, 78 (1969).

83. _____, Ibid., 10, 230 (1971).

84. _____, Trans. Soc. Rheol., 16, 405 (1972).

85. Mendelson, R.A., F.L. Finger, and E.B. Bagley, J. Poly. Sci., C35, 177 (1971).

86. Middleman, S., Chem. Eng. Sci., 20, 1037 (1965).

87. _____, "The Flow of High Polymers," Wiley, N.Y., 1968.

88. _____, Trans. Soc. Rheol., 13, 123 (1969).

89. Miller, J.C., Soc. Plast. Eng. Trans., 3, 134 (1963).

90. Miller, M.J. and E.B. Christiansen, A.I.Ch.E.J., 18, 600 (1972).

91. Minagawa, N. and J.L. White, Poly. Eng. Sci., 15, 825 (1975).

92. Morland, L.W. and E.H. Lee, Trans. Soc. Rheol., 4, 233 (1960).

93. Nadai, A. and M.J. Manjoine, J. Appl. Mech., A, 77 (1941).

94. Nadai, A., "Theory of Flow and Fracture of Solids," Vol. 1, 2nd ed., Mc Graw-Hill, N.Y., 1950.

95. Nadella, H., M.S. Thesis, Dept. of Chem. and Met. Eng. Univ. of Tennessee, 1976.

96. Nakamura, K., T. Watanabe, K. Katayama, and T. Amano, J. Appl. Poly. Sci., 10, 1077 (1972).

97. _____, Ibid., 18, 1615 (1974).

98. Nayfeh, A.N., Phys. Fluids, 13, 841 (1970).

99. Nitschmann, H. and J. Schrade, Helv. Chim. Acta, 31, 297 (1948).

100. Noll, W., J. Rat. Mech. Anal., 4, 13 (1955).

101. _____, Arch. Rat. Mech. Anal., 2, 197 (1958).

102. Olabisi, O., and M.C. Williams, Trans. Soc. Rheol., 16, 727 (1972).

103. Oldroyd, J.G., Proc. Roy. Soc., A200, 52 (1950).

104. _____, Q. J. Mech. Appl. Math., 4, 271 (1951).

105. Onogi, S., T. Masuda, and K. Kitagawa, Macromolecules, 3, 109 (1970).

106. Onogi, S., T. Matsumoto, and E. Kamei, Poly. J., 3, 531 (1972).

107. Orowan, E., Rept. Prog. Phys., 12, 185 (1949).

108. Pearson, J.R.A. and M.A. Matovich, Ind. Eng. Chem. Fund., 8, 605 (1969).

109. Pearson, J.R.A., Y.T. Shah, and R.D. Mhaskar, Ind. Eng. Chem. Fund., 15, 31 (1976).

110. Petrie, C.J.S., and M.M. Denn, A.I.Ch.E.J., 22, 209 (1976).

111. Rayleigh, Lord, Proc. London Math. Soc., 10, 4 (1879).

112. _____, Phil. Mag., 34, 145 (1892).

113. Rayleigh, Lord, Nature, 44, 249 (1891).

114. _____, "The Theory of Sound," 2nd ed., Vol. 2, p. 351, Dover, N.Y., 1945.

115. Reiner, M., "Deformation and Flow," Lewis, London, 1948.

116. Rivlin, R.S. and A.G. Thomas, J. Poly. Sci., 10, 291 (1953).

117. Roman, J., M.S. Thesis, Dept. of Chem. and Met. Eng. Univ. of Tennessee, 1974.

118. Shah, Y.T. and J.R.A. Pearson, Ind. Eng. Chem. Fund., 11, 145 (1972).

119. _____, Ibid., 11, 150 (1972).

120. _____, Poly. Eng. Sci., 10, 219 (1972).

121. Smith, T.L., J. Poly. Sci., 32, 99 (1958).

122. _____, Ibid., A1, 3597 (1963).

123. _____, "Strength and Extensibility of Elastomers," Rheology, Vol. 5, edited by F. Eirich, Academic Press, N.Y., 1969.

124. Southern, J.H. and R.L. Ballman, Appl. Poly. Symp., 20, 175 (1973).

125. Spearot, J.A. and A.B. Metzner, Trans. Soc. Rheol., 16, 495 (1972).

126. Spriggs, T.W. and R.B. Bird, Ind. Eng. Chem. Fund., 4, 182 (1964).

127. _____, Chem. Eng. Sci., 20, 931 (1965).

128. Spriggs, T.W., J.D. Huppler, and R.B.Bird, Trans. Soc. Rheol. 10, 191 (1966).

129. Stevenson, J.F., A.I.Ch.E.J., 18, 540 (1972).

130. Stokes, G.G., Trans. Comb. Phil. Soc., 8, 287 (1845).

131. Takaki, T., M.S. Thesis, Dept. of Chem. and Met. Eng. Univ. of Tennessee, 1973.

132. Takaki, T. and D.C. Bogue, J. Appl. Poly Sci., 19, 419 (1975).

133. Tanner, R.I., Trans. Soc. Rheol., 17, 365 (1973).

134. Taylor, G.I., Proc. Roy. Soc. (London), A146, 501 (1934).

135. Tobolsky, A.V. and K. Murakami, J. Poly. Sci., 40, 443 (1959).

136. Tomita, Y., "Rheology," Korona Sha, Tokyo, 1975.

137. Tomotika, S., Proc. Roy. Soc. (London), A150, 322 (1935).

138. _____, Ibid., A153, 302 (1936).

139. Treolar, L.R.G., "Physics of Rubber Elasticity," 2nd ed., Clarendon Press, Oxford, 1958.

140. Trouton, F., Proc. Roy. Soc., A77, 426 (1906).

141. Truesdell, C. and R.A. Toupin, "The Classical Field Theories," in Handbuch der Physik, Wol. III/1, Springer Verlag, Berlin, 1960.

142. Vincent, P.I., Polymer, 1, 7 (1960).

143. Vinogradov, G.V., J. Poly. Sci., A-2, 8, 1 (1970).

144. Vinogradov, G.V., V.D. Fikhman, R.V. Raduchkevich, and A.Y. Malkin, J. Poly. Sci., A-2, 8,657 (1970).

145. Vinogradov, G.V., V.D. Fikhman, and B.V. Radushkevich, Rheol. Acta, 11, 286 (1972).

146. Weber, C.Z., Angew. Math. Mech., 11, 136 (1931).

147. White, J.L., J. Appl. Poly. Sci., 8, 2339 (1964).

148. _____, Rubber Chem. Tech., 42, 257 (1969).

149. _____, Rheol. Acta, 14, 600 (1975).

150. White, J.L. and A.B. Metzner, J. Appl. Poly. Sci., 8, 1367 (1963).

151. White, J.L. and J.F. Roman, J. Appl. Poly. Sci. (in press).

152. White, J.L. and N. Tokita, J. Appl. Poly. Sci., 12, 1589 (1968).

153. Williams, M.C. and R.B. Bird, Phys. Fluids, 5, 1126 (1962).

154. Williams. M.L., R.F. Landel, J.D. Ferry, J. Amer. Chem. Soc., 77, 3701 (1955).

155. Yamamoto, M., J. Phys. Soc. Japan, 11, 413 (1956).

156. _____, Ibid., 12, 1148 (1957).

157. Yuen, M.C., J. Fluid Mech., 33, 151 (1968).

158. Zapas, L.J. and T. Craft, J. Res. Nat. Bur. Stand., 69B, 451 (1965).

159. Zaremba, S., Bul. Acad. Cracovie, 594 (1903).

160. Zeichner, G.R., M.S. Thesis, Dept. of Chem. Eng. Univ. of Delaware, 1973.

161. Ziabicki, A., in "Man-Made Fibers," Vol. 1, ed. by H.F. Mark, S.M. Atlas, and E. Cernia, Wiley, N.Y., 1967.

162. Ziabicki, A. and K. Kedzierska, Kolloid Zeit., 171, 51 (1960).

163. _____, Ibid., 175, 14 (1961).

164. Ziabicki, A. and R. Takserman-Krozer, Kolloid Zeit., 198, 60 (1964).

165. _____, Ibid., 199, 9 (1964).

APPENDIX

APPENDIX

```
$JOB


C ELONGATIONAL STRESS DEVELOPMENT OF THE ROGUE AND WHITE MODEL
      DIMENSION G(7),TAU(7),ST(4),VI(4)
      READ(5,5) N
    5 FORMAT(I10)
      READ(5,10)(G(K),TAU(K),K=1,N1
   10 FORMAT(8F10.3)
      DT=0.25
      DO 60 L=1,3
      DO 50 M=1,4
      E=10.**(M-4)*(1.+(L-1)**2)
      WRITE(6,20)E
   20 FORMAT(///10X,'E=',F10.3)
      WRITE(6,22)
   22 FORMAT(20X,'A=0.',18X,'A=0.5',18X,'A=1.0',18X,'A=1.5',/)
      WRITE(6,23)
   23 FORMAT(10X,'TIME',9X,4('STRESS',3X,'VISCOSITY',5X)/)
      T=10**(-1.25)
      DO 35 J=1,17
      T=T*10**DT
      DO 32 I=1,4
      A=(I-1)/2.
      SM=0.
      DO 30 K=1,N
      P=TAU(K)*E
      TT=T/TAU(K)
      X=1.+(1.732*A-2.)*P
      Y=1.+(1.732*A+1.)*P
      ARG1=-X*TT
      ARG2=-Y*TT
      IF(ARG1.GE.20) GO TO 31
      IF(ARG1.LT.-20) GO TO 25
      E1=EXP(ARG1)
      IF(ARG2.LT.-20) GO TO 26
      E2=EXP(ARG2)
      GO TO 27
   25 E1=0.
   26 E2=0.
   27 Q=(X+2.*Y)/3.
      IF (TT.GT.1.) GO TO 28
      EI = -0.57721566-ALOG(TT)+0.99999193*TT-0.24991055*TT**2
     #+0.0551968*TT**3-0.00976004*TT**4+0.00107857*TT**5
      R=(Q-1.)*EI*TT*EXP(TT)
      GO TO 29
   28 R  = (TT**2+2.334733*TT+0.250621)/(TT**2+3.330657*TT+1.681534)
   29 CONTINUE
      IF(X.EQ.0.) GO TO 24
      SM=SM+G(K)*(E1*(1.-Q/X+R)-E2*(1.-Q/Y+R)+Q*(1./X-1./Y))
      GO TO 30
   24 SM=SM+G(K)*(1.+R-E2*(1.-Q/Y+R)-Q/Y+2.*Y*TT/3.)
   30 CONTINUE
   31 XM=SM/E
      ST(I)=SM
   32 VI(I)=XM
   35 WRITE(6,40) T,(ST(I),VI(I),I=1,4)
   40 FORMAT(4X,F10.3,7X,4(1PE10.2,1PE10.2,3X))
   50 CONTINUE
   60 CONTINUE
      STOP
      END

$ENTRY
```

VITA

The author, Yoshiaki Ide (井手義明) was born in Fukuoka, Japan, on September 11, 1948, as the eldest son of Mr. and Mrs. Yoshio Ide. After completing his elementary education from kindergarten to high school in that community, he was admitted to Kyushu University in April, 1967. He studied mixing problems of viscoelastic fluids for his senior thesis at the university and received a Bachelor of Science in Chemical Engineering in March, 1971.

He continued his education in graduate school at the same university until July, when he traveled to the United States for further study in Rheology. He entered the University of Tennessee in the fall of 1971. A Master of Science was awarded in December, 1973, for the study of viscoelastic flow patterns around agitators.

He married the former Mary H. Newby in August, 1973. After the completion of his Ph.D., he will work for Celanese Research Company as a research engineer.